NASA CR 54822
AGC 8800-68

HYDRAULIC DESIGN OF THE M-1 LIQUID HYDROGEN TURBOPUMP

By

J. Farquahr
B. K. Lindley

Prepared for

National Aeronautics and Space Administration

Contract NAS 3-2555

AEROJET-GENERAL CORPORATION

SACRAMENTO, CALIFORNIA

Requests for copies of this report should be referred to:

National Aeronautics and Space Administration
Office of Scientific and Technical Information
Attention: AFSS-A
Washington, D. C. 20546

NASA CR-54822
AGC 8800-68

TECHNOLOGY REPORT

HYDRAULIC DESIGN OF THE M-1 LIQUID HYDROGEN TURBOPUMP

Prepared for

NATIONAL AERONAUTICS AND SPACE ADMINISTRATION

15 July 1966

CONTRACT NAS 3-2555

Prepared by:

AEROJET-GENERAL CORPORATION
LIQUID ROCKET OPERATIONS
SACRAMENTO, CALIFORNIA

AUTHORS: J. Farquahr
B. K. Lindley

APPROVED: W. E. Watters
Manager
M-1 Turbopump Project

Technical Management:

NASA LEWIS RESEARCH CENTER
CLEVELAND, OHIO

TECHNICAL MANAGER: W. W. Wilcox

APPROVED: W. W. Wilcox
M-1 Project Manager

ABSTRACT

This report presents the design method and resulting design details as well as performance predictions for a ten-stage, axial flow, hydrogen pump for the M-1 oxygen/hydrogen liquid rocket engine. The pump is designed to supply 600 lb/sec of hydrogen at a pressure rise of 1890 psi. The pump stage complement consists of a low hub ratio inducer stage with untwisted rotor blading followed by a lightly-loaded stage, called the transition stage, and eight main stages. The main stages are designed for free vortex head generation, with 50% reaction at the blade rest and a tip diffusion factor of 0.4. The transition stage is designed to provide uniform radial head distribution for the first main stage. A C-4, or modified C-4 circular arc blading is utilized for all blade rows with the exception of the inducer rotor and discharge housing turning vanes.

TABLE OF CONTENTS

TABLE OF CONTENTS

LIST OF TABLES

LIST OF FIGURES

LIST OF FIGURES (continued)

LIST OF FIGURES (continued)

I. SUMMARY

This report presents the results of the hydraulic design effort for the liquid hydrogen pump of the 1,500,000 lb thrust M-1 liquid hydrogen/liquid oxygen rocket engine. The pump was designed to produce a total pressure rise of 1890 psi at a flow rate of 600 lb/sec, while operating at a maximum suction specific speed of 20,000 and a speed of 13,225 rpm. The pump suction was sized to permit eventual upgrading to satisfy a suction specific speed requirement of 40,000.

One-stage centrifugal, two-stage centrifugal and multiple staged axial flow pumps were considered. The axial flow pump was selected primarily because of its upgrading capability and weight considerations. The pump consists of an inducer stage, a lightly-loaded axial transition stage, and eight axial main stages.

Figure No. 1 is cut-away sketch of the turbopump while Figure No. 2 shows the completed turbopump assembly. A main-stage rotor assembly is shown in Figure No. 3 and a stator assembly in Figure No. 4. The component parts of the turbopump are illustrated in Figure No. 5 along with the materials of construction.

Blading design and pump off-design performance predictions were calculated using blade element techniques that considered the effect of radial equilibrium, losses, fluid-to-blade flow deviations, and fluid density variations. The predicted performance is shown in Figures No. 6 and No. 7.

II. INTRODUCTION

The M-1 liquid hydrogen pump is the result of an effort, started in April 1962, to design a pump for a large liquid hydrogen, liquid oxygen rocket engine. The initial application was for a 1,200,000 lb thrust level for the second-stage engines in the National Aeronautics and Space Administration's first moon landing vehicle. In July 1962, the requirement for the M-1 engine in this vehicle was eliminated because of the decision to use the rendezvous technique for the mission. At this time, a study of new missions and associated engine concepts was started. This study resulted in the establishment, in November 1962, of a requirement for a 1,500,000 lb thrust level engine incorporating concepts that would allow eventual thrust upgrading to 1,800,000 lb. The pump design described in this report is for this latter application. The pump hydraulic design requirements are shown in Table I.

An analysis of alternative turbopump concepts was conducted in parallel with the mission and engine analyses discussed above. One-stage and two-stage centrifugal pumps and multi-stage axial pumps were considered. Turbopump weights and vehicle performance parameters for a typical second-stage application (ten F-1 first-stages, two M-1 second-stages of 1,500,000 lbs thrust each and one J-2 third-stage escape vehicle) are compared below:

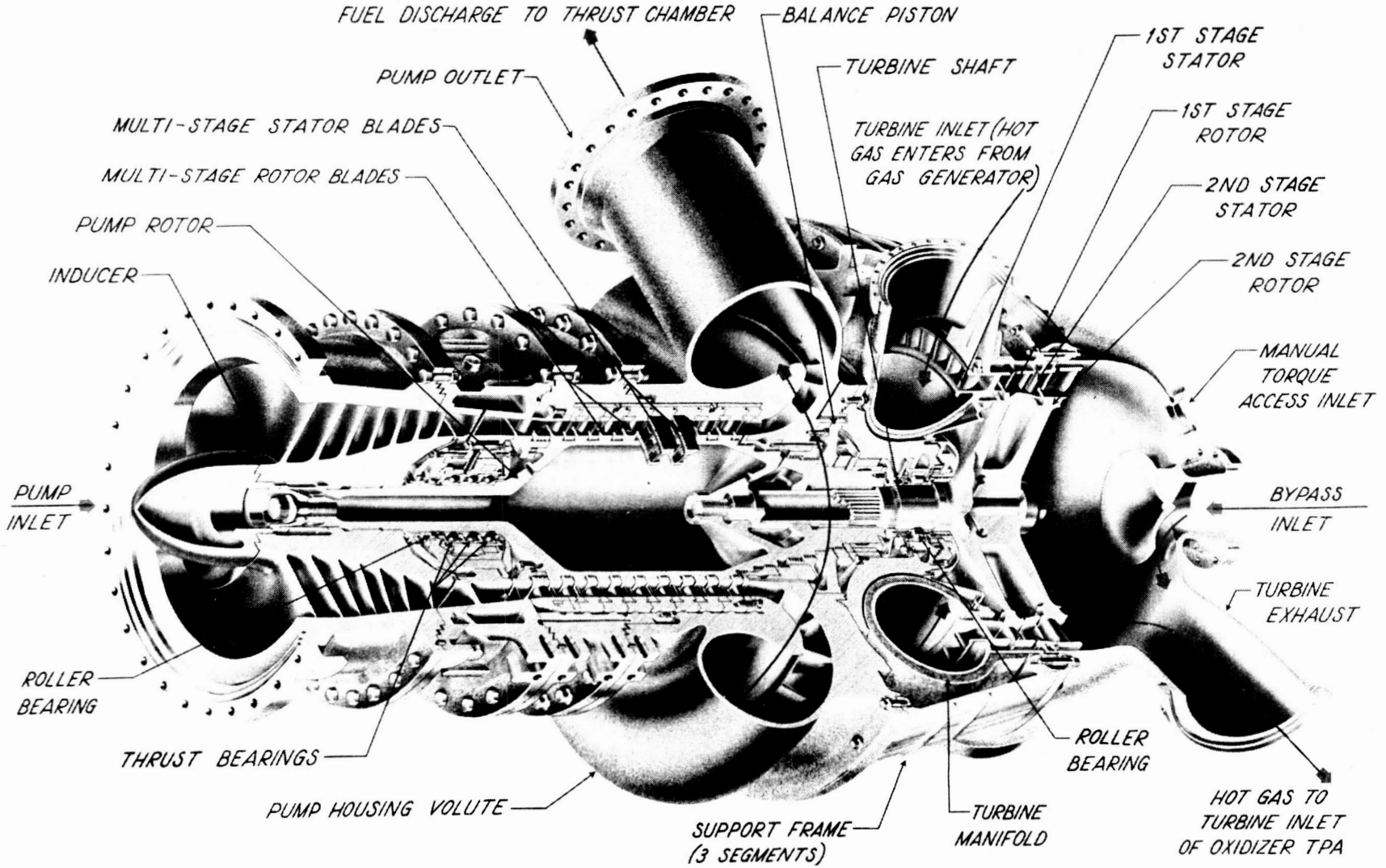

Figure 1

M-1 Liquid Hydrogen Turbopump (Cut-Away Isometric)

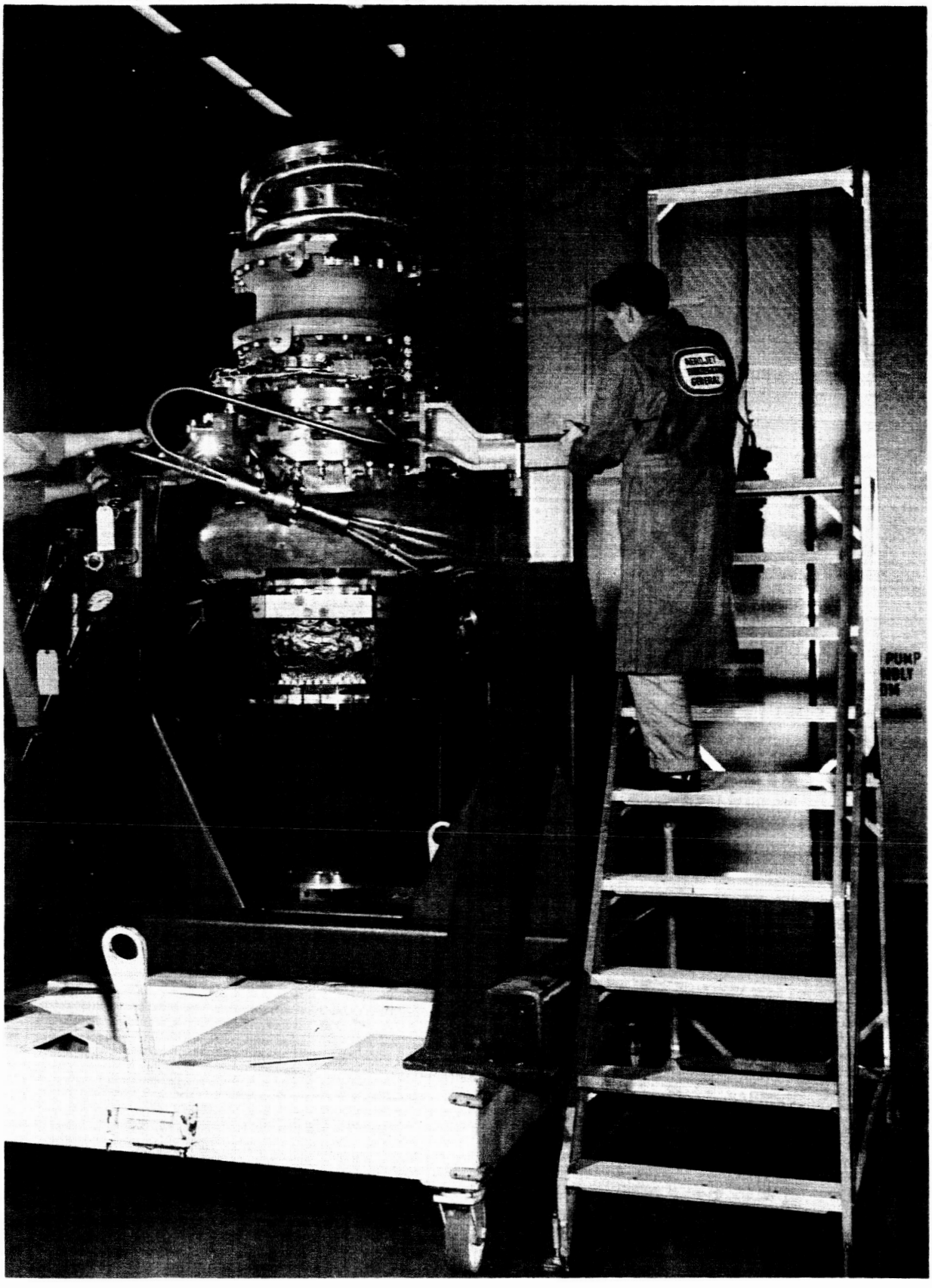

Figure 2

M-1 Liquid Hydrogen Turbopump Assembly

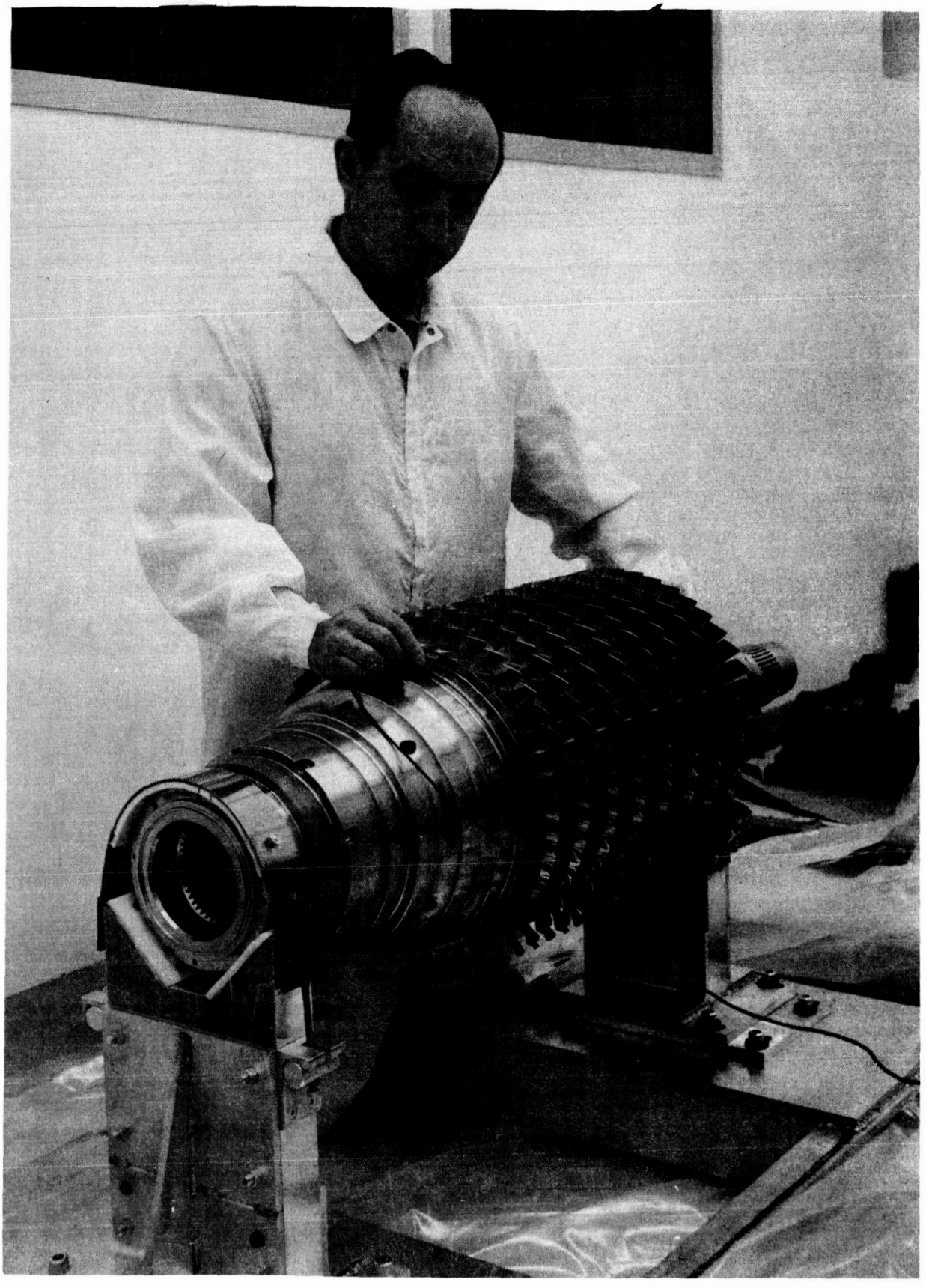

Figure 3

M-1 Liquid Hydrogen Pump Rotor Assembly

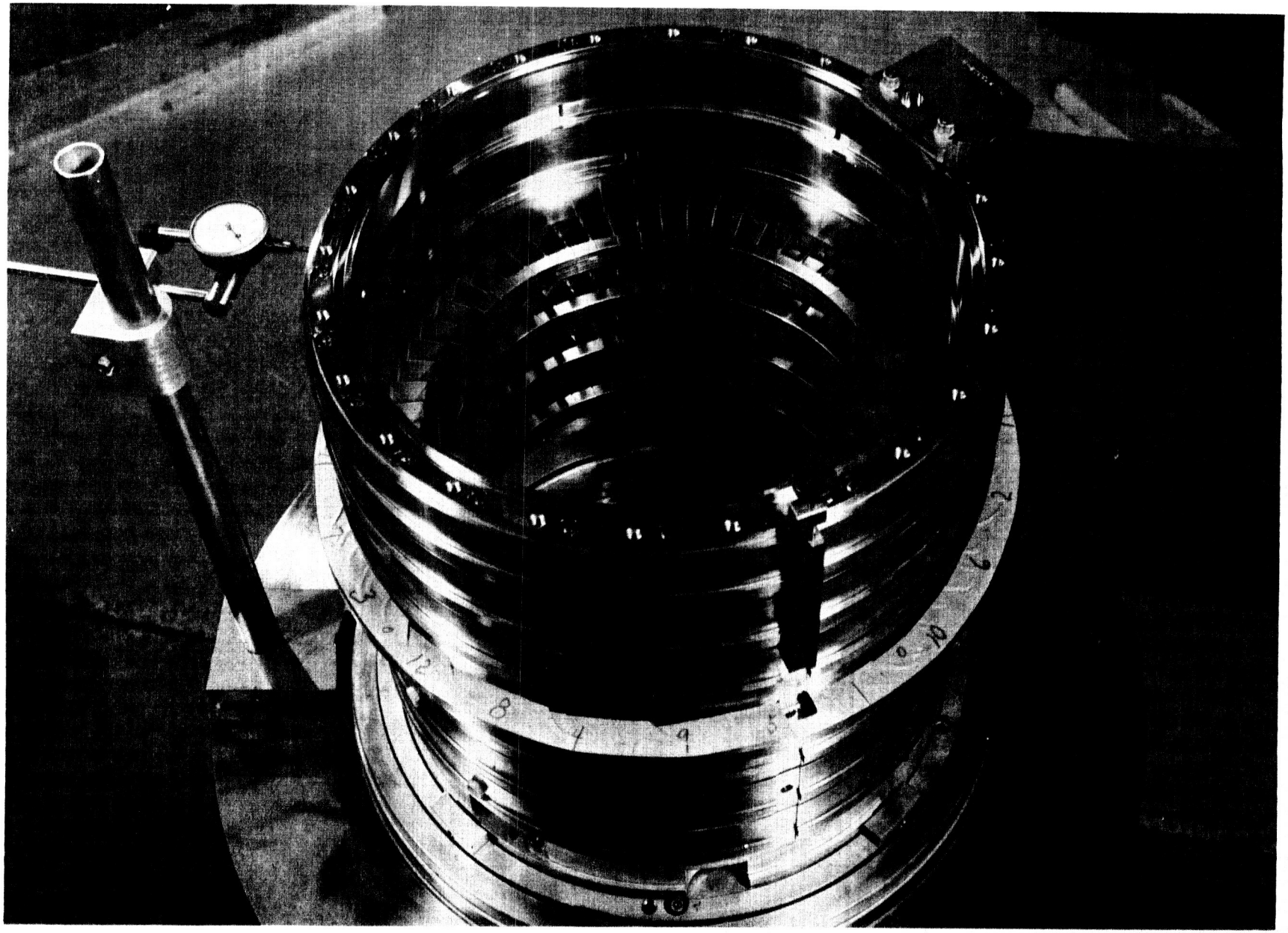

Figure 4

M-1 Liquid Hydrogen Pump Stator Assembly

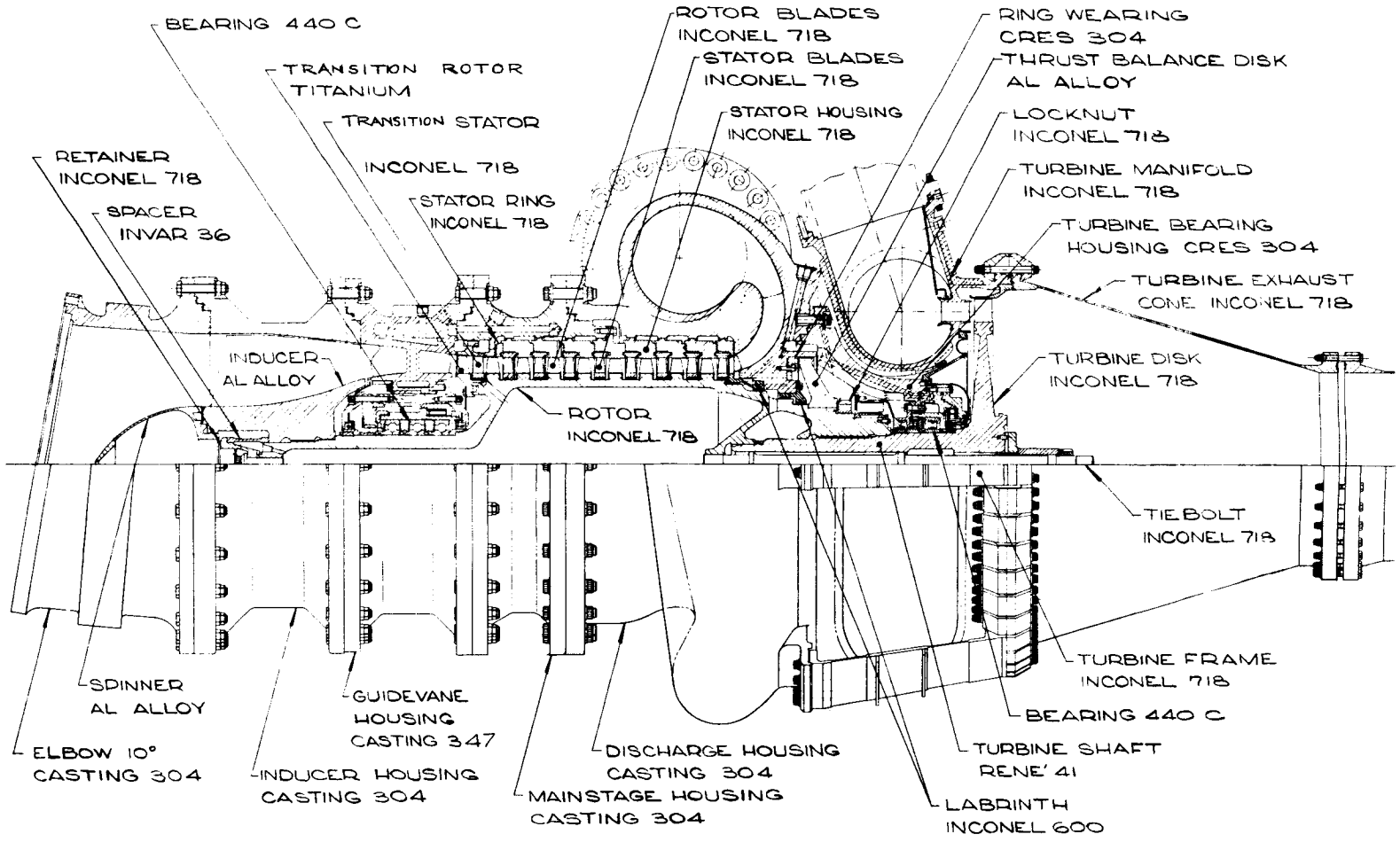

Figure 5

M-1 Liquid Hydrogen Turbopump Nomenclature and Material

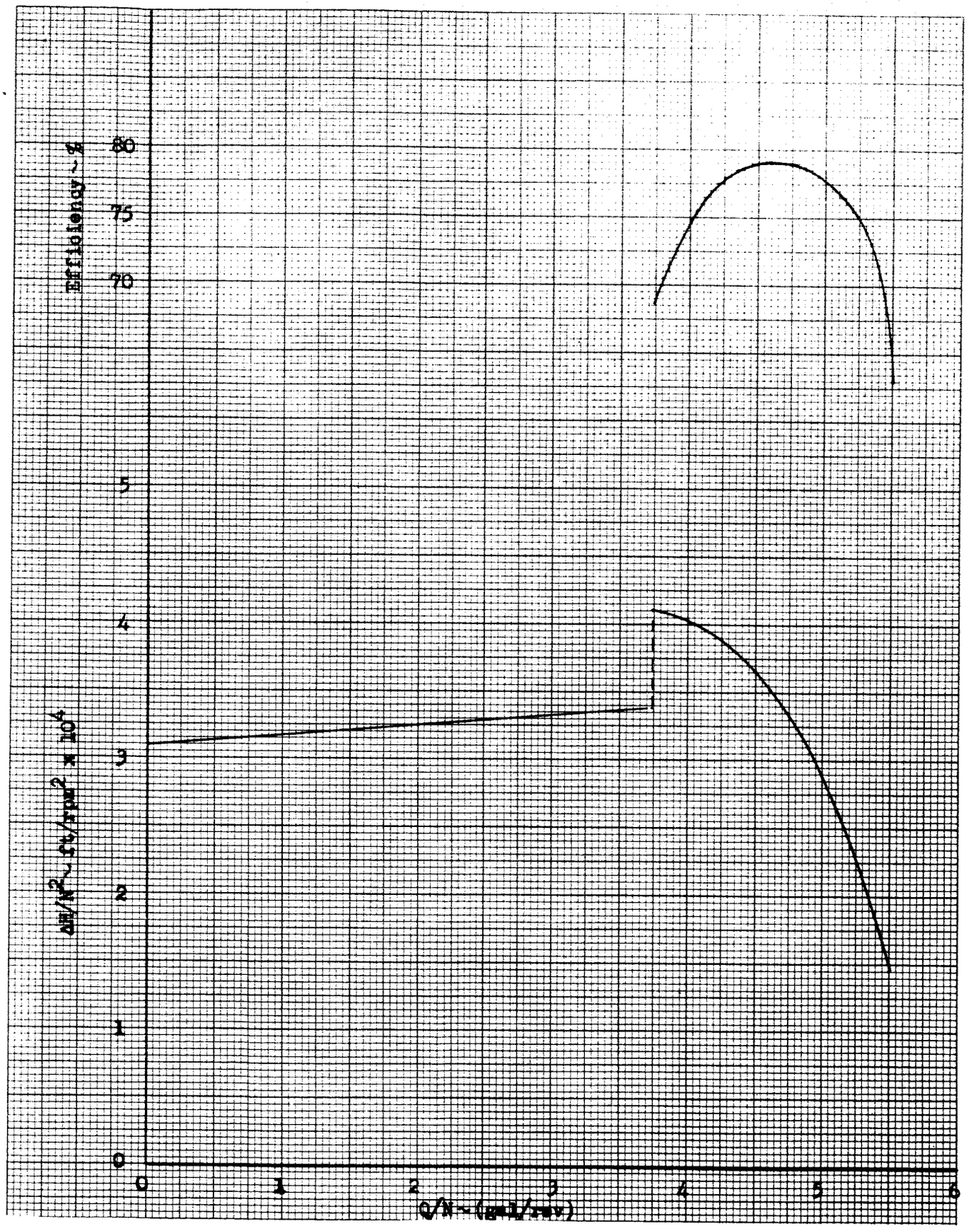

Figure 6

Over-All Performance
(Normalized Pump Head Rise and Efficiency vs. Normalized Pump Flow Rate)

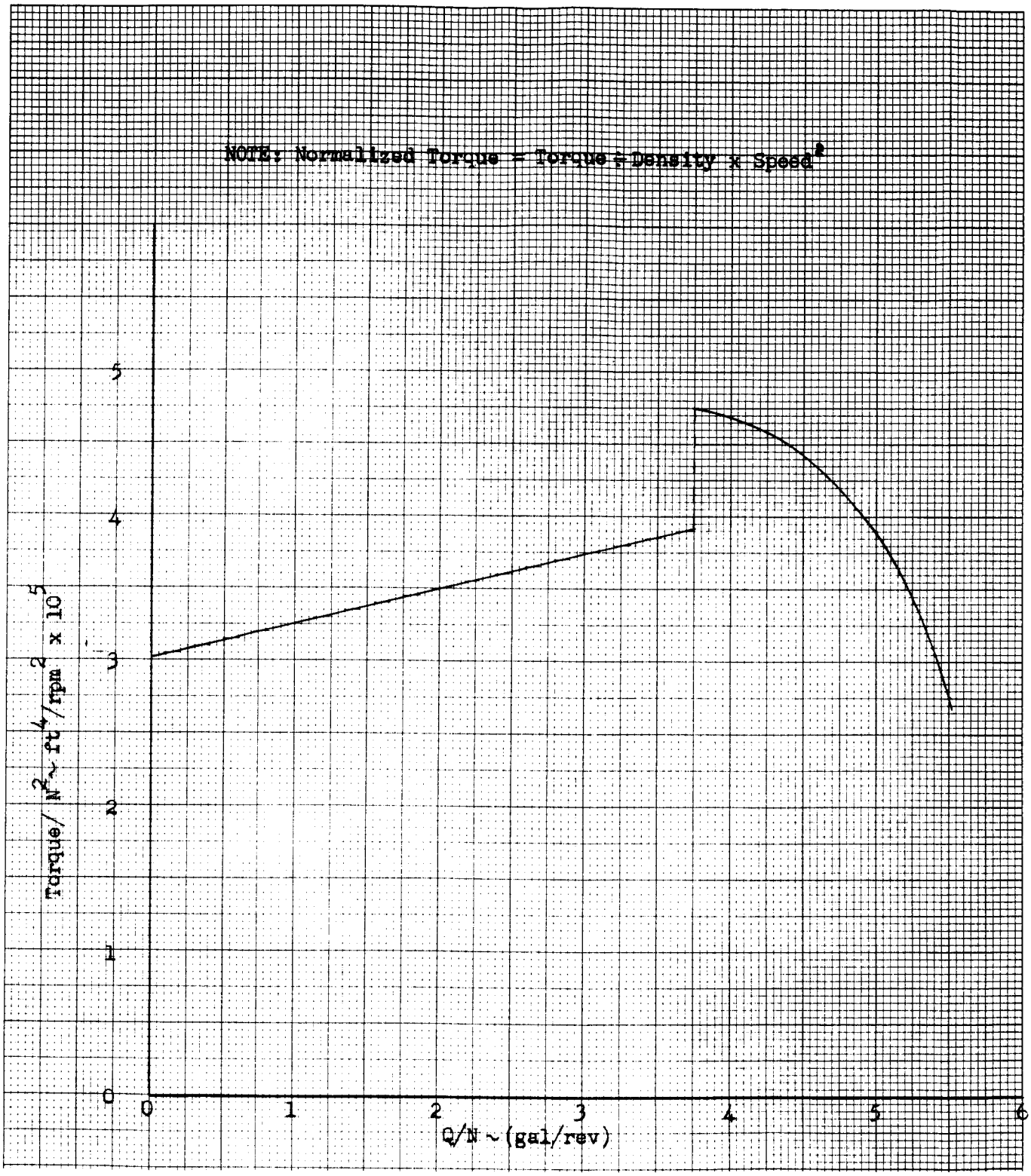

Figure 7

Over-All Performance
(Normalized Pump Required Torque vs. Normalized Pump Flow Rate)

TABLE I

M-1 FUEL PUMP HYDRAULIC DESIGN REQUIREMENT FOR LIQUID HYDROGEN

	W (Inducer Stage)	lb/sec	600
*	W (Transition & Main Stages)	lb/sec	640
	Discharge Pressure	psia	1800
	Speed	RPM	13,225
**	NPSP (Minimum)	psi	10
	Inlet Temperature (Min.)	°F	-423.5
	Inlet Temperature (Nom.)	°F	-421.0
	Inlet Temperature (Max.)	°F	-418.0
	OFF-DESIGN RANGE:		
	Flow Coefficient	%	± 13
	Speed	%	± 10

---

* Includes Balance Piston and Bearing Recirculating Flow

** Final Flight Design

Type of Pump	Change in Engine Specific Impulse (Sec)	Change in Escape Vehicle Payload (%)	Turbopump Weight (lb)
Two-Stage, Centrifugal	Not Calculated	Not Calculated	5350
Single-Stage, Centrifugal	Reference	Reference	3350
Multi-Stage, Axial (2 sec start transient)	+ 0.4	+ .30 to + .32	2850
Multi-Stage, Axial (5 sec start transient)	+ 0.4	+ .09 to .19	2850

The figures for the axial pump specific impulse and payload are differentials between the single-stage centrifugal pump figures (used as a datum) and the axial pump figures. The two-stage centrifugal pump was eliminated because of excessive weight and no comparative vehicle performance figures were obtained. A start duration of two seconds was used in initial computations; however, the effect of a longer start transient (five seconds) was also considered for the axial pump. It was believed that a longer transient would be required to prevent axial pump stall. The variation in the payload figures for a given case reflects the estimated possible variation in engine performance and weight.

The variations in vehicle performance between the single-stage centrifugal and multi-stage axial pumps were small; however, the requirement for growth to a 1,800,000 lb thrust engine by increasing engine pressures imposed a severe structural requirement upon the single-stage, aluminum centrifugal pump impeller. Analyses indicated that available aluminum alloys would have marginal structural capability at the higher tip speeds required to generate the larger discharge pressures (1900 psia to 2000 psia). Titanium alloys offered some promise for upgrading pump discharge pressure; however, the development of such alloys and fabrication techniques for those alloys was judged to be inadequate to permit the fuel pump design to be connected to a centrifugal concept. Consequently, the multi-stage axial concept was selected.

It should be emphasized that the philosophy in selecting the axial flow pump was to incorporate a pump design concept which could be utilized for larger thrust level engines without any change in concept (i.e., from centrifugal to axial flow pumps) when engine thrust is upgraded by increasing engine pressures. However, the specific design presented in this report was not required to meet specifications for the 1,800,000 lb thrust level, either hydraulically or mechanically.

Figure No. 8 is a comparison between the M-1 engine hydrogen pump estimated performance with those for three other current liquid rocket engine hydrogen pumps. The NERVA nuclear rocket pump is a single-stage centrifugal pump, the RL-10 is a

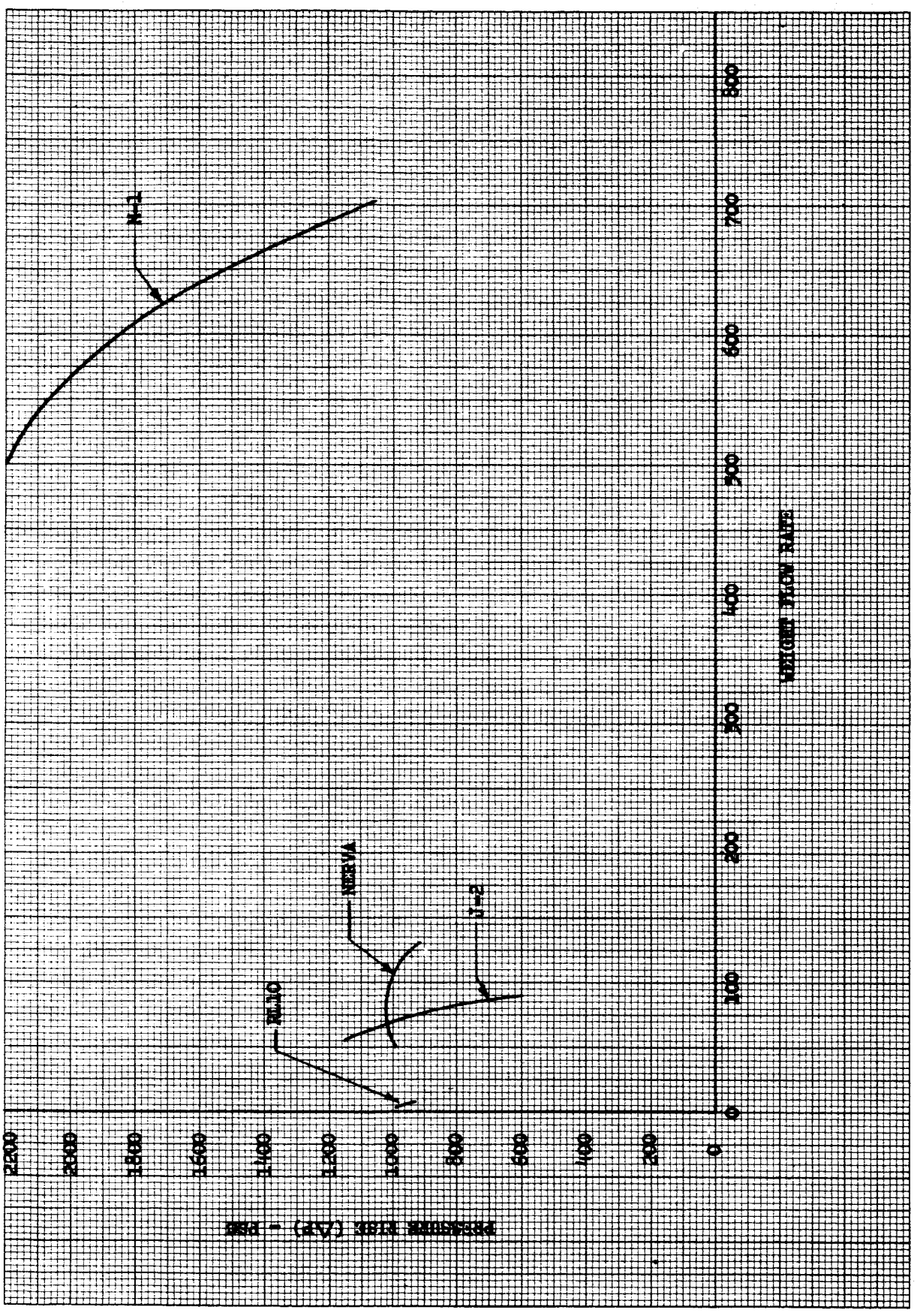

Figure 8

Comparison of Pumps (M-1, J-2, RL-10, NERVA);
Pump Pressure Rise vs. Pump Weight Flow Rate

two-stage centrifugal pump, and the J-2 is a multiple-stage axial flow pump. It can be noted from Figure No. 8 that the M-1 pump flow rate is an order of magnitude larger than any other existing rocket engine hydrogen pump.

III. HYDRAULIC DESIGN

The selected pump design point specifications are shown on Table II. With the exception of the pump pressure or head rise, the specifications are identical to those for the design requirement shown in Table I. The pump was designed for more pressure rise than the requirement to provide contingency for achieving design objectives. The design suction specific speed was 43,000 which includes an allowance for a recirculation flow caused by tip clearance leakage in the inducer. Five percent of the total pump flow rate was assumed to recirculate. The pump transition stage and main stages were designed to accept engine inlet flow plus 40 lb/sec of additional flow. This additional flow includes bearing coolant flow, internal leakage, and leakage around the thrust balance piston as shown by Figures No. 9 and No. 10.

The operating speed of the turbopump was determined by pump cavitation performance limitations. A suction specific speed of 43,000 was estimated to be an approximate maximum for reliable pump operation based upon the demonstrated capabilities of inducers. No allowance was made for thermodynamic effects in hydrogen which permit considerably higher suction specific speeds. Although reliable hydraulic performance of a 43,000 suction specific speed inducer was judged feasible, a survey of possible inducer designs, materials, methods of fabrication, and stress analysis techniques indicated that there were uncertainties regarding the structural integrity of a 43,000 suction specific speed design. A more lightly-stressed 20,000 suction specific speed design was incorporated for initial testing. This design is referred to as an "interim" design in this report because it would be replaced by a high performance design during the final phases of engine development.

The pump speed and suction eye diameter were based upon the design suction specific of 43,000; however, the design presented in this report is for the interim inducer designed for a maximum suction specific speed of 20,000. The basic differences between the two designs are inlet blade angle and blade hub thickness. The interim design was intended for use in turbopump and engine static tests during the early phases of the engine development program where operation at low suction pressures would not be required.

The hydraulic design of the pump and much of the mechanical design of the entire turbopump was largely dependent upon the number of main stages selected as well as the diameter and hub/tip diameter ratio of these stages. A parametric study of these variables was conducted using the following criteria:

The design point rotor tip diffusion factor would be 0.4.
The stator tip diffusion factor should not exceed 0.6.
At the minimum flow coefficient (87% of the design flow coefficient), the rotor tip and hub diffusion factors should not exceed values of 0.44 and 0.47, respectively.

TABLE II

M-1 FUEL PUMP DESIGN POINT

	Propellant	---	LH_2
	Propellant Inlet Temperature	°F	-421
	Propellant Inlet Density	lb/ft^3	4.33
	Shaft Speed	RPM	13,225
	Total Discharge Pressure (Cavitating)	psia	1920
	Total Suction Pressure	psia	30.6
	Total Pressure Rise (Cavitating)	psi	1890
	Total Head Rise (Cavitating)	ft	59,500
	Weight Flow Rate	lb/sec	600
	Capacity	GPM	62,300
	Efficiency	%	79
	Fluid Horsepower (Cavitating)	HP	65,000
	Shaft Horsepower (Cavitating)	SHP	82,000
*	Net Positive Suction Head	ft	333
*	Suction Specific Speed	$\frac{RPM \times GPM^{1/2}}{FT^{3/4}}$	43,000

---

* Final Flight Design

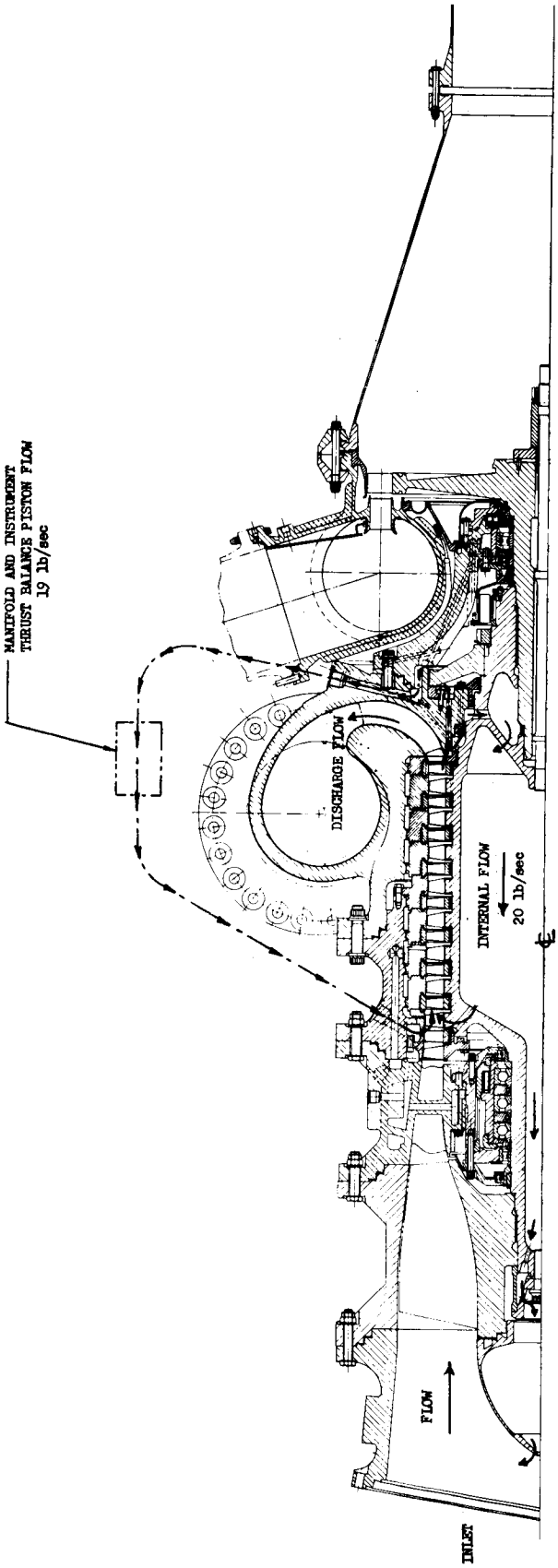

Figure 9

Pump Rotor Internal Flow and Thrust Balance System Flow

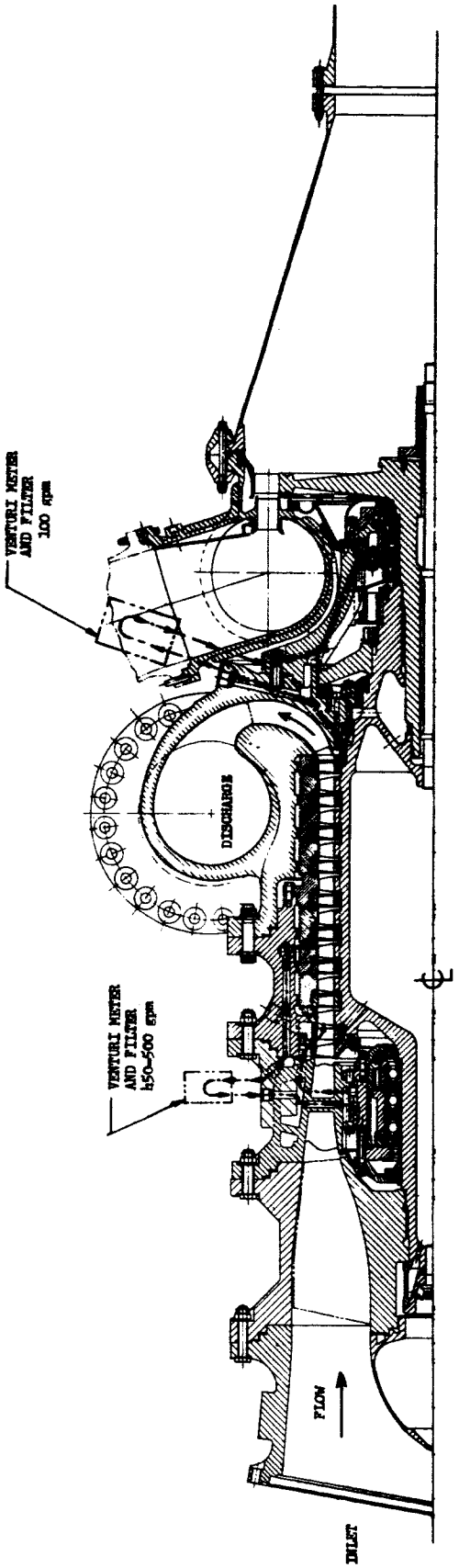

Figure 10

Bearing Coolant Flow Systems

The design point head operation should be essentially of a free vortex type (uniform radial distribution of theoretical head).

Using the above criteria, to achieve maximum head rise per stage, with high efficiency, it was necessary to have approximately 50% reaction at the blade root.

Axial stages with tip diameters varying from 14-in. to 18-in. were considered. The factors influencing the selection of the final configuration were: turbopump weight; turbopump critical speed margin; pump efficiency; and depth of the stall point head discontinuity.

The 14-in. diameter rotor required an excessive number of stages to generate the required pressure, based upon the prescribed blade diffusion factor limits. The large number of stages resulted in critical speeds that were too low and close to the selected operating speed. The 18-in. diameter rotor resulted in a heavier turbopump, the savings in the number of stages did not compensate for the weight increase resulting from the greater diameter.

In addition, the large hub-to-tip diameter ratio required to stay within the blade loading limits resulted in lower blade aspect ratios and reduced efficiency for the 18-in. diameter rotor. The relatively short blading would also result in a steep stall point discontinuity because of the tendency for the entire blade to stall within a relatively narrow range of flow coefficient. The 16-in. diameter machine was selected as optimum based upon weight, stall margin, and critical speed considerations.

Preliminary analyses indicated that an inducer stage could supply 10% to 15% of the total pump head rise; however, such a stage would not supply uniform head and axial velocities for the main stages. A lightly-loaded "transition" stage was designed to supply approximately five percent of the total pump head rise. The primary purpose of this stage was to convert the non-uniform head discharging from the inducer stage into a uniform head distribution for the first main stage. To satisfy the blade loading requirements, eight main stages were required for the 16-in. diameter configuration in addition to the inducer and transition stages. Figure No. 11 shows the resulting pump flow path. The following sections describe the design of the various stages and discharge housing as well as the off-design analysis. The hydraulic characteristics of all stages at the design condition are summarized in Appendix A.

A. INDUCER STAGE

The geometry of the inducer design is shown in Figures No. 12, No. 13, and No. 14. The speed and tip diameter of the inducer are based upon a suction specific speed of 40,000 (neglecting recirculating flows), a net positive suction pressure of 10 psi and a hub/tip diameter ratio of 0.4. The blading shown in the figures is for the interim inducer design with a hub/tip ratio of 0.45 and thick blades.

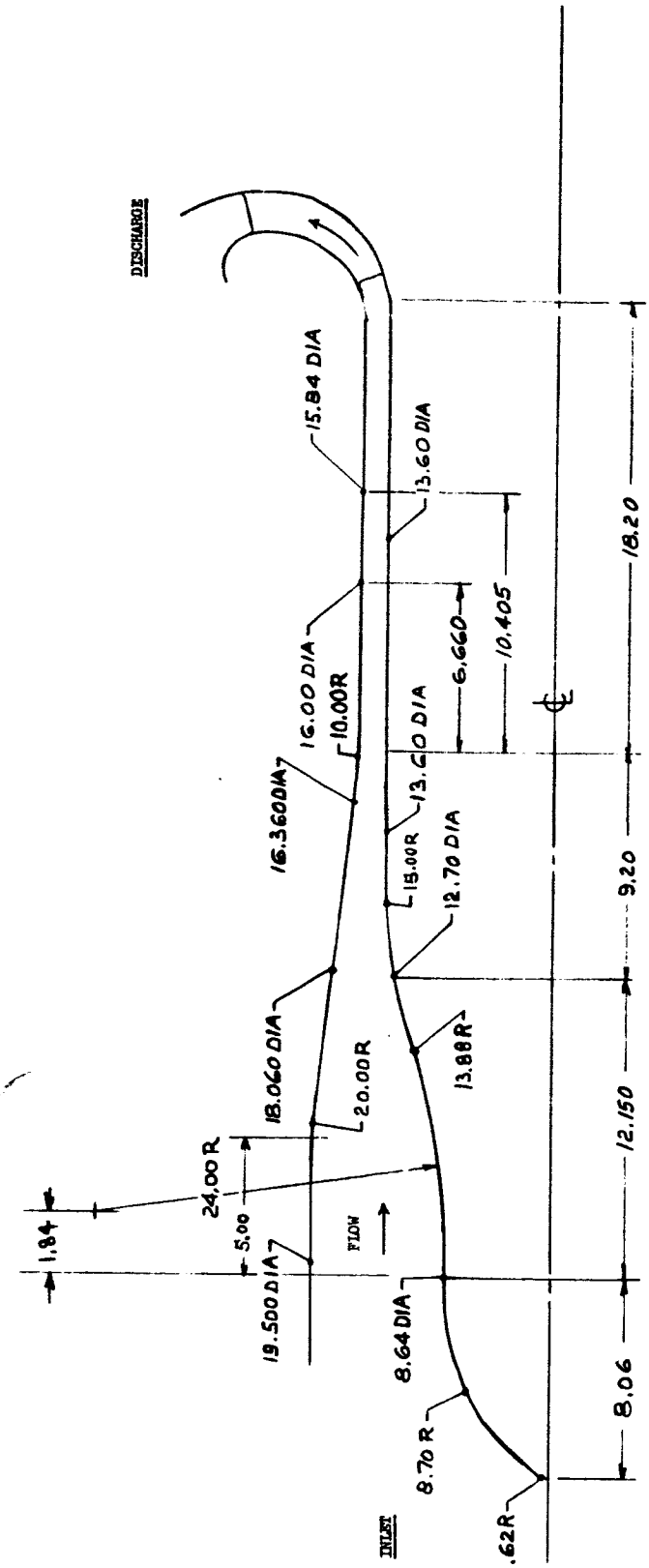

Figure 11

Hydraulic Passage Contour

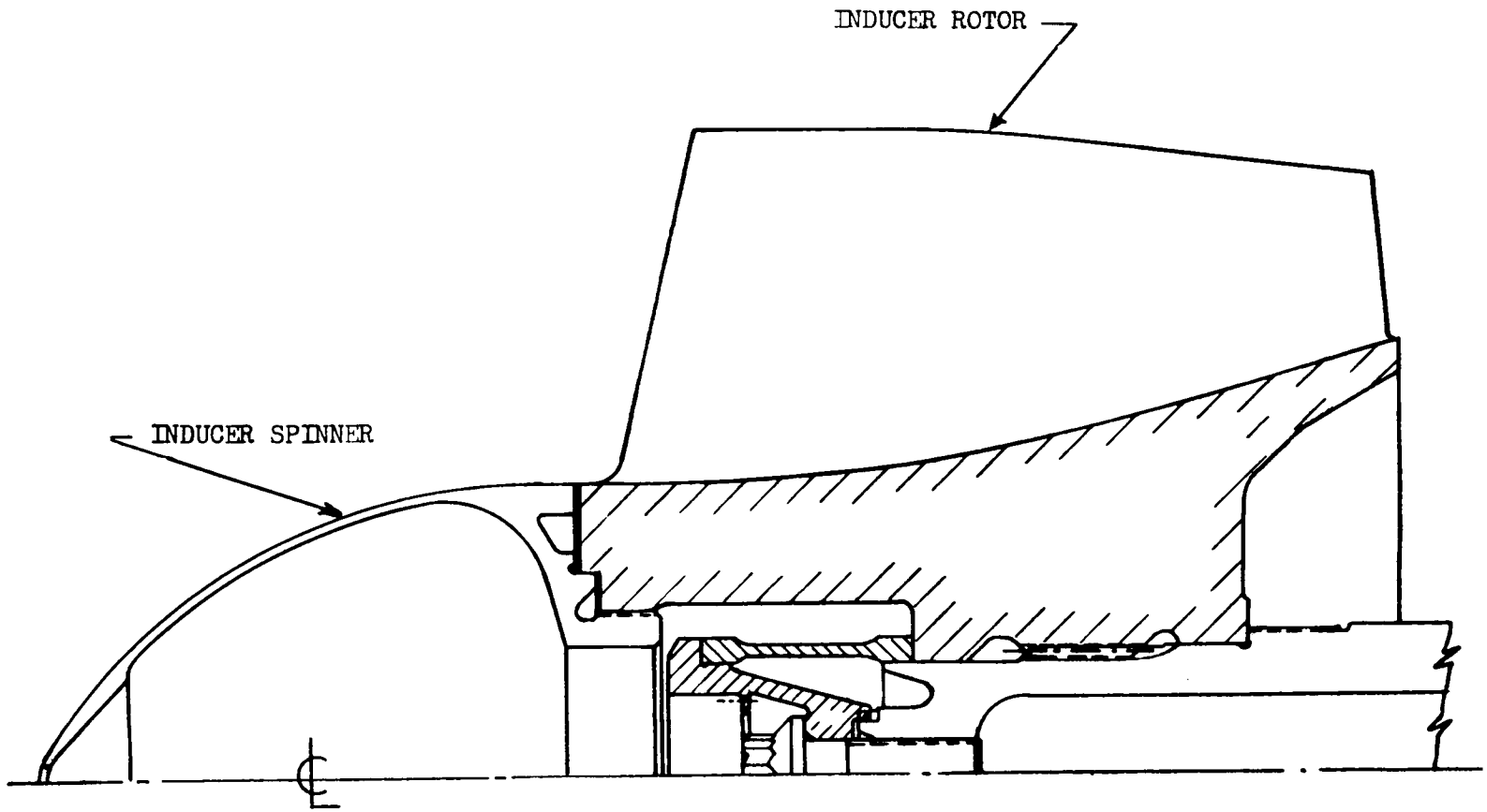

Figure 12

Inducer Rotor Profile

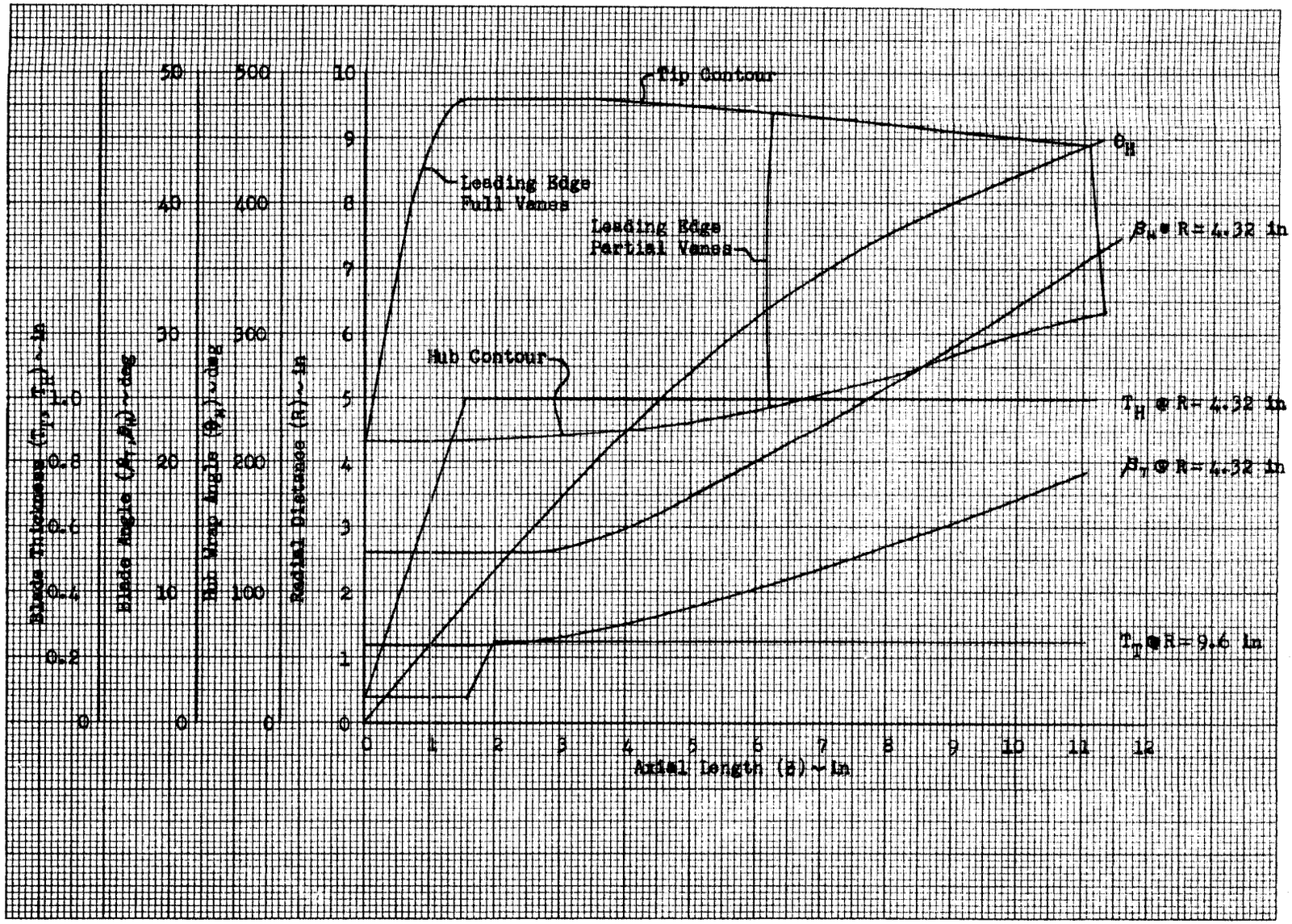

Figure 13

Inducer Rotor Blade Angle, Thickness, and Wrap Angle vs. Axial Length

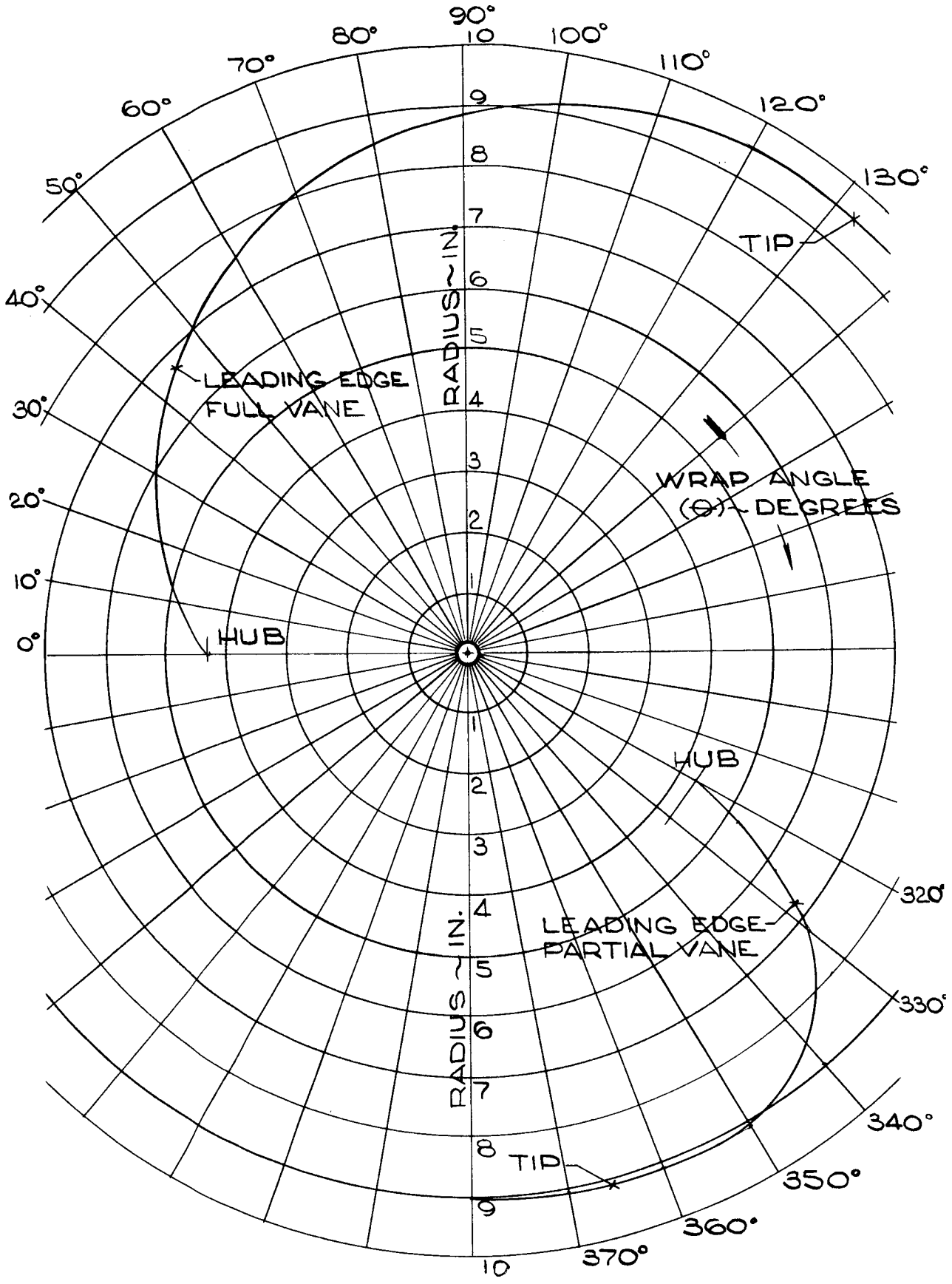

Figure 14

Inducer Rotor Leading Edge Trim, Full and Partial Blades; Radius vs. Wrap Angle

Because some of the bearing coolant flows and leakage flows were to enter the pump passages at the transition stage, the inducer discharge static pressure was designed to be in excess of the fluid critical pressure (187.6 psia) to prevent choking in the return flow passages. A total head rise through the inducer stage of 9500 ft was used as a design point to allow for some off-design capability as well as the uncertainty of the losses in the unconventional inducer stator.

1. Inlet Eye Diameter

The inlet eye diameter was determined by a method[1] where the optimum value results when the inlet velocity head of the fluid is approximately one-third of the net positive suction head. No allowances were made for the thermodynamic effects of liquid hydrogen. The estimated 75 ft to 100 ft of thermodynamic head obtainable was left as a margin to allow for dimensional variations and upgrading potential; therefore, excluding thermodynamic effects.

V_Z^2 Inlet 2/g = 1/3 NPSH (V_Z = axial velocity)

NPSH = 333 ft (design requirement)

V_Z Inlet = 84.0 ft/sec

g = 32.2 ft/sec^2 (acceleration due to gravity)

Q = 62,300 + 5% for tip leakage through clearances
= 65,500 gpm

D_H/D_T = .4 = hub to tip diameter ratio

D_T = 19.5 in. = tip shroud diameter

2. Blade Inlet Geometry

The blade inlet tip angle was determined from a study of the cavitation performance of existing Aerojet-General pumps at various fluid-to-blade incidence angles. Test data from the NERVA, MARK III, Mod 3 nuclear rocket pump (Contract SNP-1) and the Integrated Components Program fuel and oxidizer chemical rocket pumps (Contract AF04(647)-548 were examined. The test data for these pumps, which have slightly cambered inducer blades, indicated that adequate performance to achieve 20,000 suction specific speed (interim inducer design) could be obtained down to incidence-to-vane angle ratios of 0.15. Fairly severe deterioration of

(1) Ross, C. C. and Banerian, G., Some Aspects of High Suction Specific Speed Pump Inducers, Trans, AGME, Vol. 78, No. 8, November 1956, pp 1715-1721

performance occurs at values lower than 0.15. The fluid incidence is defined as the difference between the fluid relative flow angle and the blade angle, assuming uniform axial velocity and no tangential velocity in the suction eye; the blade angle and fluid angles measured from the plane perpendicular to the axis of rotation.

Because the pump was required to operate at 113% of the nominal flow coefficient, the blade tip angle was set so that the .15 incidence-to-vane angle ratio would occur at this higher flow condition. This resulted in a ratio of approximately 0.25 at the design point.

Because of the high tip speeds of the inducer (1100 ft/sec at the design speed) stress considerations determined the vane cant and taper requirement. The vanes are canted forward three degrees on the blade centerline at the leading edge to offset fluid bending loads with centrifugal bending loads. A maximum blade thickness at the tip of 0.250-in. was used to facilitate fabrication while providing a reasonably thin section for good suction performance. Stress calculations dictated a requirement for a blade maximum root thickness of 1.0-in. The blade tip was swept back 120 degrees from the hub in the radial plane view to reduce stresses resulting from blade overhang as shown in Figure No. 14.

3. Head Rise and Hub Shape

The inducer must provide a transition from the low flow coefficient at the inlet to the higher flow coefficients of the transition and main stages while supplying the necessary head rise. These two requirements were considered in establishing the inducer blade angle distribution, partial vane location, and hub contour shape. The design head rise results in an inducer specific speed of 3400 $\frac{\text{rpm gpm}^{1/2}}{\text{ft}^{3/4}}$. The one dimensional flow area and Euler's head rise at tip, mean, and hub are given in Figures No. 15 and No. 16.

4. Suction Performance

The design of the suction and of the M-1 interim inducer rotor was very similar to the Integrated Components pumps; therefore, the predicted suction performance was based upon data from these pumps. The total pump head loss and pump torque loss at three flow coefficients (design, 87% design, and 113% design) are shown as a function of suction specific speed in Figures No. 17 and No. 18.

5. Type of Analysis

The inducer non-cavitating performance, head rise, and discharge velocity distribution was determined by a two dimensional axi-symmetric solution where simple radial equilibrium is assumed to exist (see Appendix B). This assumption appears to be justified in this design because the streamline curvature is small near the discharge (Figure No. 13). The solution of the radial equilibrium equation was performed inside the blade where the fluid angle is assumed to be

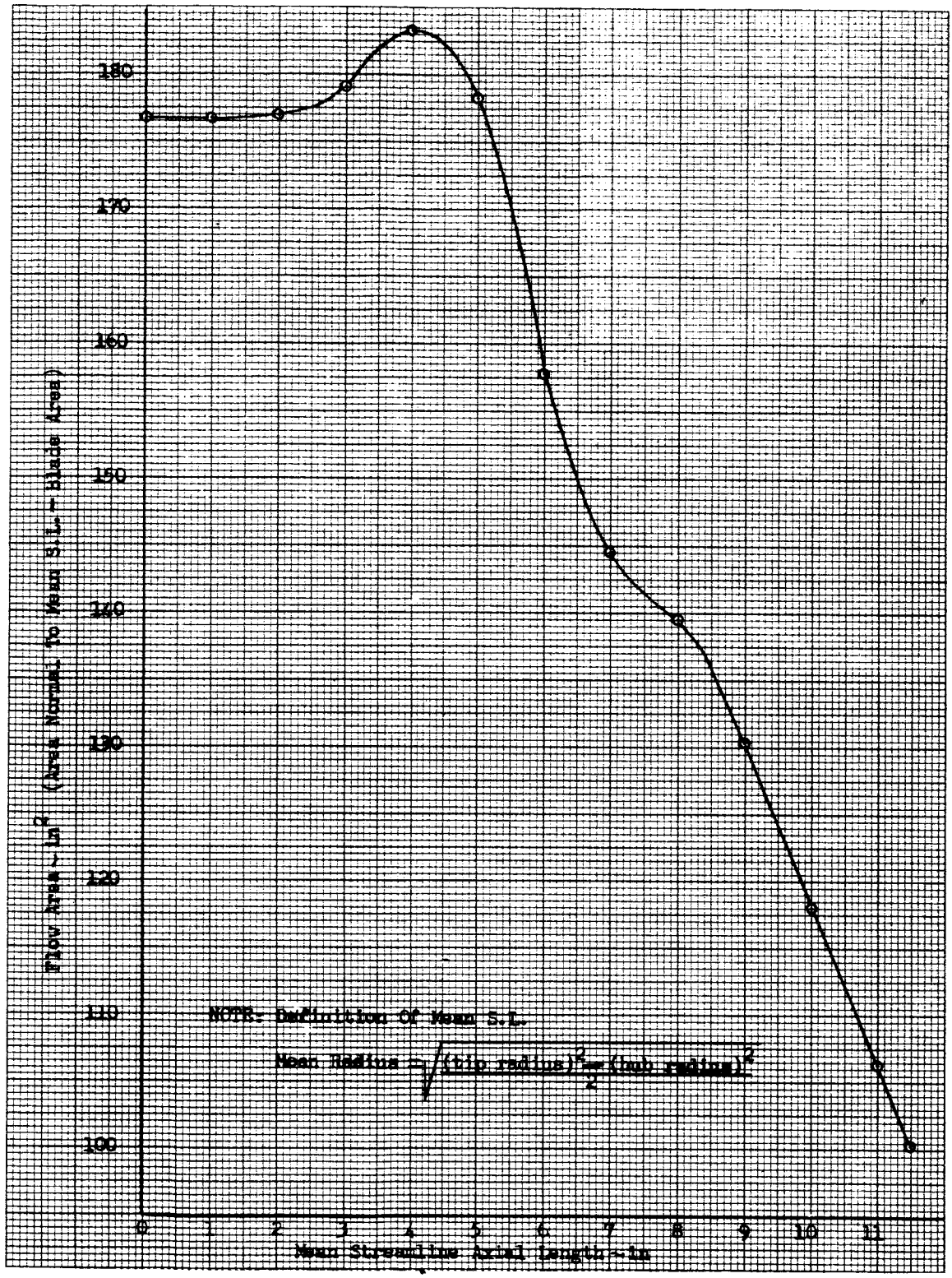

Figure 15

Inducer Rotor Through Flow Area

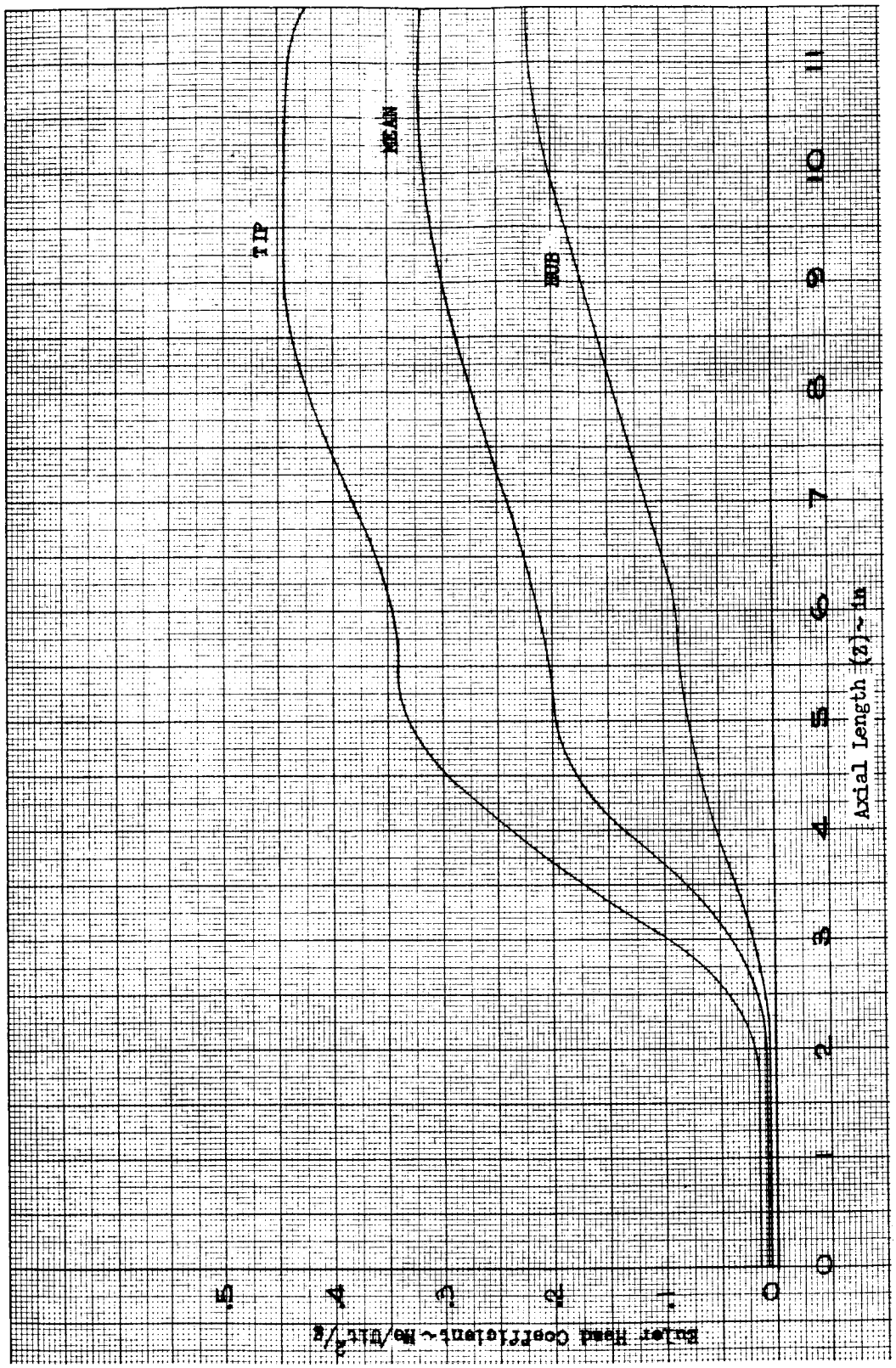

Figure 16

Inducer Rotor One-Dimensional Head Rise; Tip, Mean, Hub

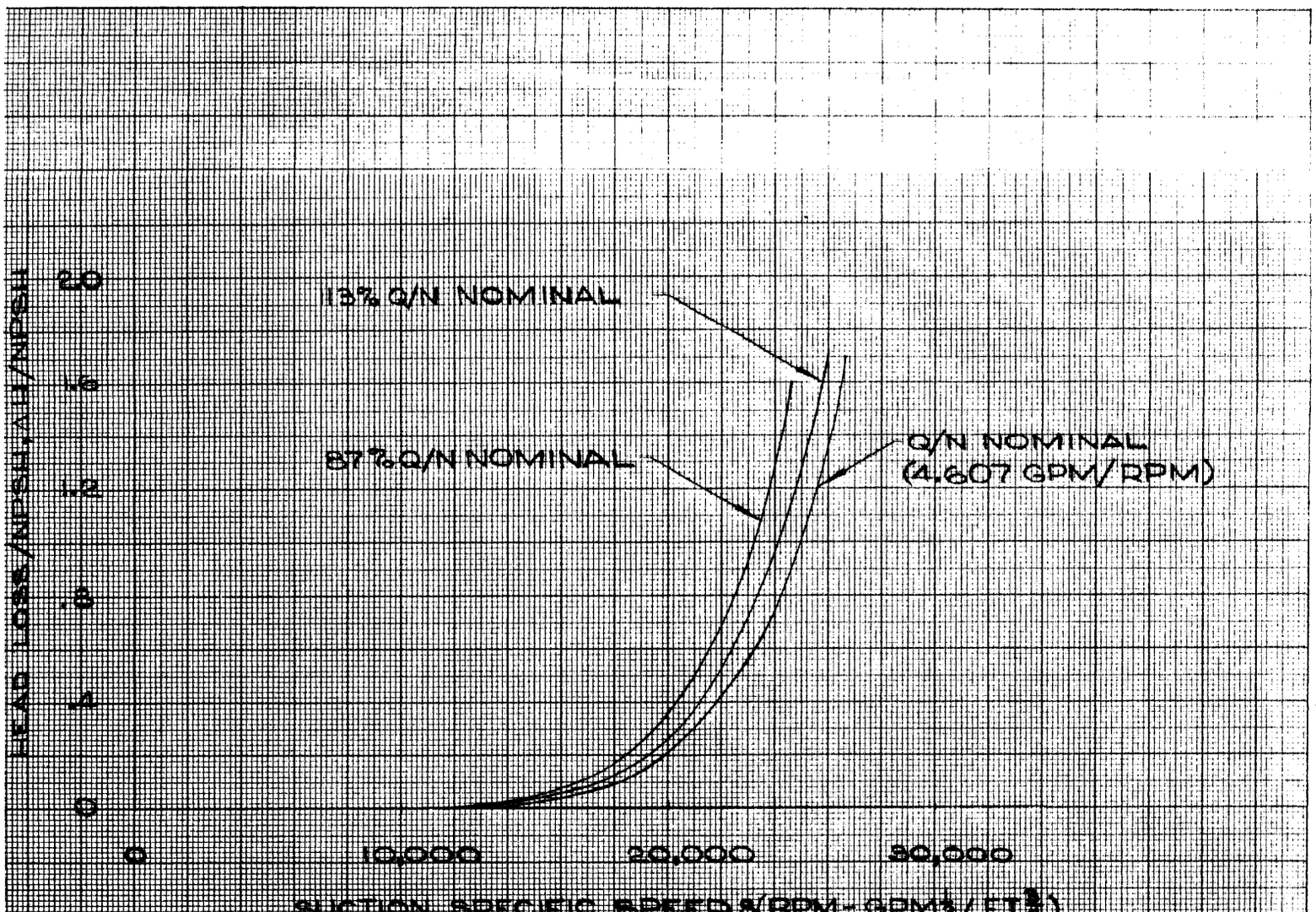

Figure 17

Pump Suction Performance; Head Loss vs. Suction Specific Speed

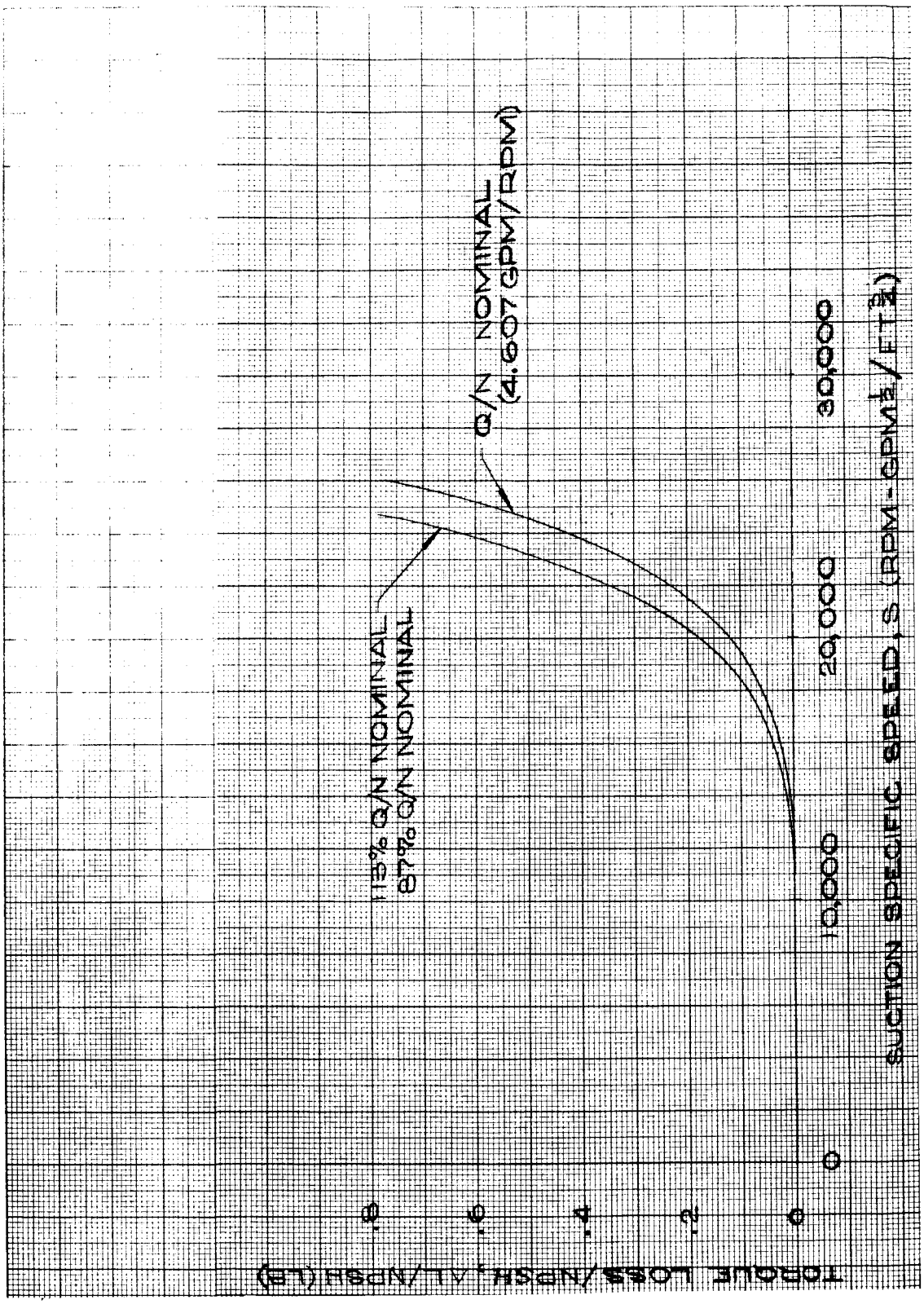

Figure 18

Pump Suction Performance; Torque Loss vs. Suction Specific Speed

equal to the blade angle. Outside of the blade, it is assumed that the angular momentum remains constant as the fluid leaves the blade. Another study[2] has shown that deviating from a radial blade element design to one where the blade is generated by a straight cutter, but not otherwise restricted, does not result in significant improvement in discharge head distribution if uniform axial velocities are maintained. Consequently, the inducer stator was required to accept a non-uniform radial head distribution.

6. Losses and Deviation Angles

A survey of flat plate inducer traverse data was made[3][4][5] to establish the inducer losses and deviation angles versus discharge radius. These data indicate that, independent of blade lead angle, the deviation angle varies almost linearly from the tip to the hub, while the loss coefficient was approximately .22 at the hub, .12 near the mid streamlines, and .46 at the tip. These are the values assumed for this design (Figure No. 19).

7. Stator

The inducer stator design serves three functions, as hydraulic guide vanes, as structural support members for the pump bearings, and as a passage through the vanes for bearing coolant flow. The stator casting and blade shapes are shown in Figures No. 20 and No. 21.

It was observed during the stator design that because of the high heads generated at the inducer tip, high decelerations of the tip axial velocity would result as the rate of fluid turning in the stator was increased. Therefore, to minimize this adverse effect, the turning was kept at a minimum which resulted in low blade loading. As a result of the extremely long blade cords, which are caused by the structural requirement, a velocity distribution analysis was performed to determine if critical areas exist where boundary layer separation could occur. The analysis indicated that this was not the case and the static pressure

(2) Knuth, W., M-1 Fuel Pump Tandem Inducer Design Investigation, Aerojet-General Report No. 0153 (Rotating Machinery Department, LRO), 16 December 1963

(3) Mullen, P. J., An Investigation of Cavitating Inducers for Turbopumps, MIT Gas Turbine Laboratory Report No. 53, May 1959

(4) Montgomery, J. C., Analytical Performance Characteristics and Outlet Flow Conditions of Constant and Variable Lead Helical Inducers for Cryogenic Pumps, NASA TN D-583, 1961

(5) Sandercock, D. M. and Crouse, J. E., Design and Over-All Performance of a Two-Staged Axial-Flow Pump with Tandem Row Inlet Stage, NASA TN D-2879

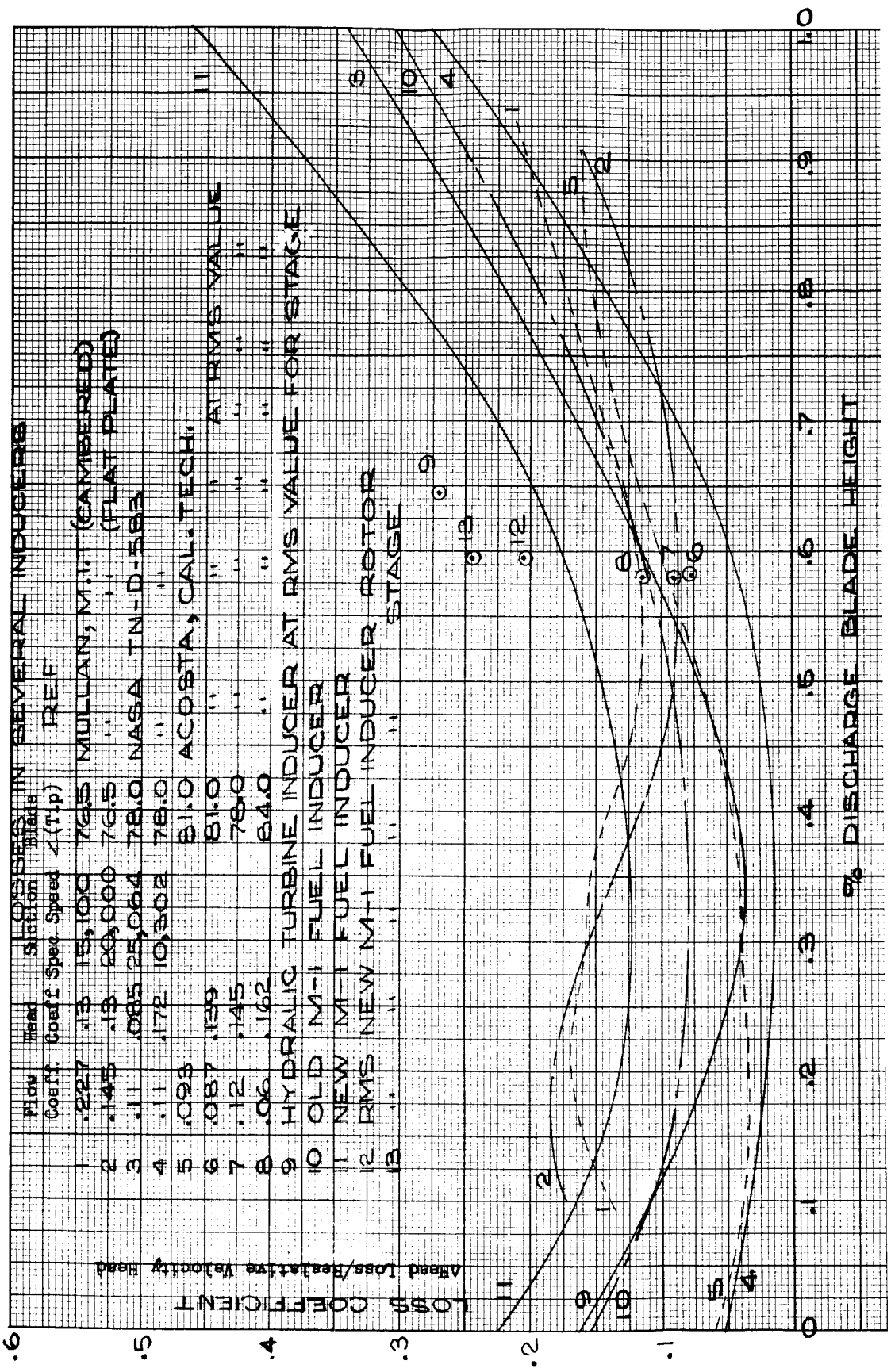

Figure 19

Losses in Several Inducers

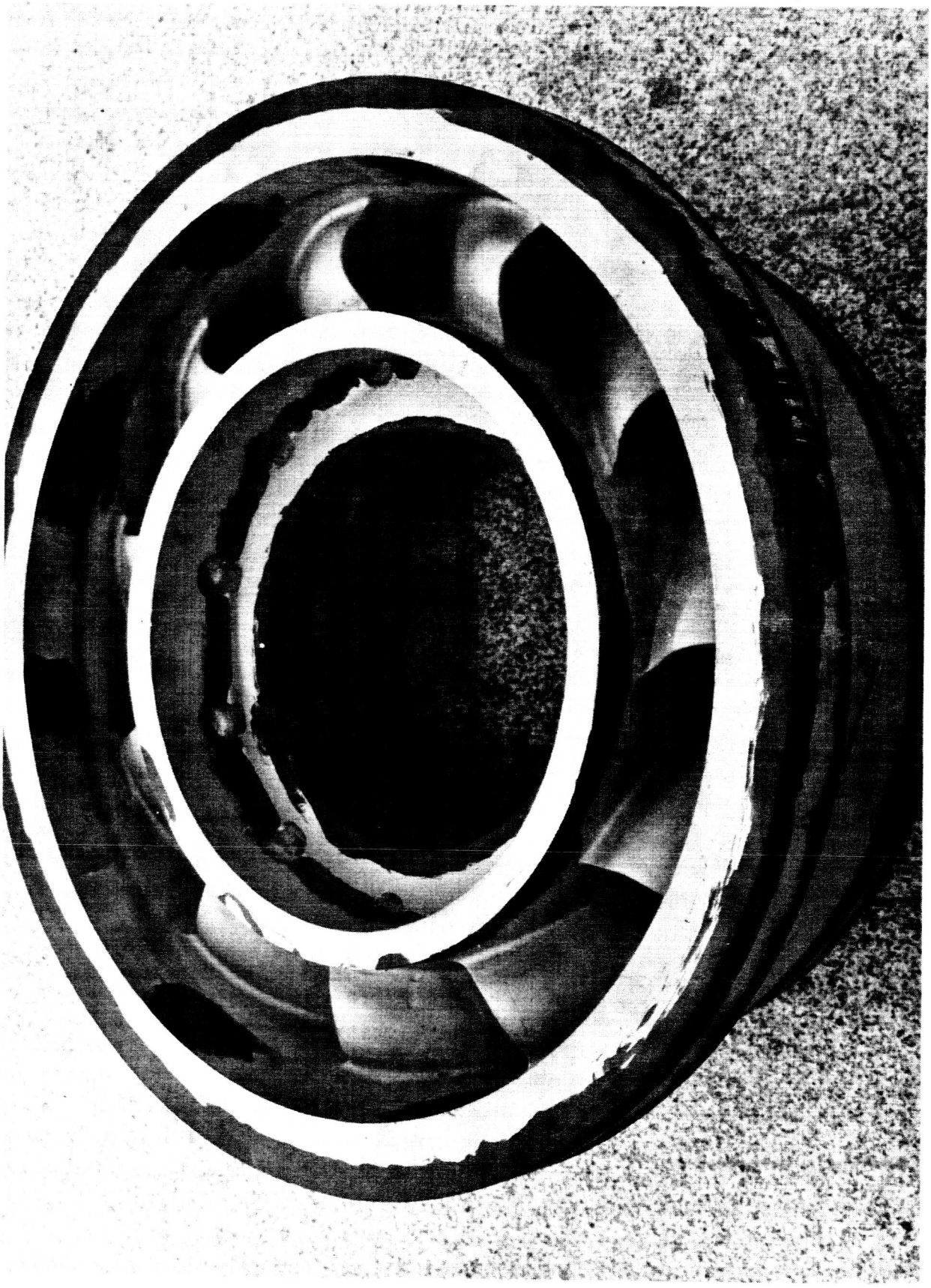

Figure 20

Inducer Stator Casting

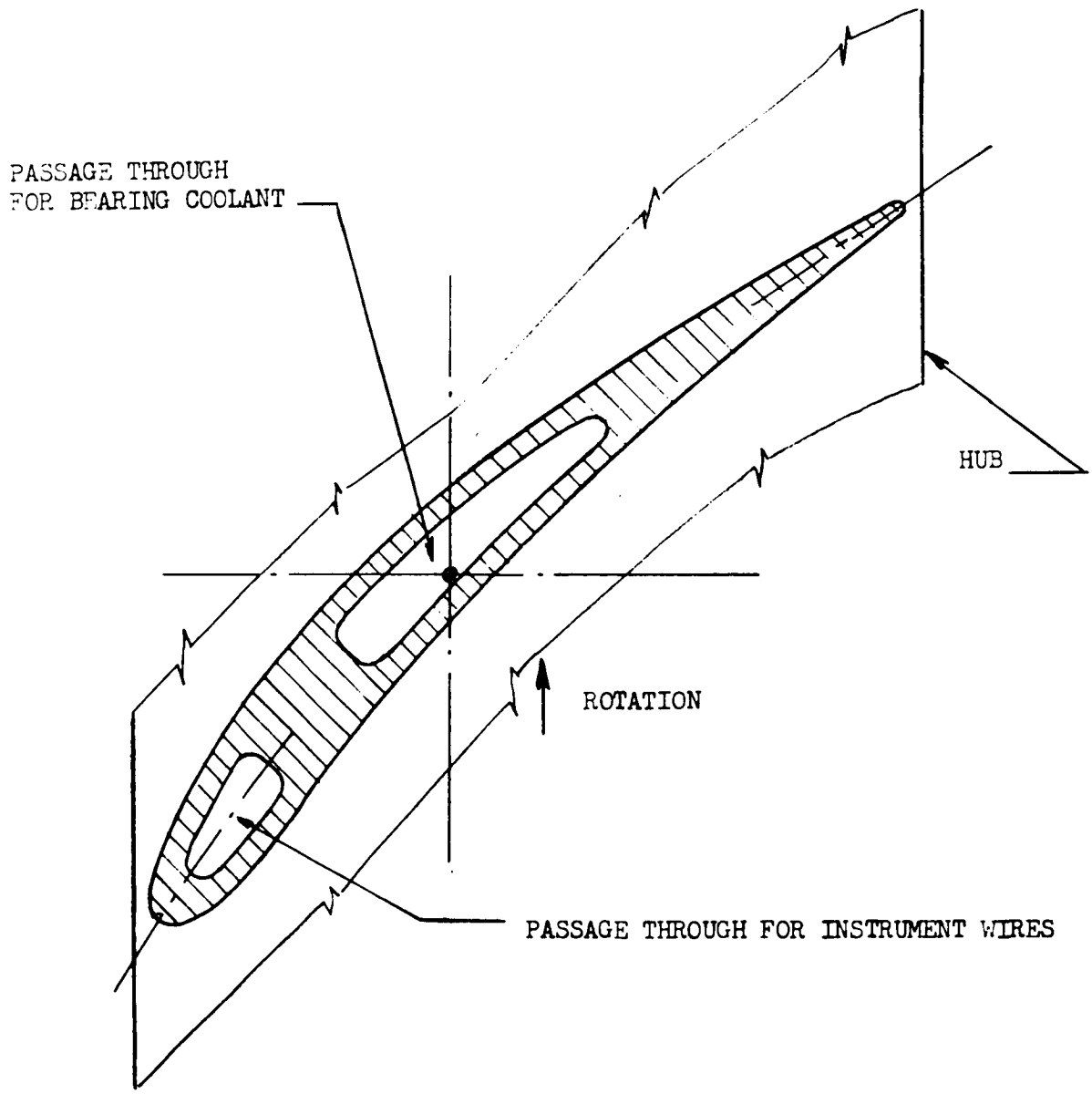

Figure 21

Inducer Stator Blade Shape

gradients on the suction surface were far below critical separation values (Figures No. 22 and 23). The less-than-optimum loading of the vane results in excessive losses; however, they had to be accepted to provide the necessary vane cross-sections for internal flow paths.

The British C-4 airfoil was selected for the inducer stator and the succeeding stages of the fuel pump design for two basic reasons: (1) it has characteristics similar to the successful NACA 65 (A_{10}) series and double circular arc blades at low Mach No. and (2) the larger area of the C-4 blade vs NACA 65 (A_{10}) and double circular arc reduces the stresses by approximately 20%. The blade bending stress is approximately 80% of the total static stress in the mainstage rotors. The blade section properties are given in Figure No. 24.

The incidence and deviation angles were determined using previously developed methods[6] although the losses were adjusted to higher values than would result from using these methods. This was done because of the low aspect ratio design, which results when hub and shroud losses become the larger percentage of the over-all blade losses.

B. TRANSITION STAGE

The transition stage compensates for the non-uniform head generated by the inducer stage. To achieve this, the transition rotor adds sufficient energy to each streamline to produce a relatively constant inlet head to the first main stage rotor. In addition, the design is lightly-loaded to assure a broad operating range which minimizes the effects of any mismatch occurring under inducer stage outlet conditions.

The design criteria for establishing incidence angles, deviation angles, and loss coefficients is identical to that discussed in the following section, which discusses the main stages.

C. MAIN STAGES

The main stages of the fuel pump consist of eight identical high pressure stages, except for the blade heights which were reduced by decreasing the outside diameter to compensate for a 6.5% increase in fluid density. The reduction which corresponds to a 16.00-in. to 15.84-in. diameter decrease occurs linearly between the third main stage stator discharge and the fifth main stage rotor discharge. This results in a reasonably constant design flow coefficient for all main stages.

The design is essentially free vortex, with a constant net energy

(6) Aerodynamic Design of Axial Flow Compressors, Vol. II, NACA RM-E56B03a, 1 August 1956

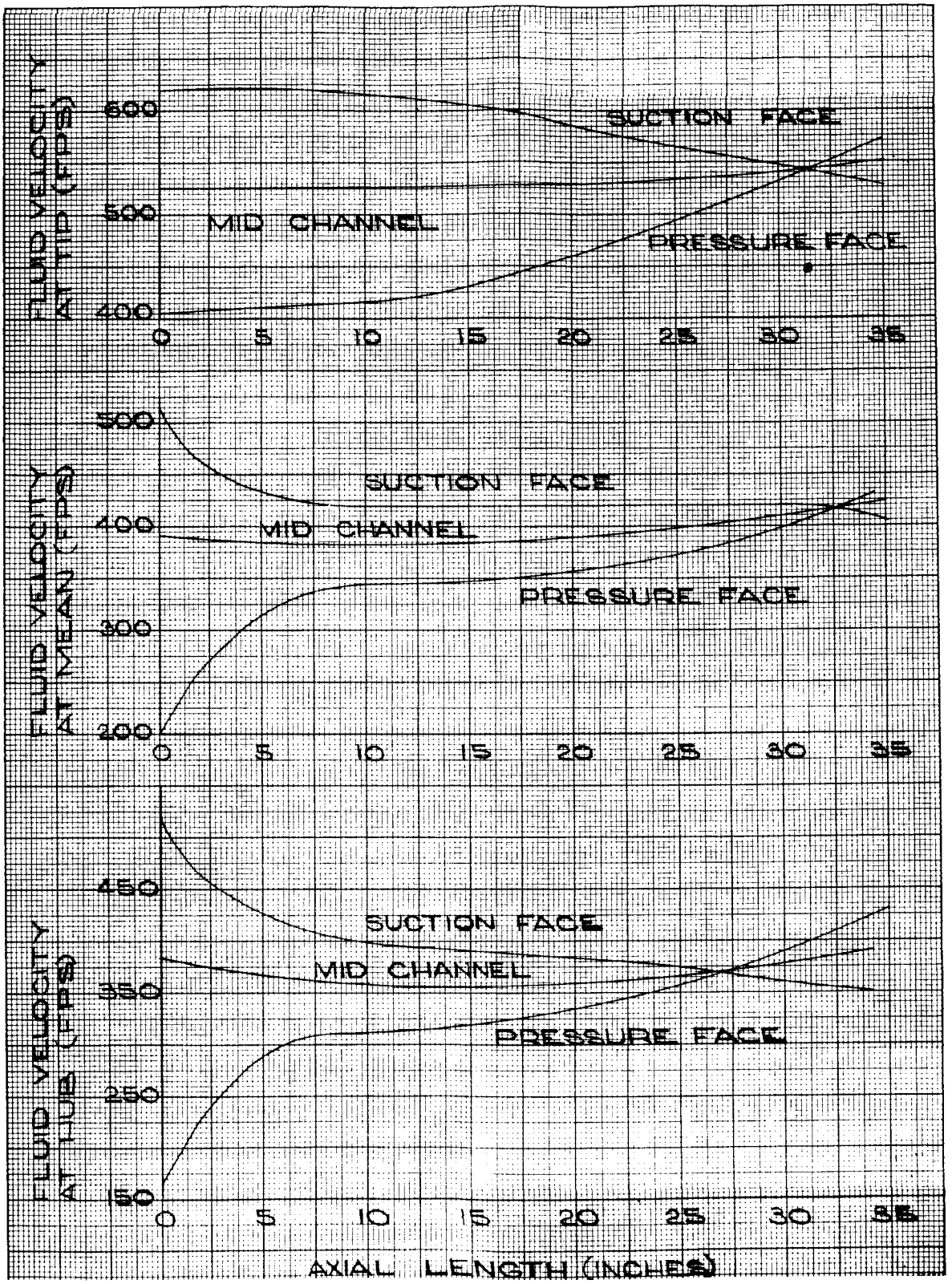

Figure 22

Inducer Stator Fluid Velocity vs. Axial Length; Tip, Mean, Hub

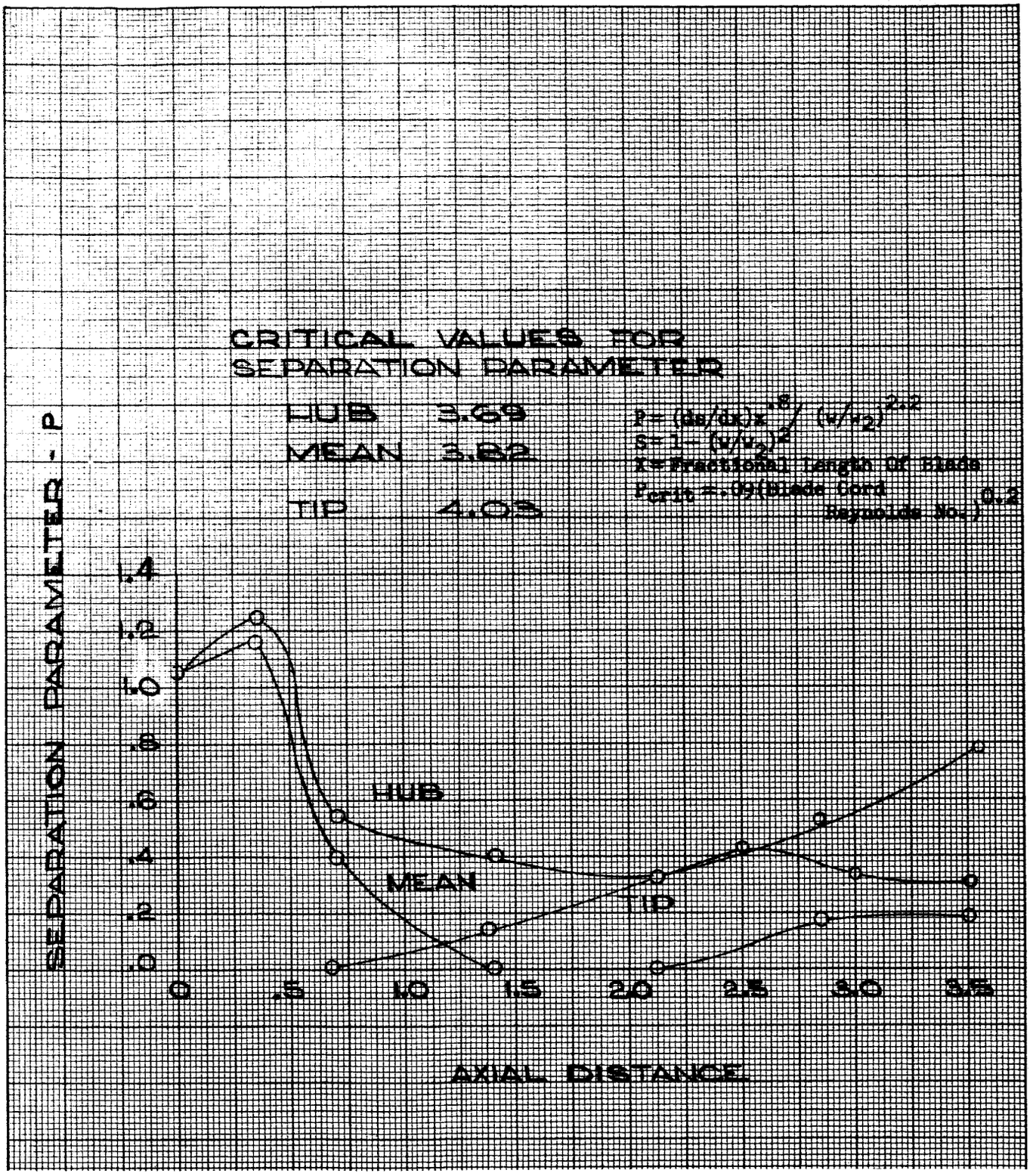

Figure 23

Inducer Stator Separation Parameter vs. Axial Length; Tip, Mean, Hub

BLADE SECTION PROPERTIES - C-4 TYPE

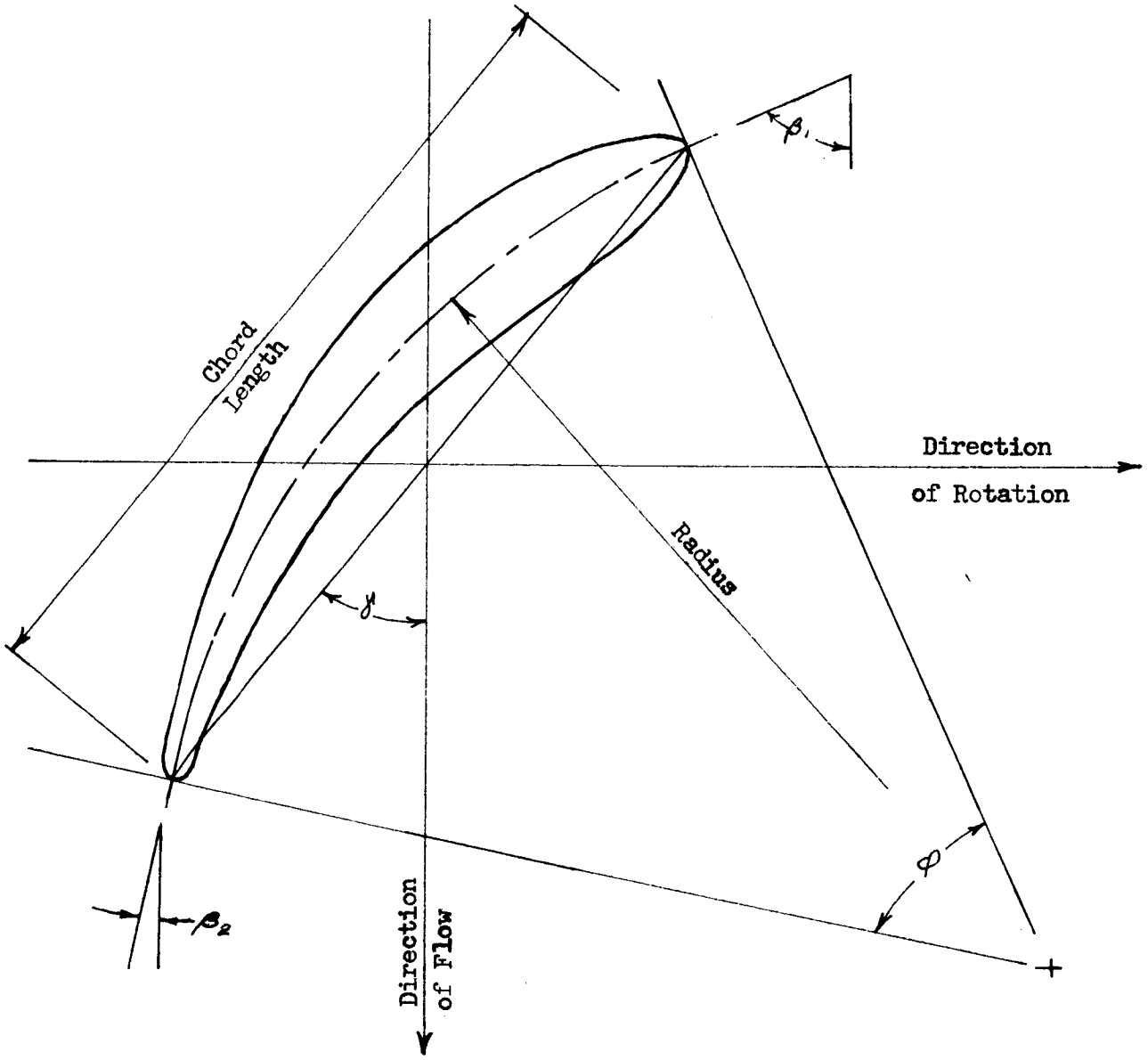

γ – Stagger Angle

φ – Camber Angle

β_1 – Blade Inlet Angle $= \gamma + \frac{\varphi}{2}$

β_2 – Blade Outlet Angle $= \gamma - \frac{\varphi}{2}$

Figure 24 (Page 1 of 3)

C-4 Blade Properties for Inducer Stator, Transition Stage, and Main Stages

BLADE SECTION PROPERTIES

BLADE	RADIAL STATION	CAMBER ANGLE	STAGGER ANGLE	CHORD LENGTH	RADIUS OF CURVATURE	THK_{MAX} CHORD
Main Stage Rotor	8.0	18.50	51.17	1.0695	3.327	.075
47 Blades	7.8	19.30	49.50	1.1015	3.286	.0824
Drawing #286325	7.6	20.42	47.45	1.1370	3.207	.090
	7.4	21.86	45.02	1.1755	3.100	.0974
	7.2	23.60	42.32	1.2155	2.972	.1050
	7.0	25.60	39.44	1.2575	2.838	.1125
	6.8	27.86	36.39	1.3020	2.704	.120
Main Stage Stator	8.0	37.56	34.12	.8818	1.3696	.10 *
57 Blades	7.8	33.84	34.45	.9097	1.563	.10 *
Drawing #710905	7.6	31.25	34.83	.9391	1.743	.10 *
	7.4	29.57	35.27	.9682	1.897	.10 *
	7.2	28.30	35.74	.9980	2.041	.10 *
	7.0	27.14	36.26	1.0275	2.190	.10 *
	6.8	26.04	36.83	1.0565	2.345	.10 *
Inducer Stage Stator	8.80	27.60	62.20	8.164	17.113	.10
11 Blades	8.55	27.05	56.20	8.164	17.454	.10
Drawing #286342	8.30	26.47	51.40	8.164	17.830	.10
	8.05	25.97	48.10	8.164	18.167	.10
	7.80	25.50	45.90	8.164	18.496	.10
	7.55	25.04	43.80	8.164	18.830	.10
	7.30	24.60	44.60	8.164	19.162	.10
	7.05	24.15	45.40	8.164	19.513	.10
	6.80	23.75	47.45	8.164	19.837	.10
	6.55	23.35	51.70	8.164	20.172	.10

* Blade surfaces were moved apart to give thickness 50% greater than shown

Figure 24 (Page 2 of 3)

C-4 Blade Properties for Inducer Stator, Transition Stage, and Main Stages

BLADE SECTION PROPERTIES

(cont'd)

BLADE	RADIAL STATION	CAMBER ANGLE	STAGGER ANGLE	CHORD LENGTH	RADIUS OF CURVATURE	$\frac{THK_{MAX}}{CHORD}$
Transition Stage Rotor	8.03	3.40	59.20	1.200	20.225	.070
31 Blades	7.91	6.70	58.00	1.223	10.465	.075
Drawing #289537	7.79	9.15	56.67	1.246	7.811	.080
	7.66	11.03	55.50	1.269	6.590	.085
	7.54	12.45	54.30	1.292	5.958	.090
	7.41	13.85	53.10	1.315	5.453	.095
	7.29	15.00	51.98	1.338	5.125	.100
	7.17	16.10	50.80	1.361	4.859	.105
	7.05	17.20	49.70	1.384	4.628	.110
	6.92	18.32	48.50	1.407	4.419	.115
	6.80	19.30	47.30	1.430	4.261	.120
Transition Stage Stator	8.00	43.60	39.90	.991	1.334	.08
51 Blades	7.88	33.90	36.30	.991	1.700	.08
Drawing #286551	7.76	27.70	34.50	.991	2.070	.08
	7.64	23.05	33.50	.991	2.480	.08
	7.52	19.95	32.98	.991	2.861	.08
	7.40	17.50	32.72	.991	3.257	.08
	7.28	15.70	32.60	.991	3.628	.08
	7.16	14.90	32.64	.991	3.822	.08
	7.04	14.60	32.80	.991	3.900	.08
	6.92	14.50	33.10	.991	3.926	.08
	6.80	14.60	33.50	.991	3.900	.08

Figure 24 (Page 3 of 3)

C-4 Blade Properties for Inducer Stator, Transition Stage, and Main Stages

addition to each streamline and has an approximately 50% reaction at the hub. Rotor and stator blade sketches are shown in Figures No. 25 and No. 26, respectively. The design objective was to limit the tip diffusion parameter "D" to .4 or less at the rotor tip which results in "D" values of approximately the same magnitude for the remainder of the blade. The diffusion limit for the stator was set at .6, or less; however, the rotor tip limit resulted in stator "D" values of less than .47. A flow coefficient of .431 was selected to supply the necessary head for the eight, 16-in. diameter stages while restricting the tip and root diffusion factors at the minimum (87%) flow coefficient to maximum values of 0.44 and 0.47, respectively. These values were selected as desirable limits based upon the correlations previously cited(7).

The main stages are designed to have axial clearance between blade rows (at the blade root) of .155-in. for the rotor trailing edge/stator leading edge clearance and .173-in. for the stator trailing edge/rotor leading edge clearance. These dimensions are somewhat larger than those used in compressor design practice but they are necessary because of turbopump mechanical design constraints. However, it is expected that this will have very little affect upon performance. The selected nominal operating clearances of .020-in. for the rotor tip and .049-in. between the stator inner platform and rotor drum are conventional and no attempt was made to evaluate the affect of these clearances upon pump performance.

1. Blade Design Parameters

The blade solidities and maximum chord-to-thickness ratios were established primarily by the maximum allowable stresses at the blade root; however, the blade solidity and chord-to-thickness ratio values are in the range of normal design practice.

The blade properties are shown on pages 2 and 3 of Figure No. 24. The rotor blade foils are C-4 type. The main stage stator blades were originally designed to be C-4 foils with a constant thickness-to-chord ratio of .10. The affect of pressure loading upon the blade inner platform was neglected in arriving at the 10% thickness value and resulted in an overstressed blade. This blade overstress was not discovered until the tooling for the 10% blade was fabricated. In the interests of both time and cost, thicker blades corresponding to a maximum thickness equal to 15% of the chord were fabricated by spreading the 10% thickness inside form and back form surfaces apart. This resulted in a blade with thicker sections than a 15% C-4 section in the leading and trailing edge regions. The performance predictions shown in this report are for the standard C-4 stator of 10% thickness. The blading modifications are estimated to result in a 2.2 point loss in pump efficiency at the design point together with a 3.2% reduction in pump head rise. The reduction in performance is primarily attributed to increased trailing edge thickness with the increase in maximum thickness having a secondary affect. It was assumed that the increase in leading edge thickness would have a negligible affect. It was planned to have standard C-4 thin trailing edge stator blades for the final pump design.

(7) ibid.

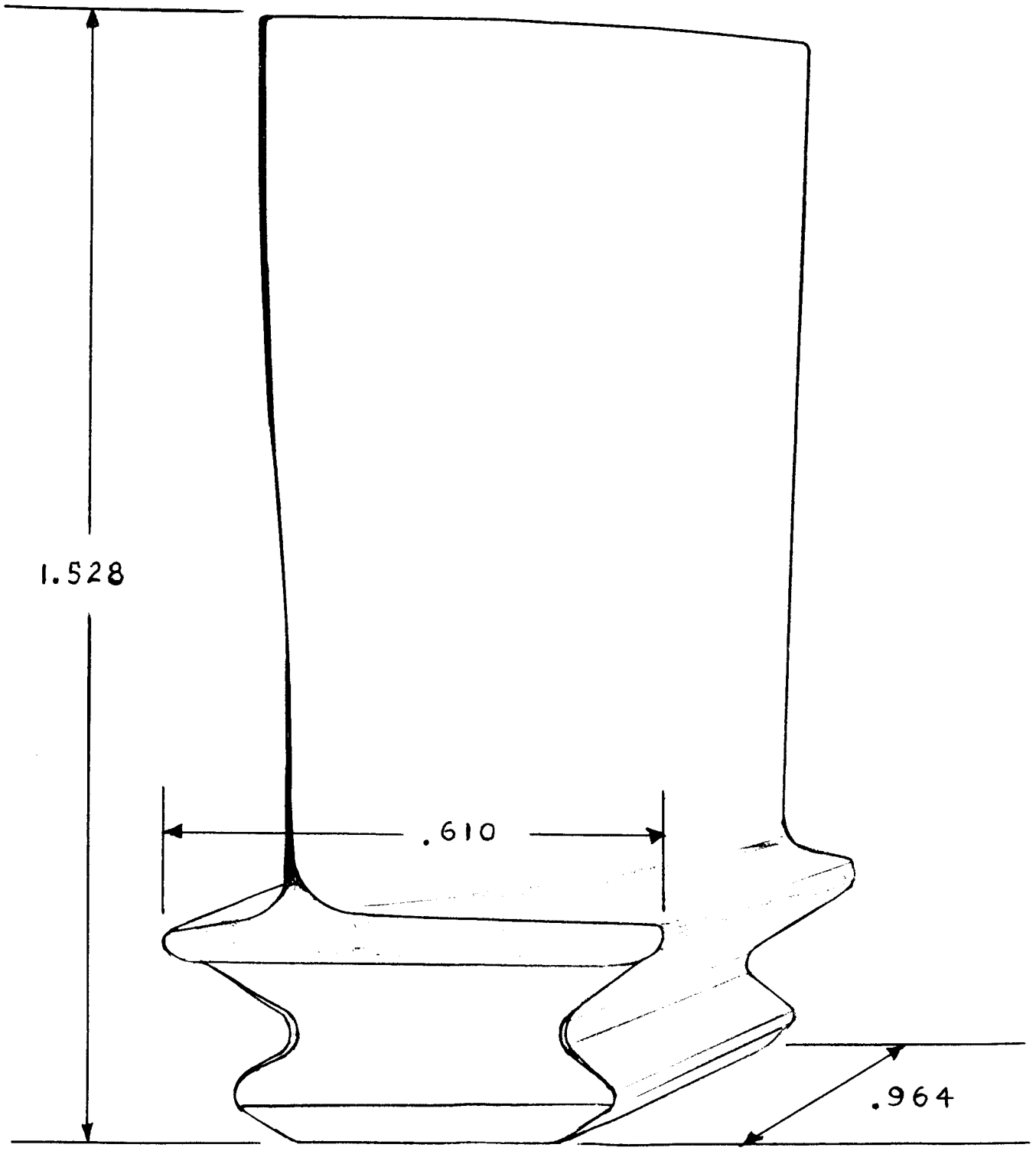

Figure 25

Typical Rotor Blade

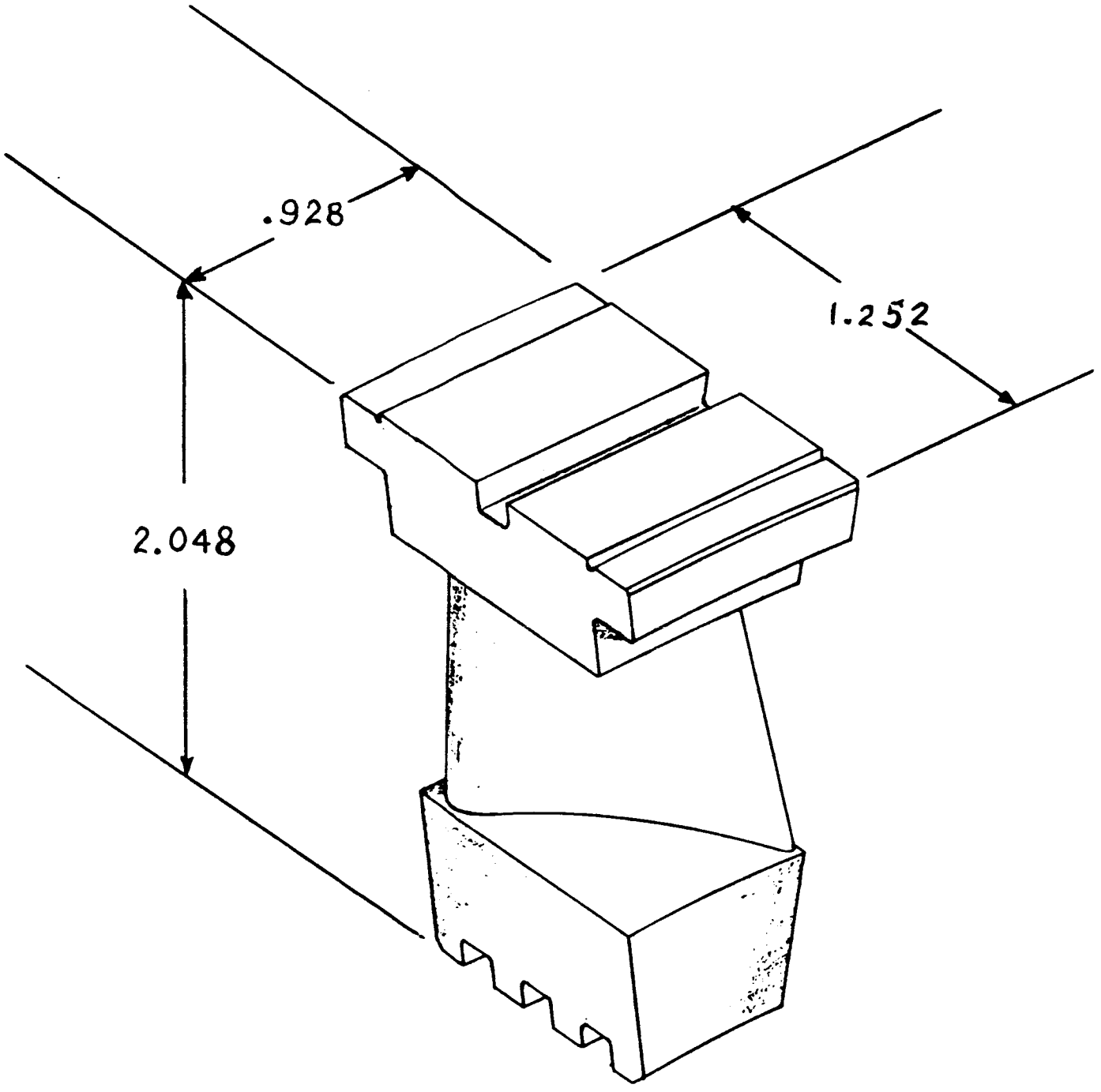

Figure 26

Typical Stator Blade

The incidence and deviation angles were determined by the previously cited methods[8] for C-4 blade settings at the minimum loss condition established by two dimensional cascade data. Three-dimensional corrections were not applied because information[9] indicated that in the cited methods[10] derived from compressor data did not apply for an incompressible fluid, however, no other convenient correction was available. The losses, except for minor modifications near the tip, were also determined using the cited method,[11] wherein the fluid diffusion, fluid turning, blade solidity and fluid exit angle are related to losses. The tip losses were reduced slightly based upon the reported test results.[12][13] A smoother transition between the tip losses and the remaining streamline losses was also included, as shown in Figure No. 27.

2. Method of Analysis

The streamline analysis that was used was obtained from existing literature.[14][15] A mathematical model taken from this literature was formulated into a computer program, Aerojet-General Corporation Job No. 10001, and used to establish the transition stage and main stage blade geometry. The basic assumptions made in this analysis are:

a. Flow is steady and axially symmetric.

b. Flow is two-dimensional and satisfies simple radial equilibrium.

c. Shearing effects of viscosity between blade rows is neglected.

---

(8) ibid

(9) Crouse, J. E., Soltis, R. F., and Montgomery, J. C., Investigation of the Performance of an Axial-Flow Pump Designed by the Blade-Element Theory-Blade-Element Data, NASA TN D-1109, December 1961

(10) NACA RM-E56B 03a, Vol. II, op. cit.

(11) ibid

(12) Crouse, J. E., et al, NASA TN D-1109, op. cit.

(13) Crouse, J. E. and Sandercock, D. M., Investigation of an Axial Flow Pump Rotor with a 0.7 Hub-Tip Radius Ratio and Blade Tip Diffusion Factor of .43 - Blade Element Performance, NACA E-1968

(14) NACA RM-E56B03a, op. cit.

(15) Lieblein, S., Analysis of Experimental Low Speed Loss and Stall Characteristics of Two-Dimensional Compressors Blade Cascades, NASA RM-E57A28

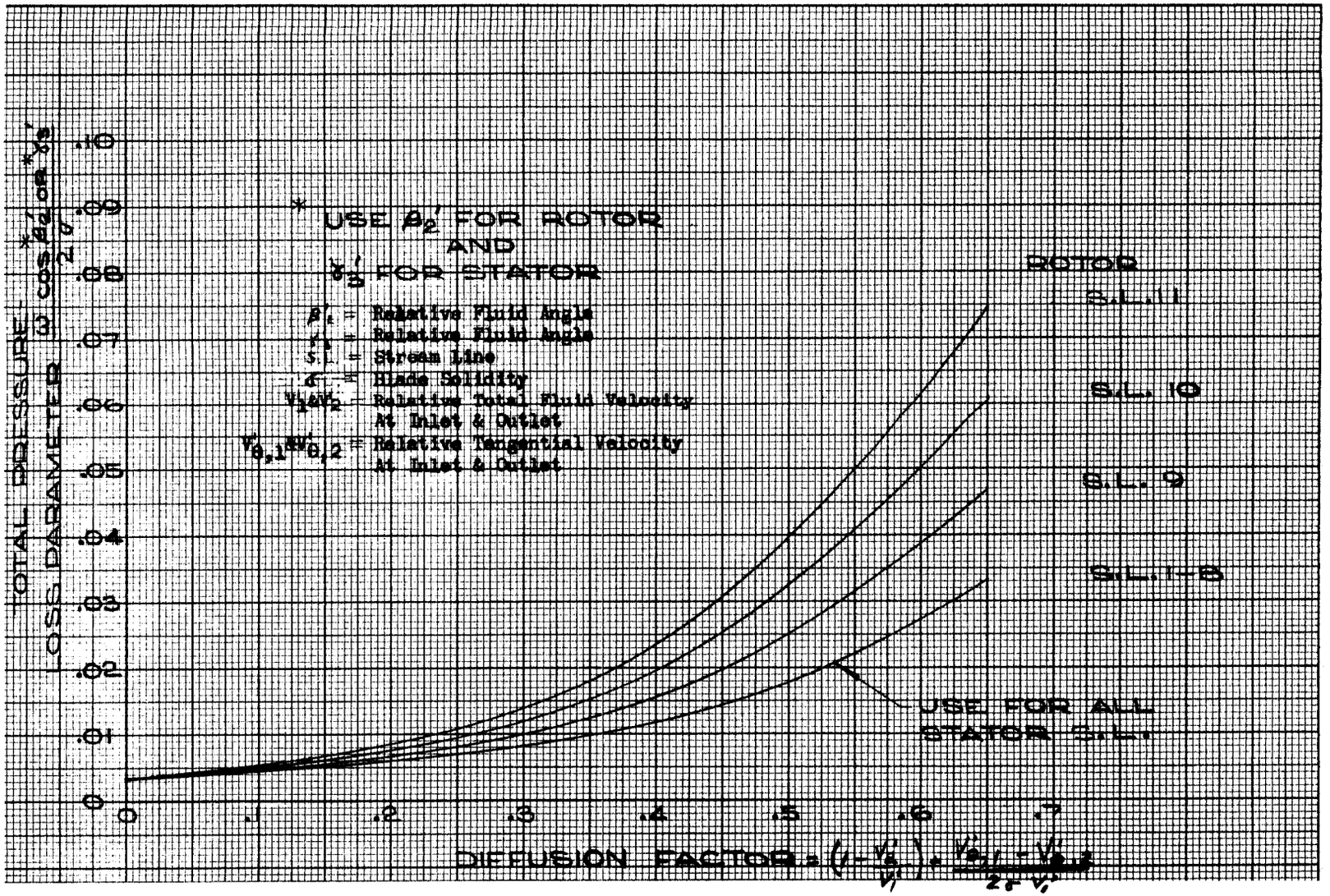

Figure 27

Total Pressure Loss Parameter

d. Heat transfer is neglected.

e. Losses and fluid-to-blade flow deviations effects are considered.

D. DISCHARGE DIFFUSER VANES AND HOUSING

A pump discharge pipe diameter of 12-in. was defined by engine design considerations. A conical diffusing section with a constant half angle of approximately 4.5 degrees was incorporated between the discharge pipe and the constant velocity volute. Engine design constraints limited the length of this section so that a 10-in. diameter volute discharge section was required, which resulted in a volute velocity of 250 ft/sec.

The housing vanes are non-airfoil sections that are designed to provide a smooth transition from the entrance velocity of approximately 500 ft/sec to the volute velocity of approximately 250 ft/sec. The profile of the passage is shown in Figure No. 28. The root, tip, and mean passage vane angle distributions are shown in Figure No. 29. Essentially, the hub vane angle distribution was selected to provide a free vortex velocity distribution. To simplify pattern making, the vanes were generated by straight line elements that are approximately normal to the root (back shroud) contour. The resultant velocity distribution is shown in Figure No. 30.

The pressure loss based upon a one-dimensional analysis indicates the diffuser losses will be approximately 50 psi or approximately 2.5% of the total pump pressure rise.

E. OFF-DESIGN ANALYSIS

1. Inducer Stage

To predict the off-design performance of axial flow pump by the blade element method, the fluid deviation angle and loss coefficient must be known or assumed for each radial streamline on the blade at each off-design flow condition. The inducer off-design deviation angles were assumed to be unchanged from those at the design point because for high solidities other investigators[16][17] show that the deviation is little affected by the inlet fluid flow angle. The inducer rotor off-design loss coefficient was determined by assuming the performance would be

(16) ibid

(17) Shigeo, Kubota, Cascade Performance with Accelerated or Decelerated Axial Flow, MIT Gas Turbine Laboratory Report No. 56, September 1959

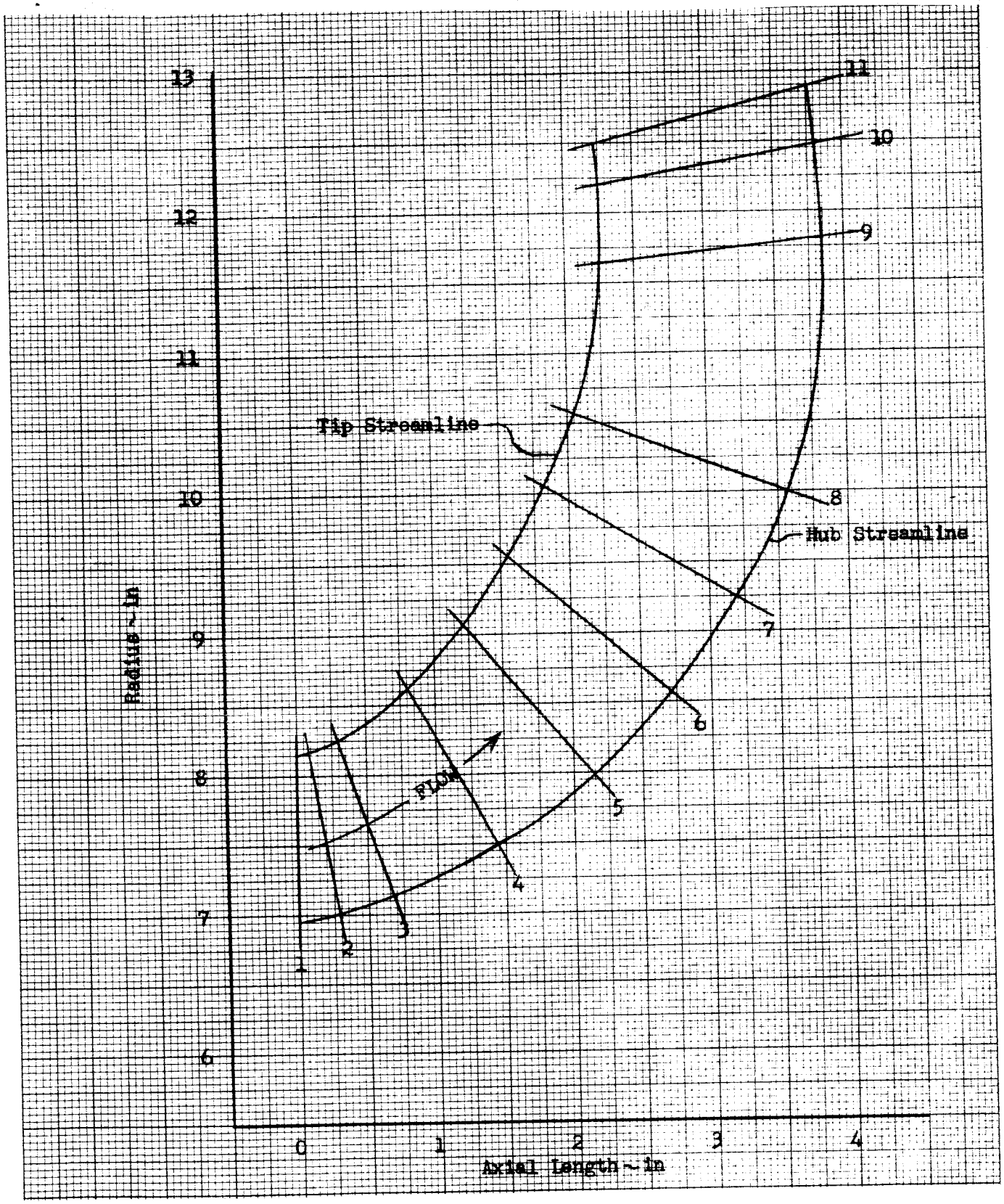

Figure 28

Diffuser Vane Profile

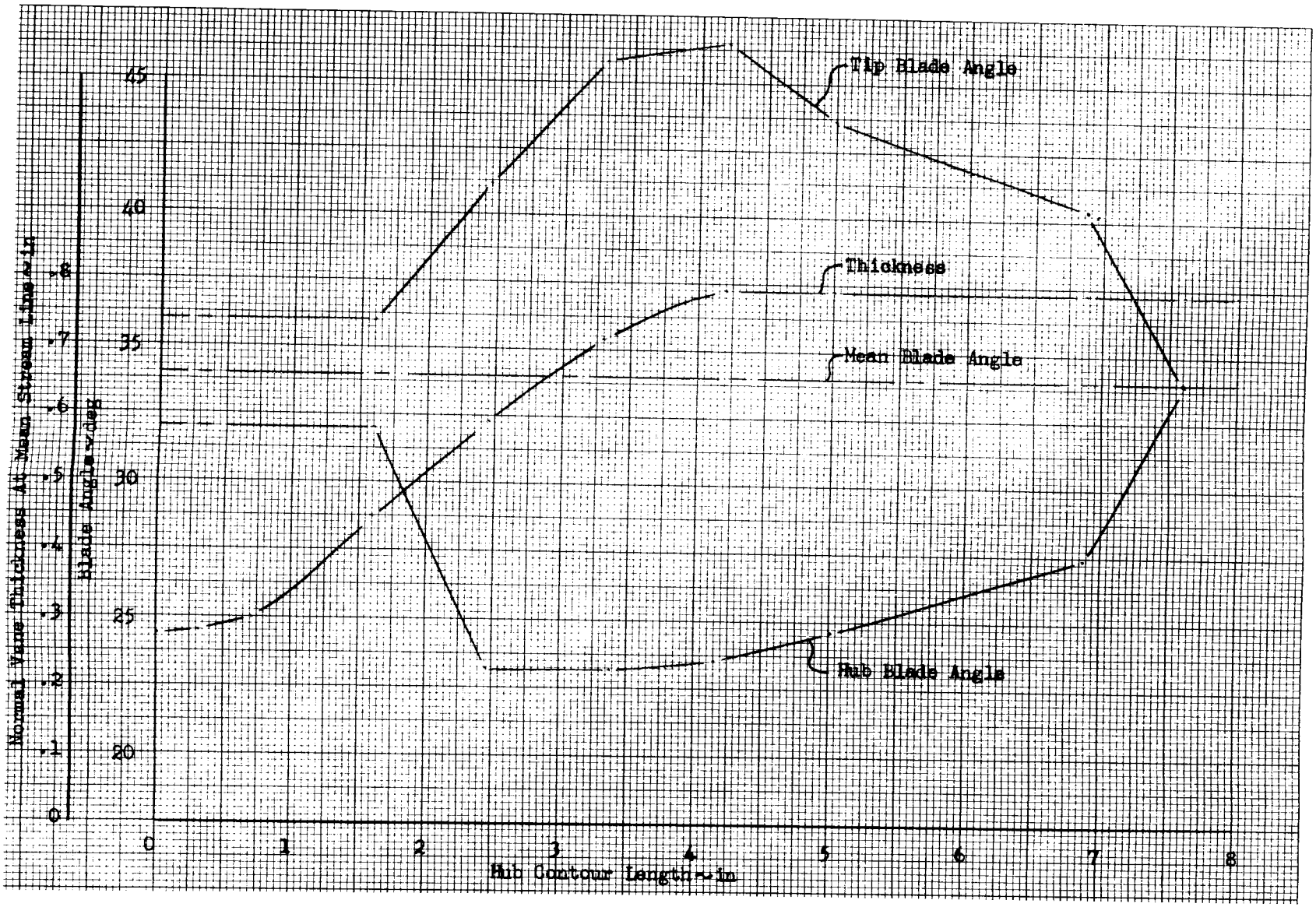

Figure 29

Blade Angle and Blade Thickness vs. Length

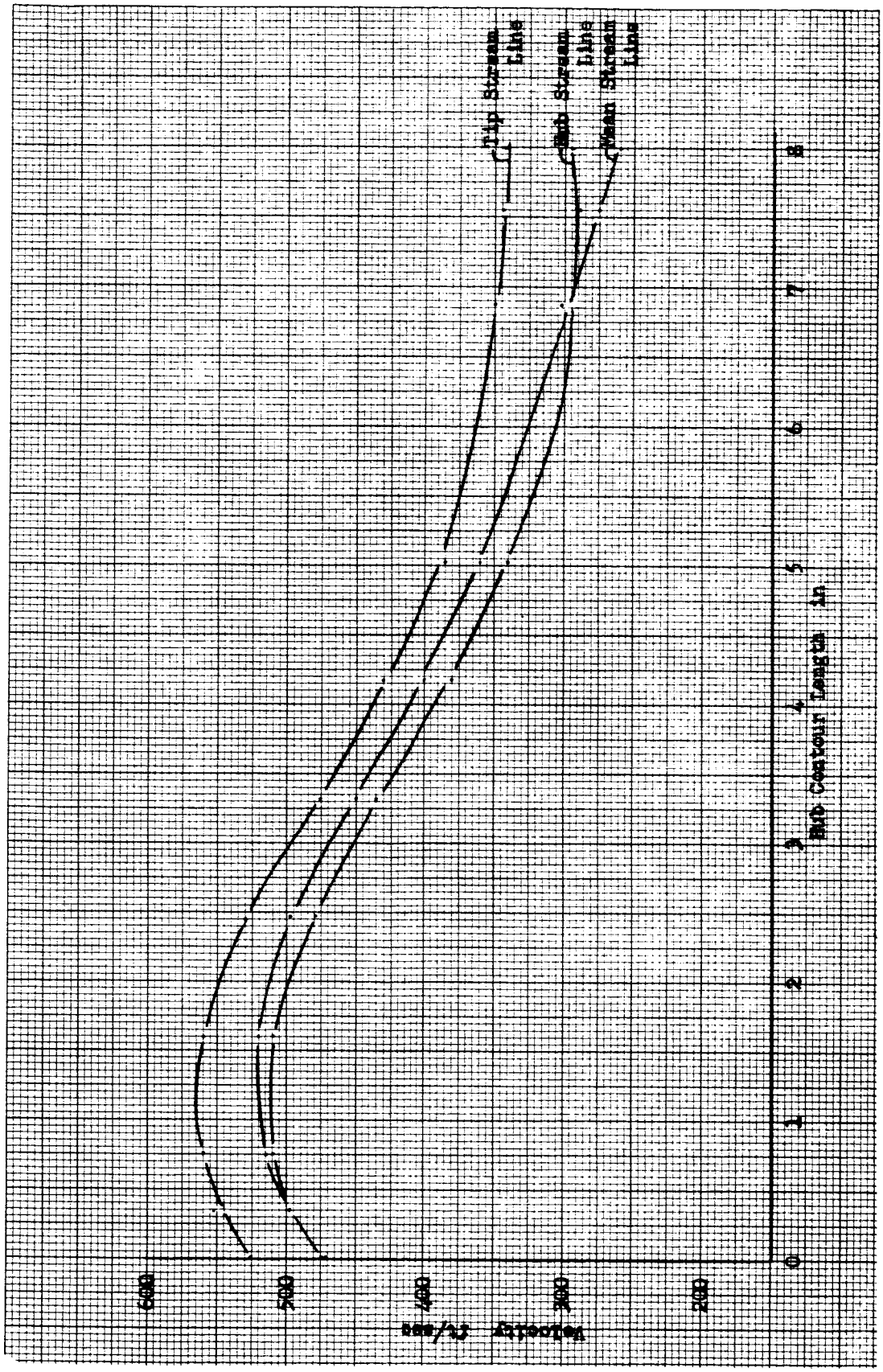

Figure 30

Velocity vs. Length; Tip, Mean, Hub

similar to a turbine-driven inducer[18] which has the same specific speed. The method for determining the inducer off-design loss coefficients is described in Appendix C.

The rotor off-design performance was computed in the same manner as the design point performance (Appendix B). The stator off-design performance was computed in the same manner as the design point performance. Rotor and stage off-design performance is shown in Figure No. 31.

2. Transition and Main Stages

The off-design performance analysis of these more conventional axial-flow stages was performed using two methods. The first method was one-dimensional wherein the deviation angle was assumed to be constant while the off-design loss characteristics were similar to those of cascade tests (see Figure No. 32) but at a higher level to account for tip leakage and hub boundary layer losses. The second was a two-dimensional blade element method.[19] The deviation angle variation, stall criteria, and loss criteria at stall in this method have been detailed by Lieblein.[20] The equations and their numerical form are shown in the off-design section of Appendix D. Stall was assumed to occur when the off-design losses were twice those at the design point (Figure No. 32), corresponding to a value of two for the equivalent diffusion parameter "Deq."[21]

The results of the off-design analysis are shown in Figure No. 33 for the one-dimensional and two-dimensional studies. It can be seen that Method two substantiates Method one, but gives a slightly steeper head versus flow curves with stall occurring at 89% of design flow. However, the predicted performance (Figures No. 6 and No. 7) is based upon the one-dimensional analysis[22] where the stall margin occurs at a lower flow coefficient. It appeared that the one-dimensional analysis was more reliable than the two-dimensional predictions for a ten stage machine because the two-dimensional analysis requires accurate radial loss predictions to avoid large radial flow shifts while the one-dimensional analysis does not have this problem.

(18) (u) The Design and Evaluation of a Low Speed Hydraulic Turbine-Driven Pump Discharge Fed Inducer Stage, Aerojet-General Corp. (LRO), Final Report, Phase II, Contract AF04(611)-7446 (Conf.)

(19) Serovy, G. K. and Tyler, J. C., Prediction of Axial Flow Turbomachine Performance by Blade Element Methods, ASME Paper No. 61 WA-134

(20) Lieblein, S., op. cit.

(21) ibid

(22) Final Report, Phase II, Contract AF 04(611)-7446, op. cit.

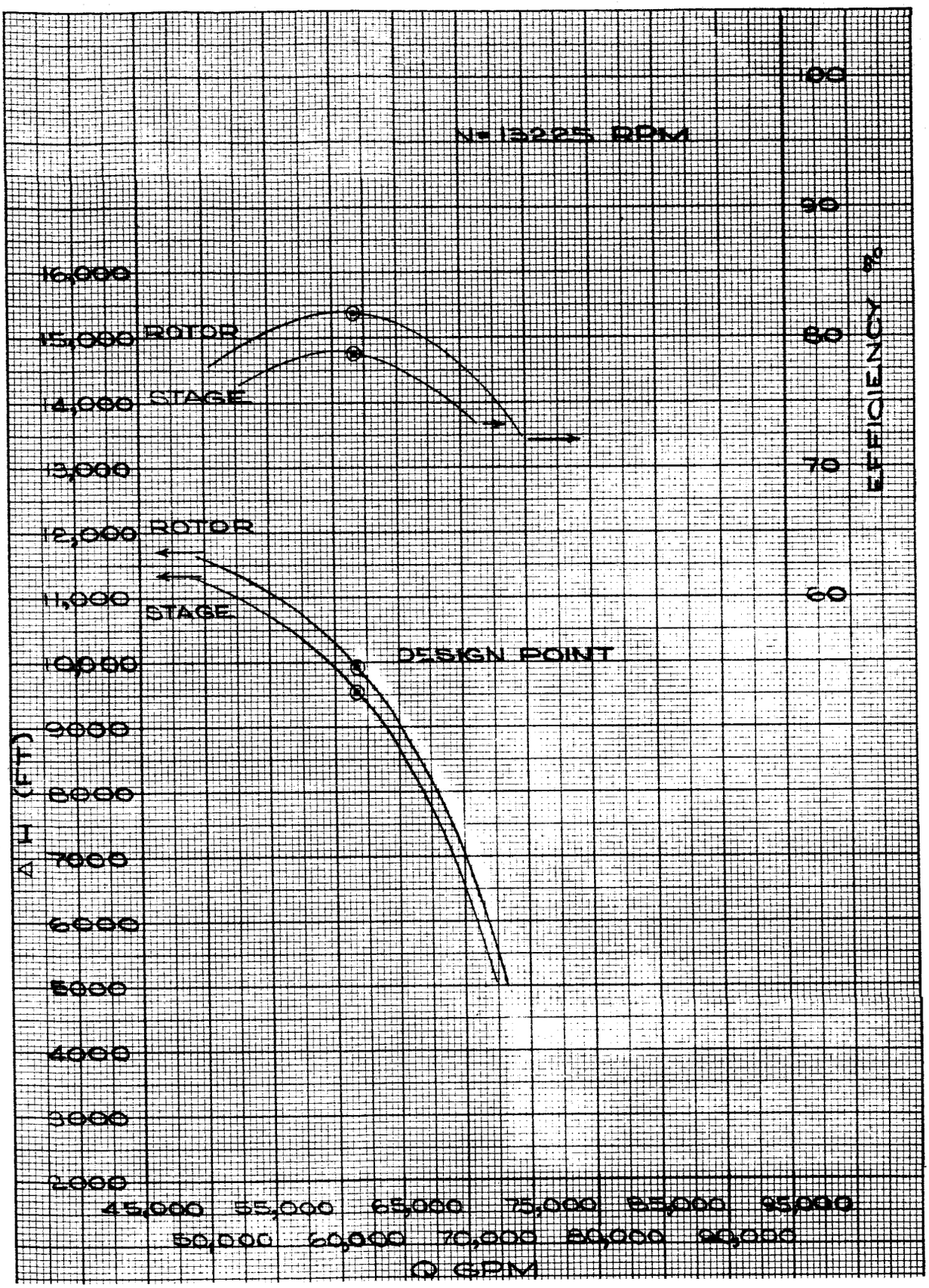

Figure 31

Inducer Rotor and Stage Head Rise; Efficiency vs. Flow Rate

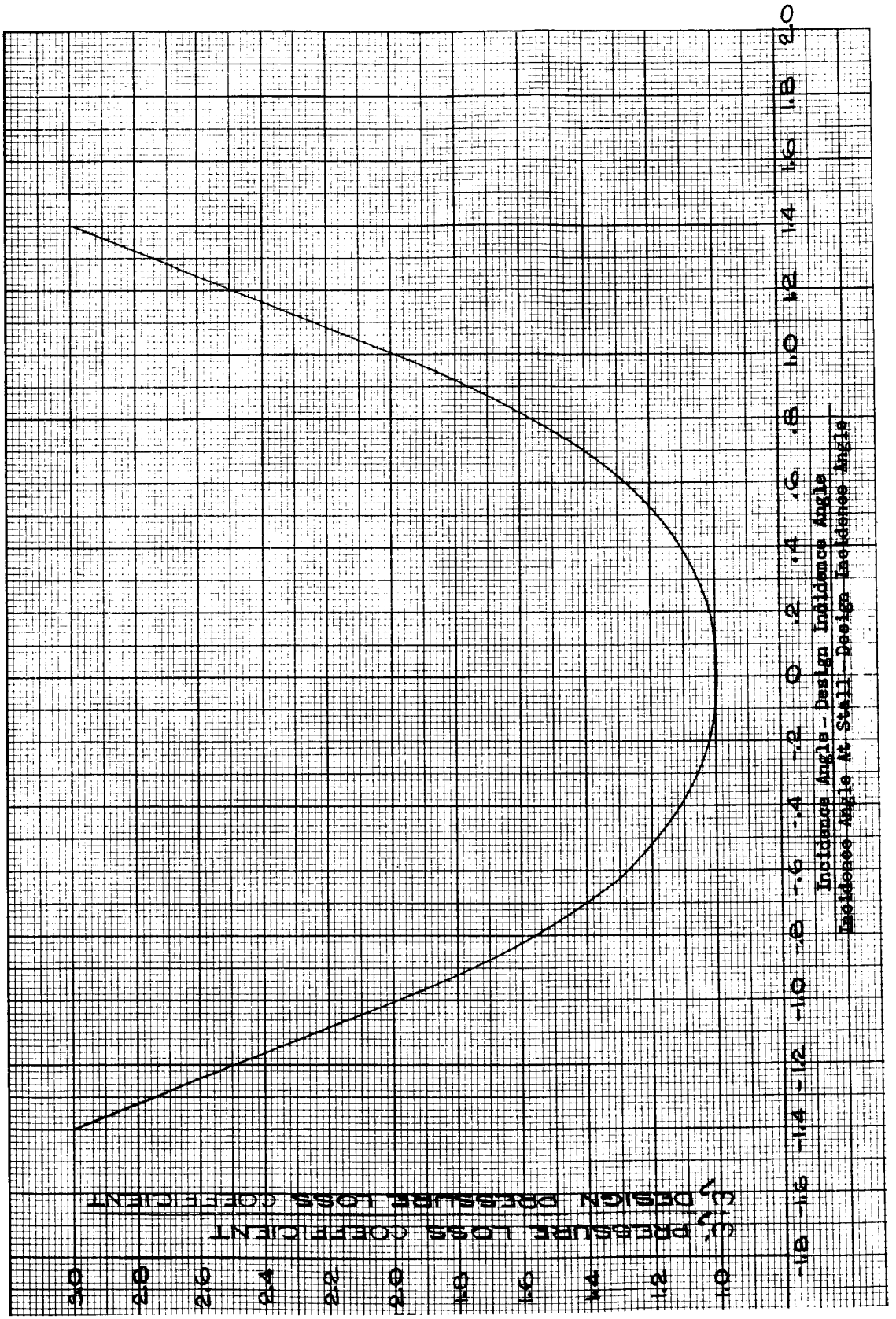

Figure 32

Pressure Loss Coefficient

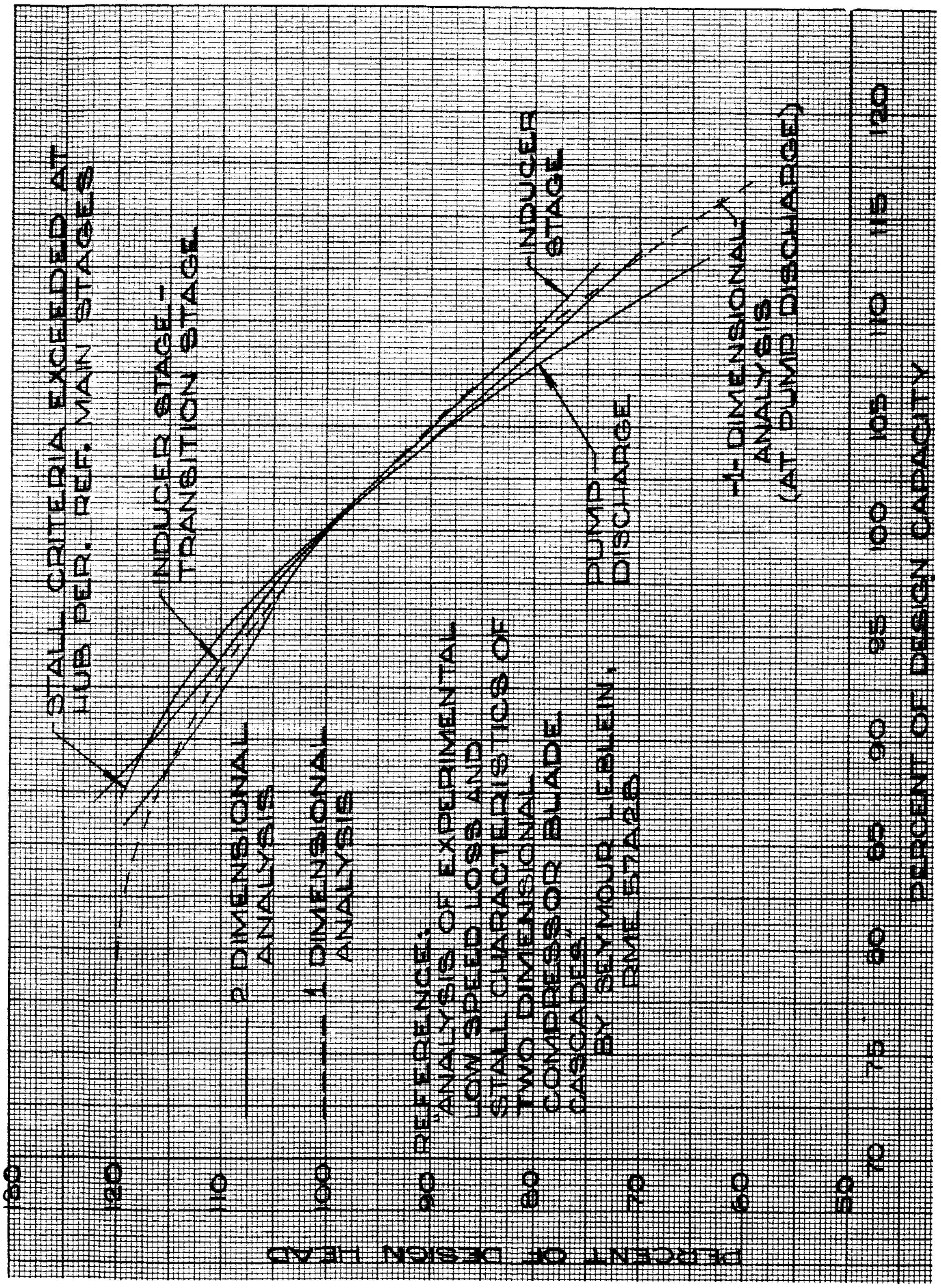
STALL CRITERIA EXCEEDED AT HUB PER. REF. MAIN STAGES
INDUCER STAGE - TRANSITION STAGE
INDUCER STAGE
PUMP DISCHARGE
1 DIMENSIONAL ANALYSIS (AT PUMP DISCHARGE)
2 DIMENSIONAL ANALYSIS
1 DIMENSIONAL ANALYSIS
REFERENCE: ANALYSIS OF EXPERIMENTAL LOW SPEED LOSS AND STALL CHARACTERISTICS OF TWO DIMENSIONAL COMPRESSOR BLADE CASCADES, BY SEYMOUR LIEBLEIN, RME 57A28
130
120
110
100
90
80
70
60
50
PERCENT OF DESIGN HEAD
70
75
80
85
90
95
100
105
110
115
120
PERCENT OF DESIGN CAPACITY

Figure 33

The effect of the non-standard main stage stator blades was estimated to be a one percent to two percent decrease in stall margin. This analysis (flow coefficient margin to stall) predicted the performance change would be caused by the increased thickness at the trailing edge; the thicker leading edge was assumed to have no effect.

A one percent pressure loss at design flow was predicted because of the untwist of the rotor blades. This prediction was based upon a calculated one degree untwist at the tip caused by blade loading and centrifugal loading. This effect was not considered in the design predictions shown in this report.

BIBLIOGRAPHY

1. Crouse, J. E. and Sandercock, D. M., Investigation of an Axial Flow Pump Rotor with a 0.7 Hub-Tip Radius Ratio and Blade Tip Diffusion Factor of .43 - Blade Element Performance, NACA E-1968

2. Crouse, J. E., Soltis, R. F., and Montgomery, J. C., Investigation of the Performance of an Axial Flow Pump Stage Designed by the Blade-Element Theory - Blade Element Data, NASA TN D-1109, December 1961

3. Inouye, F.T., Subscale Fuel Inducer, Aerojet-General Report FA 64-360, 31 July 1964

4. Knuth, W., M-1 Fuel Pump Tandem Inducer Design Investigation, Aerojet-General Corporation Report No. 0153 (Rotating Machinery Department, LRO) 16 December 1963

5. Lieblein, S., Analysis of Experimental Low Speed Loss and Stall Characteristics of Two-Dimensional Compressor Blade Cascades, NACA RME57A28.

6. Montgomery, J. C., Analytical Performance Characteristics and Outlet Flow Conditions of Constant and Variable Lead Helical Inducers for Cryogenic Pumps, NASA TN D-583, 1961

7. Mullen, P. J., An Investigation of Cavitating Inducers for Turbopumps, MIT Gas Turbine Laboratory Report No. 53, May 1959

8. Ross, C. C. and Banerian, G., Some Aspects of High Suction Specific Speed Pump Inducers, Trans. ASME, Vol. 78, No. 8, November 1956, pp. 1715-1721

9. Sandercock, D. M. and Crouse, J. E., Design and Over-All Performance of a Two-Staged Axial-Flow Pump with Tandem Row Inlet Stage, NASA TN D-2879

10. Serovy, G. K. and Tysen, J. C., Prediction of Axial Flow Turbomachine Performance by Blade Element Methods, ASME Paper No. 61 WA-134

11. Shigeo, Kubota, Cascade Performance with Accelerated or Decelerated Axial Flow, MIT Gas Turbine Laboratory Report No. 56, September 1959

12. Aerodynamic Design of Axial Flow Compressors, Vol. II, NACA RM-E56B03a, 1 August 1956

13. (U) The Design and Evaluation of a Low-Speed, Hydraulic Turbine-Driven Pump Discharge Fed Inducer Stage, AGC, LRP Final Report Phase II, Contract AF04(611)-7446 (Confidential)

14. M-1 Design Information Report, Section P. 10, Contract NAS3-2555 (Conf.)

APPENDICES

APPENDIX A

SUMMARY OF M-1 LIQUID HYDROGEN PUMP DESIGN DATA

SYMBOL NOMENCLATURE

r	RADIUS	IN.
U	BLADE SPEED	FT./SEC.
V	ABSOLUTE FLUID VELOCITY	FT./SEC.
V_z	AXIAL FLUID VELOCITY	FT./SEC.
V_T	ABSOLUTE TANGENTIAL FLUID VELOCITY	FT./SEC.
W	RELATIVE FLUID VELOCITY	FT./SEC.
β	RELATIVE FLUID ANGLE	DEGREES
γ	ABSOLUTE FLUID ANGLE	DEGREES
σ	SOLIDITY	- - - -
D	DIFFUSION PARAMETER	- - - -
$\bar{\omega}$	TOTAL PRESSURE LOSS COEFFICIENT	- - -
ΔH_{Loss}	HEAD LOSS	FT.
i	INCIDENCE ANGLE	DEGREES
δ	DEVIATION ANGLE	DEGREES
c	CHORD	IN.
t_{max}	THICKNESS	IN.
ΔH	ROTOR HEAD RISE	FT.
η	EFFICIENCY	%
ϕ	FLOW COEFFICIENT	- - - -
ψ	HEAD COEFFICIENT @ 8.0-in. radius	- - - -
ρ	FLUID DENSITY @ 8.0-in. radius	LB./FT.^{3}
ΔH_A	ACTUAL HEAD, STAGE	FT.
ΔH_i	IDEAL HEAD, STAGE	FT.

SYMBOL NOMENCLATURE (Cont'd)

$\overline{\Delta H_A}$	MASS AVERAGED ACTUAL HEAD	FT.
$\overline{\eta}$	MASS AVERAGED EFFICIENCY	%
$\overline{\phi}$	MASS AVERAGED FLOW COEFFICIENT	- - -
$\overline{\psi}$	MASS AVERAGED HEAD COEFFICIENT	- - -
$\overline{\dot{w}}$	MASS AVERAGED WEIGHT FLOW	LB/SEC.
HP	HORSEPOWER	

SUBSCRIPTS

1. ROTOR INLET
2. ROTOR EXIT AND/OR STATOR INLET
3. STATOR EXIT

VECTOR DIAGRAM OF TYPICAL FLUID VELOCITIES

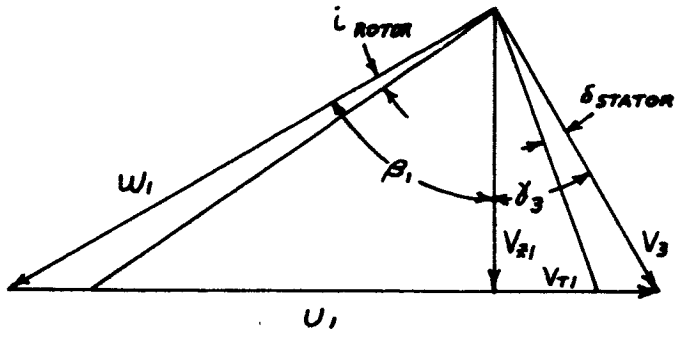

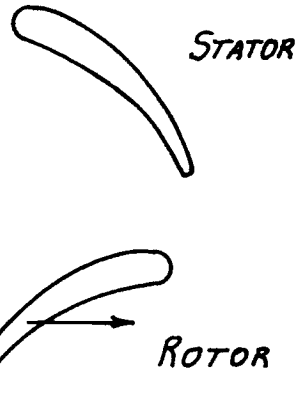

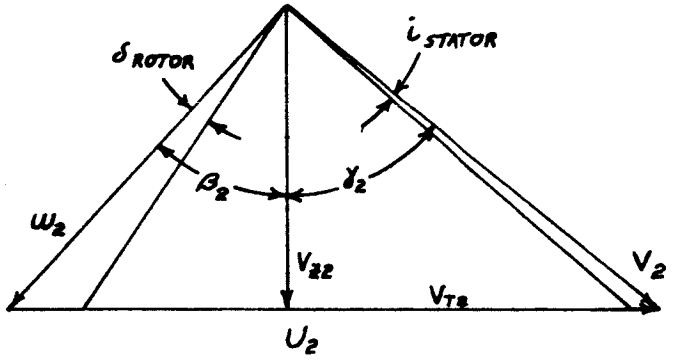

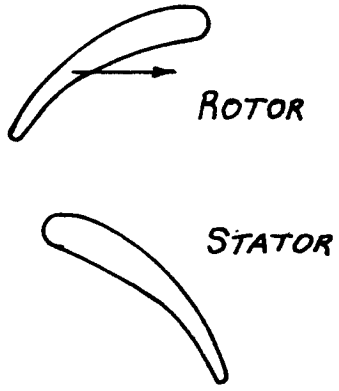

INDUCER ROTOR
DESIGN DATA SUMMARY SHEETS

STATION	1	2	3	4	5	6	7	8	9	10	11
r_1	4.32	4.85	5.38	5.90	6.43	6.96	7.49	8.02	8.54	9.07	9.60
r_2	6.35	6.60	6.86	7.11	7.37	7.62	7.88	8.13	8.39	8.64	8.90
U_1	499	560	621	681	741	804	864	925	985	1049	1109
U_2	734	762	792	820	351	880	910	937	967	996	1029
ρ_1	◄					4.33					►
V_{Z1}	◄					82.4					►
V_{Z2}	110	159	185	199	206	206	203	188	160	115	36
V_{T1}	◄					0					►
V_{T2}	476	426	397	381	375	378	389	424	492	601	794
W_1	510	565	626	686	747	806	865	926	987	1050	1110
W_2	280	372	435	481	519	542	558	545	500	412	238
β_1	80.6	81.6	82.5	83.1	83.7	84.1	84.5	84.9	85.2	85.4	85.6
β_2	66.7	64.7	64.9	65.6	66.6	67.7	68.7	69.8	71.4	73.8	81.3
$\overline{W}$	.228	.155	.129	.123	.126	.145	.170	.220	.296	.375	.456
λ	3.6	3.9	4.1	4.0	3.9	3.6	3.3	3.0	2.4	2.1	1.6
σ	7.7	4.5	3.6	3.2	3.0	2.9	2.8	2.6	2.3	2.0	1.5
ΔH	9380	8830	8690	8760	8870	9050	9250	9720	10620	12480	16610
η	86.7	87.5	88.9	90.2	89.6	87.4	84.1	78.6	71.8	66.9	65.5
ϕ	.119	.172	.200	.216	.223	.223	.220	.204	.173	.125	.039
ψ	.354	.333	.327	.330	.335	.341	.349	.366	.400	.470	.626

INDUCER ROTOR (Cont'd)

NO. BLADES	3 FULL AND 3 PARTIAL BLADES
TYPE BLADE	RADIAL BLADE - CONSTANT THICKNESS
BLOCKAGE FACTOR	.96
$\overline{\Delta H_A}$	9920
$\overline{\eta}$	82%
$\overline{\phi}$	.159
$\overline{\psi}$	.374
$\overline{\omega}$	600

INDUCER STATOR

STA	1	2	3	4	5	6	7	8	9	10	11
r_2	6.51	1.75	6.99	7.23	7.48	7.72	7.96	8.20	8.44	8.68	8.92
r_3	6.80	6.94	7.08	7.21	7.35	7.49	7.63	7.77	7.90	8.04	8.18
V_{B2}	110	159	185	199	206	206	203	188	160	115	36
V_{B3}	280	258	255	265	274	285	296	319	358	422	529
V_{T2}	476	426	397	381	375	378	389	424	492	601	794
V_{T3}	228	202	193	197	201	209	218	240	279	346	468
V_2	488	455	438	430	428	431	439	464	517	612	794
V_3	362	326	320	330	339	354	357	401	454	545	706
γ_2	77.0	69.5	65.0	62.4	61.2	61.4	62.5	66.1	72.0	79.2	87.3
γ_3	39.2	38.1	37.1	36.6	36.2	36.3	36.4	37.0	37.8	39.4	41.5
σ	2.20	2.12	2.04	1.98	1.91	1.85	1.80	1.76	1.69	1.65	1.60
D	.428	.434	.431	.426	.421	.418	.412	.407	.413	.420	.427
$\overline{W}$	.243	.213	.197	.182	.182	.182	.182	.182	.182	.198	.213
H_{Loss}	400	325	305	320	320	310	310	320	360	550	1050
i	17.8	10.2	7.6	5.2	4.1	3.7	2.8	3.5	3.6	5.9	7.0
ε	3.7	3.9	3.9	3.9	4.2	4.9	4.8	4.3	3.8	4.4	4.9
ρ_3	4.37	4.38	4.38	4.38	4.38	4.38	4.38	4.38	4.33	4.30	4.24

NUMBER OF BLADES	11
TYPE OF BLADES	C-4
BLOCKAGE FACTOR	.04

INDUCER STAGE

ΔH_i	10,830	10,100	9,760	9,710	9,900	10,350	11,000	12,370	14,800	18,640	25,350
ΔH_A	8980	8,405	8,385	8,440	8,550	8,740	8,940	9,400	10,260	11,930	15,460
η	83	83	86	87	86	85	81	76	69	64	61
ϕ	.303	.279	.276	.287	.296	.308	.320	.345	.389	.456	.572
ψ	.338	.317	.316	.318	.322	.330	.337	.354	.387	.450	.583

$\overline{\Delta H_A}$	9540
$\overline{\eta}$	78.5
$\overline{\phi}$	.370
$\overline{\psi}$	.360
$\dot{\omega}$	600
HP	1320

TRANSITION ROTOR
DESIGN DATA SUMMARY SHEET

M-1 FUEL PUMP
DESIGN FLOW
INLET TEMP. 39°R

STR	1	2	3	4	5	6	7	8	9	10	11
r_1	6.80	6.94	7.08	7.21	7.35	7.49	7.63	7.77	7.90	8.04	8.18
r_2	6.80	6.93	7.06	7.18	7.31	7.44	7.57	7.70	7.82	7.95	8.08
U_1	785	801	817	834	849	864	880	896	912	928	944
U_2	785	800	814	829	844	859	873	888	903	918	933
V_{Z1}	280	258	255	266	274	285	296	319	358	422	529
V_{Z2}	346	364	362	358	349	352	341	327	322	323	328
V_{T1}	228	202	193	197	201	209	218	240	279	346	468
V_{T2}	426	398	395	396	403	395	402	417	416	404	383
W_1	623	652	673	689	703	715	725	729	727	719	711
W_2	499	542	554	562	563	582	582	574	584	607	640
β_1	63.3	66.7	67.8	67.3	67.1	66.5	65.9	64.1	60.5	54.1	42.0
β_2	46.0	47.8	49.2	50.4	51.6	52.8	54.1	55.3	56.5	57.8	59.2
σ	1.037	1.000	.966	.933	.902	.872	.844	.818	.792	.768	.745
D	.352	.320	.336	.343	.365	.342	.356	.373	.328	.224	.037
$\bar{\omega}$	.030	.027	.028	.029	.031	.028	.029	.021	.034	.026	.012
i	6.32	9.08	9.48	8.43	7.58	6.47	5.37	3.05	-.734	-7.29	-18.9
ρ_1	4.37	4.38	4.38	4.38	4.38	4.38	4.38	4.38	4.33	4.30	4.24
ρ_2	4.39	4.40	4.40	4.40	4.40	4.40	4.40	4.40	4.35	4.32	4.25

TRANSITION ROTOR

STR	1	2	3	4	5	6	7	8	9	10	11
δ	8.38	8.45	8.13	7.61	7.13	6.61	6.00	5.32	4.39	3.19	1.67
t_{max}/c	.100	.096	.092	.088	.084	.080	.076	.072	.068	.064	.060
ΔH	4632	4694	4895	4891	5028	4708	4691	4556	3480	1340 2400	-2730 1000
η	.962	.963	.961	.959	.955	.955	.951	.946	.927	.866	.965
ϕ	.37	.39	.39	.39	.38	.38	.37	.35	.35	.35	.35
ψ	.17	.18	.18	.18	.19	.18	.18	.17	.13	.09	.04

NO. OF BLADES	31
TYPE OF BLADE	C-4
BLOCKAGE FACTOR	.04
$\overline{\Delta HA}$	3700
$\bar{\eta}$	.934
$\bar{\Phi}$	.37
$\bar{\Psi}$	.155
$\frac{\bar{\Psi}}{\dot{\omega}}$	600

TRANSITION STATOR
DESIGN DATA SUMMARY SHEET

M-1 FUEL PUMP
DESIGN FLOW
INLET TEMP. 39°R

STR	1	2	3	4	5	6	7	8	9	10	11
r_3	6.80	6.92	7.04	7.16	7.28	7.40	7.52	7.64	7.76	7.88	8.00
r_2	6.80	6.93	7.06	7.18	7.31	7.44	7.57	7.70	7.82	7.95	8.08
V_{Z3}	360	358	359	363	367	368	371	377	378	371	356
V_{Z2}	346	364	362	358	349	352	341	327	322	323	328
V_{T3}	218	212	210	211	213	211	211	216	217	218	222
V_{T2}	426	398	395	396	403	395	402	417	416	404	383
V_3	421	416	416	420	424	424	426	434	436	430	419
V_2	549	540	536	534	533	529	527	529	526	517	504
γ_3	31.2	30.6	30.4	30.2	30.1	29.8	29.7	29.8	29.9	30.5	32.0
γ_2	50.9	47.5	47.5	47.9	49.1	48.3	49.7	51.9	52.2	51.4	49.5
σ	1.19	1.16	1.14	1.12	1.10	1.08	1.06	1.04	1.02	1.01	.99
D	.392	.378	.374	.370	.369	.361	.363	.364	.359	.350	.333
$\bar{\omega}$	.032	.030	.029	.028	.027	.026	.026	.025	.024	.023	.022
H_{Loss}	181	178	198	210	235	223	240	258	275	208	95
i	10.08	7.17	7.43	7.76	8.62	6.80	6.70	6.89	3.89	-1.88	-12.24
δ	5.01	4.78	4.85	5.00	5.34	5.83	6.67	7.81	9.27	11.11	13.90
α	33.5	33.1	32.8	32.6	32.6	32.7	33.0	33.5	34.5	36.3	39.9
ρ_3	4.40	4.41	4.42	4.42	4.42	4.41	4.41	4.41	4.36	4.33	4.26

TRANSITION STATOR

STR	1	2	3	4	5	6	7	8	9	10	11
t_{MAX}/C	.08	.08	.08	.08	.08	.08	.08	.08	.08	.08	.08

NUMBER OF BLADES 45

TYPE OF BLADE C-4

BLOCKAGE FACTOR .04

TRANSITION STAGE

Δ Hi	4813	4872	5093	5101	5263	4931	4931	4814	3755	1548	2635
Δ HA	4481	4559	4766	4768	4908	4596	4581	4446	3570	1240	2820
η	.931	.936	.936	.935	.933	.932	.929	.924	.897	.801	--
ϕ	.389	.387	.388	.392	.397	.398	.401	.408	.409	.401	.385
ψ	.17	.17	.18	.18	.19	.17	.17	.17	.13	.08	.03
$\overline{\Delta H_A}$				3346							
$\bar{\eta}$				.916							
$\bar{\Phi}$				.396							
$\frac{\psi}{\omega}$				.126							
				600							
HP				4251							
$\overline{\Delta H_i}$				3654							

TYPICAL MAIN STAGE ROTOR
DESIGN DATA SUMMARY SHEET

M-1 FUEL PUMP
DESIGN FLOW
INLET TEMP. 39°R

STR	1	2	3	4	5	6	7	8	9	10	11
r_1	6.80	6.92	7.04	7.16	7.28	7.40	7.52	7.64	7.76	7.88	8.00
r_2	6.80	6.92	7.04	7.16	7.28	7.40	7.52	7.64	7.76	7.88	8.00
U_1	785	799	813	826	840	854	868	882	896	909	923
U_2	785	799	813	826	840	854	868	882	896	909	923
ρ_1	4.40	4.41	4.42	4.42	4.42	4.41	4.41	4.41	4.36	4.33	4.26
ρ_2	4.43	4.44	4.45	4.45	4.45	4.45	4.45	4.45	4.39	4.36	4.28
V_{z1}	360	358	359	363	367	368	371	377	378	371	356
V_{z2}	405	405	404	403	398	397	394	391	381	364	320
V_{T1}	218	212	210	211	213	211	211	216	217	218	222
V_{T2}	529	519	511	505	497	489	483	480	485	498	547
W1	671	687	701	714	727	741	754	765	776	785	786
W2	479	493	504	515	526	539	551	561	560	550	494
β_1	57.6	58.6	59.2	59.5	59.7	60.2	60.6	60.5	60.9	61.8	63.1
β_2	32.3	34.6	36.8	38.6	40.7	42.6	44.3	45.8	47.2	48.5	49.6
σ	1.43	1.36	1.30	1.24	1.19	1.13	1.08	1.04	.995	.954	.915
D	.448	.447	.446	.445	.442	.439	.436	.433	.451	.487	.598
$\bar{\omega}$	.049	.048	.047	.045	.044	.043	.042	.041	.059	.088	.176
i	7.24	7.17	6.58	6.03	4.85	4.27	3.62	2.53	2.03	2.12	2.69

TYPICAL MAIN STAGE ROTOR
DESIGN DATA SUMMARY SHEET

(Continued)

STR	1	2	3	4	5	6	7	8	9	10	11
σ	9.88	9.69	9.41	9.01	8.78	8.52	8.26	8.00	7.83	7.74	7.71
t_{MAX}/c	.120	.115	.111	.106	.102	.098	.093	.088	.084	.080	.075
ΔH_A	7227	7264	7224	7201	7068	7024	6976	6868	6891	7074	7644
η	.955	.954	.953	.952	.951	.950	.950	.949	.926	.893	.819
ϕ	.438	.438	.437	.436	.431	.430	.426	.423	.412	.394	.346
ψ	.27	.27	.27	.27	.27	.26	.26	.26	.26	.27	.29

NUMBER OF BLADES	31
TYPE OF BLADE	C-4
BLOCKAGE FACTOR	.04
$\overline{\Delta HA}$	7126
$\bar{\eta}$	.934
$\bar{\phi}$	.421
$\bar{\psi}$	.27
$\overline{\sigma}$	640

TYPICAL MAIN STAGE STATOR
DESIGN DATA SUMMARY SHEET

(Continued)

STR	1	2	3	4	5	6	7	8	9	10	11
t MAX/C	.150	.150	.150	.150	.150	.150	.150	.150	.150	.150	.150

NUMBER OF BLADES	45
TYPE OF BLADE	C-4
BLOCKAGE FACTOR	.04

STAGE I

Δ Hi	7571	7615	7580	7561	7431	7391	7345	7238	7442	7220	9330
Δ H	6850	6914	6897	6897	6780	6752	6720	6625	6657	6844	7408
η	.904	.908	.910	.912	.912	.914	.915	.915	.900	.864	.794
ϕ	.410	.413	.412	.418	.414	.414	.416	.417	.422	.430	.454
ψ	.26	.26	.26	.26	.26	.25	.25	.25	.25	.26	.28

$\overline{\Delta HA}$	6854
$\overline{\eta}$	.894
$\overline{\phi}$	.420
$\overline{\psi}$	.258
$\overline{\omega}$	640
HP	8921

TYPICAL MAIN STAGE STATOR
DESIGN DATA SUMMARY SHEET

M-1 FUEL PUMP
DESIGN FLOW
INLET TEMP. 39°

STR	1	2	3	4	5	6	7	8	9	10	11
r_3	6.80	6.92	7.04	7.16	7.28	7.40	7.52	7.64	7.76	7.88	8.00
r_2	6.80	6.92	7.04	7.16	7.28	7.40	7.52	7.64	7.76	7.88	8.00
t_3	4.46	4.46	4.47	4.47	4.47	4.47	4.47	4.47	4.41	4.38	4.30
VZ3	379	382	381	386	383	383	384	385	390	397	420
VZ2	405	405	404	403	398	397	394	391	381	364	320
VT3	242	237	235	233	228	225	222	220	220	223	241
VT2	529	519	511	505	497	489	483	480	485	498	547
V3	450	449	448	451	446	444	443	444	448	455	484
V2	666	658	651	646	637	630	624	619	616	617	634
γ_3	32.5	31.8	31.6	31.2	30.8	30.4	30.1	29.7	29.5	29.3	29.8
γ_2	52.6	52.0	51.7	51.5	51.3	51.0	50.8	50.8	51.8	53.8	59.7
σ	1.42	1.36	1.31	1.27	1.22	1.18	1.14	1.11	1.07	1.03	1.00
D	.477	.475	.473	.469	.472	.473	.473	.473	.475	.477	.477
$\overline{\omega}$	.055	.052	.050	.047	.046	.044	.042	.041	.040	.039	.038
HLOSS	344	351	356	360	363	367	369	370	551	846	1686
i	2.71	1.66	1.85	1.61	1.36	.911	.535	.211	.682	1.88	6.81
δ	8.73	9.13	9.12	9.38	9.67	9.96	10.33	10.81	11.56	12.61	14.50
α	36.8	36.5	36.2	35.8	35.5	35.3	35.0	34.8	34.5	34.3	34.1

APPENDIX B

HYDRAULIC PERFORMANCE ANALYSIS
M-1 LIQUID HYDROGEN PUMP
INDUCER STAGE

1. Inducer Rotor Analysis

The M-1 inducer impeller was designed with radial blade elements, and blade angles satisfying the relation,

$$\tan \beta' = \frac{r}{r_t} \tan \beta_t \qquad \text{where}$$

β' is the blade angle to the axis, and subscript t refers to any point at the same axial station where the blade angle is known.

Preliminary investigation of the inducer performance indicated that the velocity and pressure distributions at the impeller exit plane would not provide reasonable design conditions for the design of the inducer stage stator or transition stage. In order to reduce the work done on the fluid at the impeller tip, and thereby "flatten the hub to tip total pressure distribution, it was suggested that the impeller vane be trimmed back at the exit plane.

a. Impeller Geometry

For the analysis, the trimmed portion of the impeller was divided into eleven equally spaced axial stations, A through K; and at each axial station, the passage was divided into eleven equally spaced radial stations, one through eleven. In this way an eleven by eleven grid was formed, with points on the principal diagonal corresponding to split point at each axial station between in-blade and out-of-blade flow.

b. Equations

Under the imposed geometrical conditions, velocity and pressure distributions could be determined by successive solution of the equations of simple radial equilibrium and continuity at each axial station.

The radial equilibrium equation,

$$g \frac{dh}{dr} = \frac{V_\theta^2}{r}$$

g = Acceleration of Gravity

h = Static Pressure

r = Radius

V_θ = Fluid Tangential Velocity

If the axial velocity distribution does not satisfy continuity, the initial guess for hub velocity is revised, and a new axial distribution is computed. This iteration process is continued until the continuity condition is satisfied.

Referring back to the section on geometry, it can be observed that the equation for $V_{Z(n+1)}$ can be used exclusively only at axial station A; at succeeding stations, the fluid has passed all or in part out of the blade. If it is assumed that the fluid tangential velocity remains constant after the fluid leaves the blade, the complete flow solution may be readily determined.

As the fluid passes from axial station A to B one radial station is out of the blade, one at the split point, and the remaining stations are within the blade. As each successive axial station is reached an additional radial station is out of the blade, and the split point moved one station closer to the hub. If then, the tangential velocity at radial station eleven (tip) determined at axial station A is assumed constant as the fluid passes from A to B, a solution can be had for the flow outside the blade.

Using the previously stated radial equilibrium equation, and the expression for static head, an expression for $V_{Z\ n+1}$ is again found.

$$V_{Z(n+1)} = \left[V_{Z(n)}^2 + 2g \left(-H_{L(n+1)} + H_{1(n)} + \frac{U_{(n+1)} V_{\Theta\,(n+1)}}{g} - \frac{U_{(n)} V_{\Theta\,(n)}}{g} \right. \right.$$

$$\left. \left. - \frac{V_{\Theta}^{2}{}_{(n+1)}}{2g} + \frac{V_{\Theta}^{2}{}_{(n)}}{2g} - \frac{V_{\Theta}^{2}{}_{(n)}}{rg} \Delta r \right) \right]^{1/2}$$

Using the first $V_{Z\ n+1}$ equation to compute the velocity distribution to the split point, and the above $V_{Z\ n+1}$ equation above the split point, the flow distribution at all stations can be successively determined.

2. Stator Analysis

The stator design and off design conditions were computed by solving the equation of simple radial equilibrium. The analysis consisted of first determining the blade angles required to satisfy conditions of design; having thus selected the blade inlet and outlet angles, it was then only necessary to hold these blade angles, and study the effect at (the stator outlet) of varying inlet velocity and head profiles, and flow rates.

Beginning again with the equation of simple radial equilibrium,

$$g \frac{dh}{dr} = \frac{V_{\Theta}^{2}}{r}$$

may be used to solve for axial velocity V_Z, distribution when either the tangential fluid velocity is known, or the fluid angle is known. For this case the fluid angle can be estimated knowing the blade angle, and using an approximate in-blade deviation angle. Then at axial station, A, the axial velocity distribution can be determined, knowing only the fluid angles.

$$g \frac{dh}{dr} = \frac{V_\theta^2}{r}$$

$$V_\theta = u - W_\theta = u + V_Z \tan\beta$$

$$h = H_1 - H_2 + \frac{U(V_\theta - V_\theta)}{g} - \frac{V_\theta^2}{2g} - \frac{V_Z^2}{2g}$$

H_L = Head Loss

U = Blade Speed

β = Fluid Angle Relative to Blade

H_1 = Inlet Head = 0 (Assumed)

V_{θ_1} = Inlet Tangential Velocity = 0 (Assumed)

The equations above may be combined and expressed in finite difference from

$$\Delta\left[V_Z^2 (1+\tan^2\beta)\right] = 2g\left[\Delta\left(H_1 - H_2 - \frac{U^2}{2g}\right) - \frac{U^2 + 2UV_Z\tan\beta + V_Z^2\tan^2\beta}{rg}\Delta r\right]$$

This equation may be solved explicitly for V_Z at radial station n+1, as a function of known values at radial stations n, and n+1, i.e.,

$$V_{Z(n+1)} = \left\{\frac{1}{1+\tan^2\beta_{(n+1)}}\left[V_Z^2(1+\tan^2\beta_{(n)}) + 2g\left(-H_{L(n+1)} + H_{L(n)} + \frac{U^2_{(n+1)}}{2g} - \frac{U^2_{(n)}}{2g} - \frac{U^2_{(n)} + 2U_{(n)}V_{Z(n)}\tan\beta_{(n)} + V_Z^2{}_{(n)}\tan^2\beta_{(n)}}{rg}\Delta r\right)\right]\right\}^{1/2}$$

If an initial estimate is made for the axial velocity at the hub, the velocity distribution may be determined using the expression above. The velocity distribution so determined is then checked against the continuity equation,

$$Q = \text{Volume Flow Rate} = \int_{r_{hub}}^{r_{tip}} 2\pi V_Z\, r\, dr$$

at the design point, the effect of various outlet tangential velocity distributions were studied to select the outlet V_θ distribution that would best satisfy the design conditions. The equation expressed explicitly in terms of axial velocity is

$$V_{Z(n+1)} = \left[V_{Z(n)}^2 + 2H_{2(n+1)} - 2H_{2(n)} - V_{\theta(n+1)}^2 - V_{\theta(n)}^2 - \Delta r \left(\frac{V_{\theta\, n+1}^2}{r(n+1)} + \frac{V_{\theta(n)}^2}{r(n)} \right) \right]^{1/2}$$

H_2 = Outlet head

V_θ = Outlet tangential velocity

V_2 = Outlet axial velocity

r = Radius

subscript n = Axial station

To determine off-design conditions, V_θ in the equation above was required by

$$V_\theta = V_2 \tan \gamma$$

γ = Fluid angle

The equation, again explicitly solved for

$$V_{Z(n+1)} = \left\{ \frac{2}{\tan^2 \gamma_{(n+1)} + 1} \left[\frac{V_{Z(n)}^2 \left(\tan^2 \gamma_{(n)} - 1 \right)}{2} + H_{2(n+1)} - H_{2(n)} - \frac{V_{Z(n)}^2 \tan^2 \gamma_{(n)}}{r_{(n)}} \Delta r \right] \right\}^{1/2}$$

Using these equations and the equation of continuity, the performance of the stator may be determined

APPENDIX C

OFF-DESIGN LOSS COEFFICIENT ANALYSIS
M-1 LIQUID HYDROGEN PUMP
INDUCER STAGE

The expression above for head loss at any off-design point is a function of design head (H_D), design efficiency (η_D), and C_1 and C_2 determined from the performance curve of the turbine-driven inducer.

Using the off-design head loss so determined, the off-design loss coefficients can be determined, and a complete off-design analysis of the inducer rotor can be obtained.

The inducer stator off-design loss coefficients were assumed to be equal to the design point loss coefficients. This assumption was made because magnitude of the stator losses was small compared to the total head, so that a significant increase in the stator losses would not be important in changing the outlet total dynamic head.

INDUCER STAGE

OFF-DESIGN LOSS COEFFICIENT

The loss coefficients for the rotor off-design were determined by assuming that the M=1 fuel inducer performance would be similar to the performance of another Helical inducer of approximately the same specific speed, i.e., the turbine-driven inducer.*

Let C_1 = percent of design head at any off-design point.

C_2 = percent of design efficiency at any off-design point;

Then if

H = head

η = efficiency

subscript $_L$ = head lost

subscript $_K$ = off-design point

subscript $_D$ = point

I = ideal head,

$$C_1 = \frac{H_K}{H_D} = \frac{H_{I_K} - H_{L_K}}{H_D}$$

$$C_2 = \frac{\eta_K}{\eta_D} \quad \frac{1 - \frac{H_{L_K}}{H_{I_K}}}{\eta_D}$$

These equations may be combined to solve for H_{L_K}

$$H_{L_K} = H_D C_1 \left(\frac{1}{\eta_D C_2} - 1 \right)$$

* Shigeo, Kubota, Cascade Performance with Accelerated or Decelerated Axial Flow, MIT Gas Turbine Laboratory Report No. 56, September 1959

APPENDIX D

HYDRAULIC PERFORMANCE ANALYSIS
(DESIGN AND OFF-DESIGN)
M-1 LIQUID HYDROGEN PUMP
TRANSITION STAGE AND MAIN STAGES

I. PROBLEM TO BE SOLVED

A. COMPUTATION

This program calculates design and off-design performance for a multi-stage axial flow pump of given geometry.

The program is equipped to handle incompressible flow as well as compressible para-hydrogen.

The flow solution is two-dimensional and incorporates NACA, low mach number cascade loss data.

B. INITIAL INFORMATION

1. Inlet velocity distribution.
2. Inlet density distribution when flow is compressible.
3. Inlet head distribution when flow is incompressible.
4. Inlet temperature distribution when flow is compressible.
5. Inlet pressure distribution when flow is compressible.
6. Flow rate and shaft speed.

C. SOLUTION

1. Physical Theory

For a complete discussion refer to NACA Research Memorandum No. E56B03a "Aerodynamic Design of Axial-Flow Compressors - Volume II dated August 1, 1956.

2. Methematical Formulation (AGC Computer Program 10039)

See Section IV

D. RESTRICTIONS

1. The flow satisfies radial equilibrium conditions.
2. The pressure and temperature ranges are as follows:

$36.0001\ ^\circ R \leq \text{temperature} \leq 100^\circ R$

$147\ \text{psia} \leq \text{pressure} \leq 5000\ \text{psia}$

II. INPUT

A. DISCUSSION

Three input sheets have been constructed for this program:

The first page contains the basic data for each case such as option flags, flow rate, blockage factor, etc. including the inlet conditions and geometry for Stage No. 1.

The second page contains the pump geometry for each succeeding stage.

The third page contains the data necessary to run the off-design portion of the program. Normally, only the PDESQ coefficients will be required input as the program stores all the design point data on tape and it is read as needed. In the event different inlet conditions are desired at Stage 1, fill out the other lines on the sheet and set the value of K_I corresponding to $PDESQ_I$ equal to 1.

Any number of cases may be stacked, however, each case must be complete.

B. DATA NEEDED

The following is a list of the data required to run one case:

Input Symbol	Description
NSL	Number of streamlines
NS	Number of stages
T	BLADE TYPE: T = 1 if C-4 T = 2 if DCA T = 3 if NACA-65
FLOW	Incompressible flow flags: FLOW = 1 if incompressible FLOW = 0 if compressible
$\dot{W}$	Flow rate, lbs/sec
RPM	Shaft speed, revolutions per minute blockage factor
DFS	Diffusion at stall
$R_{i,H}$ (i = 1,2,3)	Hub radius at station i, inches
$R_{i,T}$ (i = 1,2,3)	Tip radius at station i, inches
$(t/c)_{R,H}$	Rotor hub thickness to chord ratio

Input Symbol	Description
$(t/c)_{S,H}$	Stator hub thickness to chord ratio
$(t/c)_{R,T}$	Rotor tip thickness to chord ratio
$(t/c)_{S,T}$	Stator tip thickness to chord ratio
$\sigma_{R,H}$	Rotor blade solidity
$\sigma_{S,H}$	Stator blade solidity
X_R	Radius ratio exponent
X_S	Radius ratio exponent
ϕ Rotor	Rotor blade camber angle, degrees
ϕ Stator	Stator blade camber angle, degrees
α Rotor	Rotor blade stagger angle, degrees
α Stator	Stator blade stagger angle, degrees
T_1	Represents one of the following: density lbs/ft^3 when flow is incompressible temperature °R when flow is compressible
T_2	Represents one of the following: head, ft when flow is incompressible pressure, psia when flow is compressible
V_Z	Axial component of fluid velocity, ft/sec
V_T	Tangential component of fluid velocity, ft/sec
$PDESQ_I$ (I = 1,2,...6)	Fraction of design flow rate to be used for off-design calculations
K_I (I = 1,2,...6)	A flag corresponding to each $PDESQ_I$ indicating whether additional input is required:

Input Symbol	Description
	K_I = 1 for additional input
	K_I = 0 for no additional input
Φ_1	Same as T_1
Φ_2	Same as T_2

C. INPUT FORMAT

Card 1

Symbol	Card Column
NSL	1-2
NS	3-5
T	6
FLOW	20-22
W	27-34
RPM	35-42
$\uparrow$	43-50
DFS	59-67

Card 2

Symbol	Card Column
$R_{1,H}$	1-12
$R_{2,H}$	13-24
$R_{3,H}$	25-36
$R_{1,T}$	37-48
$R_{2,T}$	49-60
$R_{3,T}$	61-72

Card 3

Symbol	Card Column
$(t/c)_{R,H}$	1-8
$(t/c)_{S,H}$	9-16
$(t/c)_{R,T}$	17-24

Symbol	Card Column
$(t/c)_{S,T}$	25-32
$\sigma_{R,H}$	33-40
$\sigma_{S,H}$	41-48
X_R	49-56
X_S	57-64

Cards numbering 4 through (NSL + 4) contain:

Symbol	Card Column
ϕ Rotor	1-8
ϕ Stator	9-16
α Rotor	17-24
α Stator	25-32
FIXDEV	33-40
T_1	41-48
T_2	49-56
V_Z	57-64
V_T	65-72

The remaining (NS - 1) sets of cards will each contain (NSL + 2) cards the first two of which repeat the format of cards 2 and 3 followed by NSL cards with the following:

Symbol	Card Column
ϕ Rotor	1-8
ϕ Stator	9-16
α Rotor	17-24
α Stator	25-32

The last card of sets of cards will contain off-design data (see third page of sample input sheets).

D. RESTRICTIONS

1. NSL must be odd and less than or equal to eleven (11).

2. See Section I. D. 2.

E. TIME

No specific formula for computing execution time is available; however,

time required for the test cases run where as follows:

4 mir for 8 stages with 11 streamlines and 4 off-design points

1 min for 3 stages with 11 streamlines and 2 off-design points

III. OUTPUT

A. DISCUSSION

Each set of output will consist of 6 pages for each stage.

The first page contains the basic pump data, inlet conditions and geometry for Stage 1. The second, third and fourth pages contain the data obtained at stations 1, 2 and 3. The fifth and sixth pages contain the data pertaining to the rotor and stator.

B. DATA OUTPUT

The following is a list of all the data output:

Symbol	Description
ALPHA	blade stagger angle, degrees
ALPHAR	rotor blade stagger angle, degrees
ALPHAS	stator blade stagger angle, degrees
BETA (1)	fluid inlet angle relative to blade, degrees
BETA (2)	fluid outlet angle relative to blade, degrees
BLADE TYPE	
BLOCKAGE FACTOR	
DEV	deviation angle, degrees
D *	equivalent diffusion ratio
D **	diffusion factor
E	enthalpy, btu/lb
ETA	efficiency

Symbol	Description
FLOW	Compressible or incompressible
FLOW RATE	Flow rate, lbs/sec
H	HEAD, feet
HEAD LOSS	Head loss, feet
INC	Incidence angle, degrees
K	Number of streamlines
NS	Number of stages
P	Pressure, psia
PS	Static pressure, psia
PHI	Blade camber angle, degrees
PHIS	Stator blade camber angle, degrees
PHIR	Rotor blade camber angle, degrees
Gamma (2)	Fluid angle relative to housing at station 2, degrees
Gamma (3)	Fluid angle relative to housing at station 3, degrees
R	Coordinate in radial direction, inches
RH (1)	Hub radius at station 1, inches
RH (2)	Hub radius at station 2, inches
RH (3)	Hub radius at station 3, inches
RHØ	Density, lbs/ft^3
RT (1)	Tip radius at station 1, inches
RT (2)	Tip radius at station 2, inches
RT (3)	Tip radius at station 3, inches

Symbol	Description
S	Entropy, BTU/lb°R
SHAFT SPEED	Shaft speed, revolutions/minute
SIGMA	σ
TCRH	$(t/c)_{R,H}$
TCSH	$(t/c)_{S,H}$
TCRT	$(t/c)_{R,T}$
TCST	$(t/c)_{S,T}$
T	Temperature
T/C	Blade solidity
U	Blade speed
V	Fluid velocity relative to pump housing, ft/sec
VT	Fluid tangential velocity relative to pump housing, ft/sec
VZ	Axial component of fluid velocity, ft/sec
W	Fluid velocity relative to blade, ft/sec
X (Rotor)	Radius ratio exponent
X (Stator)	Radius ratio exponent

1) $$R_{i,n} = \left[\frac{n-1}{K-1} \left(\frac{1 - R_{i,H}/R_{i,T}}{R_{i,H}/R_{i,T}} \right) + 1 \right] R_{i,H}$$

2) $$U_{i,n} = R_{i,n} \quad (RPM/9.549)$$

3) $$(T/C)_{R,n} = (T/C)_{R,H} + \frac{(T/C)_{R,T} - (T/C)_{R,H}}{K-1} (n-1)$$

4) $$\sigma_{R,n} = \sigma_H \left(R_{i,H}/R_{i,n} \right)^{X_R}$$

5) $$\gamma_{1,n} = \text{Arctan} \left(V_{T1,n}/V_{Z1,n} \right)$$

6) $$W_{T1,n} = U_{1,n} - V_{T1,n}$$

7) $$W_{1,n} = \left(V^2_{Z1,n} + W^2_{T1,n} \right)^{1/2}$$

8) $$V_{1,n} = \left(V^2_{Z1,n} + V^2_{T1,n} \right)^{1/2}$$

9) $$h_{1,n} = H_{1,n} - \frac{V^2_{1,n}}{2g}$$

10) $$\beta_{1,n} = \text{Arctan} \left(W_{T1,n}/V_{Z,n} \right)$$

11) Set DAC = 1.1 for blade type C-4
= 0.7 for blade type DCA
= 1.0 for blade type NACA-65

A. $$B = \left[.1197 + 3.871 \, (T/C)_{R,n} + 50 \, (T/C)^2_{R,n} \right] \quad DAC$$

B. $$M = .252 - .1045 \times 10^{-3} \beta_{1,n} + .192 \times 10^{-4} \beta^2_{1,n}$$

C. $$b = .954 + .873 \times 10^{-3} \beta_{1,n} - .929 \times 10^{-4} \beta^2_{1,n}$$

D. $$NN_n = f \left(\beta_{1,n}, \sigma_{R,n} \right)$$

E. $$(\delta_o)_{10,n} = f \left(\beta_{1,n}, \sigma_{R,n} \right)$$

F. $$\delta_n = B \, (\delta_o)_{10,n} + \frac{m \phi R,n}{\sigma^6_{R,n}} + FIXDEV_n$$

G. $i_n = \beta_{1,n} - \left| \alpha_{R,n} + \phi_{R,n/2} \right|$

H. $\beta_{2,n} = \alpha_{R,n} - \phi_{R,n} + \delta_n$

12) Satisfy radial equilibrium for rotor:

A. $V_{Z_{2,1}} = \dot{W} / \quad \rho_{1,1} (R^2_{T,1} - R^2_{1,H}) \pi$

B. Set n = 1

C. $V_{T_{2,n}} = U_{2,n} - V_{Z_{2,n}} \tan \beta_{2,n}$

D. $V_{2,n} = \left(V^2_{T_{2,n}} + V^2_{Z_{2,n}} \right)^{1/2}$

E. $\Delta H_{i,n} = (U_{2,n} V_{T_{2,n}} - U_{1,n} V_{T_{1,n}})/g$

F. Calculate $\widetilde{W}_{R,n}$

G. Calculate $\rho_{2,n}$

H. $H_{2,n} = H_{1,n} + \Delta H_{i,n} - \widetilde{W}_{R,n} W^2_{1,n}/2g$

If n = K go to step 13, otherwise continue

I. $TD = V^2_{T_{2,n}} / R_{2,n}$

J. $\widetilde{W}_{R,n+1} = W_{R,n}$

K. $V_{Z_{2,n+1}} = \cos \beta_{2,n+1} \left[2g (H_{1,n+1} - H_{2,n}) + U^2_{2,n+1} + V^2_{2,n+1} - 2U_{1,n+1} V_{T_{1,n+1}} - 2 \Delta RTD - \widetilde{W}_{R,n+1} W^2_{1,n+1} \right]^{1/2}$

L. $VT_{2,n+1} = U_{2,n+1} - VZ_{2,n+1} \tan \beta_{2,n+1}$

M. $TD = (VT^2_{2,n} / R_{2,n} + VT^2_{2,n+1} / R_{2,n+1}) / 2$

N. Return to K two times, then proceed to O.

O. Increase n by 1 and return to D.

13) $\dot{W}_c = 2\pi (1 - \lambda) \int_{R_1}^{R_K} R_{2,n} VZ_{2,n} \rho_{2,n} \, dr$

14) Define: Check = $(\dot{W} - \dot{W}_c) / \dot{W}$

15) If/check/$\leq .005$, go to 25, otherwise proceed to 16,

16) If this is the first iteration go to 17, if not go to 22.

17) If check is negative set F = .95
If check is positive set F = 1.05

18) $Check_1$ = check

19) VEL = $VZ_{2,1}$

20) $VZ_{2,1} = VZ_{2,1} \cdot F$

21) If the number of iterations performed is less than or equal to 30, go to 12)B otherwise halt.

22) If (check)($check_1$) ≥ 0, go to 18
< 0, go to 23

23) $VZ_{2,1} = (check_1 VZ_{2,1} - check \cdot VEL)/(check_1 - check)$

24) Go to 21.

25) $(T/C)_{s,n} = (T/C)_{s,H} + \frac{(T/C)_{s,T} - (T/C)_{s,H}}{(K-1)} (n-1)$

26) $\sigma_{s,n} = \sigma_H \left| R_{i,H}/R_{i,n} \right|^{X_s}$

27) $\gamma_{2,n} = \text{Arctan} (VT_{2,n}/VZ_{2,n})$

28) A. B = $.1197 + 3.871 (T/C)_{s,n} + 50 (T/C)^2_{s,n}$ DAC

B. $M = .252 - .1045 \times 10^{-3} \gamma_{2,n} + .192 \times 10^{-4} \gamma_{2,n}^2$

C. $b = .954 + .873 \times 10^{-3} \gamma_{2,n} - .929 \times 10^{-4} \gamma_{2,n}^2$

D. $NN_n = f(\gamma_{2,n}, \sigma_{s,n})$

E. $(\delta_o)_{10,n} = f(\gamma_{2,n}, \sigma_{s,n})$

F. $S_n = B(\delta_o)_{10,n} + \frac{m\phi_{s,n}}{\sigma_{s,n}^b} + FIXDEV_n$

G. $i_n = \gamma_{2,n} - (\alpha_{s,n} + \phi_{s,n/2})$

H. $\gamma_{3,n} = \alpha_{s,n} - \phi_{s,n/2} + \delta n$

29) Satisfy radial equilibrium for stator:

A. $VZ_{3,1} = \dot{W}/\rho_{2,1}(R_{2,T}^2 - R_{2,H}^2)\pi$

B. Set n = 1

C. $VT_{3,n} = VZ_{3,n} \tan \gamma_{3,n}$

D. $V_{3,n} = (VT_{3,n}^2 + VZ_{3,n}^2)^{1/2}$

E. Calculate $\tilde{W}_{s,n}$ and $\rho_{3,n}$

F. $H_{3,n} = H_{2,n} - \tilde{W}_{s,n} V_{2,n}^2/2g$

G. If n = K go to step 30, otherwise go to H.

H. $TD = VT_{3,n}^2/R_{3,n}$

I. $\tilde{W}_{s,n+1} = \tilde{W}_{s,n}$

J. $VZ_{3,n+1} = \left\{ 2\left[g(H_{2,n+1} - H_{3,n}) - TD(\Delta R) \right] + V_{3,n}^2 - \tilde{W}_{s,n+1} V_{2,n+1}^2 \right\}^{1/2} \cos \gamma_{3,n+1}$

K. $VT_{3,n+1} = VZ_{3,n+1} \tan \gamma_{3,n+1}$

L. Calculate $\tilde{W}_{s,n+1}$

M. Return to J two times, then proceed to N.

N. Increase n by 1 and return to D.

O. $$\dot{W}_c = 2\pi(1 - \tau) \int_{R_1}^{R_K} R_{3,n}\, VZ_{3,n}\, \rho_{3,n}\, dr$$

P. Define: $\text{Check} = (\dot{W}_c - \dot{W})/\dot{W}$

Q. If/check/ $\leq .005$, go to 30
$> .005$, go to R

R. If this is the first iteration go to S, if not go to 29.X

S. If check > 0, set F = .95
< 0, set F = 1.05

T. $\text{Check}_1 = \text{check}$

U. $VEL = VZ_{3,1}$

V. $VZ_{3,1} = VZ_{3,1} F$

W. If the number of iterations performed is less than or equal to 30 go to 29.B, otherwise halt.

X. If $(\text{check})(\text{check}_1) \geq 0$, go to T
< 0, go to Y

Y. $VZ_{3,1} = (\text{check}_1 VZ_{3,1} - \text{check} \cdot VEL)/(\text{check}_1 - \text{check})$

Z. Go to W

30) $W_{2,n} = VZ_{2,n}/\cos \beta_{2,n}$

31) $HLOSS_{R,M} = \tilde{W}_{R,n}\, W_{1,n}^2/2g$

32) $HLOSS_{s,n} = \tilde{W}_{s,n} V^2_{2,n}/2g$

CALCULATION OF DENSITY AT STATION 2

1) $E(IDEAL)_{2,n} = E_{1,n} + \Delta H_{i,n}/778$

2) $E_{2,n} = E(IDEAL)_{2,n} - \tilde{W}_{R,n} W^2_{1,n}/2g \times 778$

3) $P_{2,n} = f(E_{2,n}, S_{1,n})$

4) $S_{2,n} = f(E(IDEAL)_{2,n}, P_{2,n})$

5) $E(STATIC)_{2,n} = E(IDEAL)_{2,n} - V^2_{2,n}/2g \times 778$

6) $\rho_{2,n} = f(E(STATIC)_{2,n}, S_{2,n}$

7) $T_{2,n} = f(E(STATIC)_{2,n}, S_{2,n}$

8) $P(STATIC)_{2,n} = P_{2,n} - \frac{V^2_{2,n}}{2g} \frac{\rho_{2,n}}{144}$

9) $\eta_{R,n} = (E_{2,n} - E_{1,n})/(E(IDEAL)_{2,n} - E_{1,n})$

CALCULATION OF DENSITY AT STATION 3

1) $E_{3,n} = E_{2,n} - \tilde{W}_{s,n} V^2_{2,n}/2g \times 778$

2) $P_{3,n} = f(E_{3,n}, S_{1,n})$

3) $S_{3,n} = f(E(IDEAL)_{2,n}, P_{3,n})$

4) $E(STATIC)_{3,n} = E_{3,n} - V^2_{3,n}/2g \times 778$

5) $\rho_{3,n} = f(E(STATIC)_{3,n}, S_{3,n})$

6) $T_{3,n} = f(E(STATIC)_{3,n}, S_{3,n})$

7) $P(STATIC)_{3,n} = P_{3,n} - \frac{V^2_{3,n}}{2g} \frac{\rho_{3,n}}{144}$

8) $\eta_{S,n} = (E_{3,n} - E_{1,n})/(E(IDEAL)_{2,n} - E_{1,n})$

CALCULATION OF DENSITY AT STATION 1, STAGE 1

1) $E_{1,n} = f\ (P_{1,n}\ ,\ T_{1,n})$

2) $S_{1,n} = f\ (P_{1,n}\ ,\ T_{1,n})$

3) $E\ (STATIC)_{1,n} = E_{1,n} - (VZ^2_{1,n} + VT^2_{1,n})/50062.744$

4) $\rho_{1,n} = f\ (E\ (STATIC)_{1,n}\ ,\ S_{1,n})$

5) $H_{1,n} = P_{1,n} \cdot 144/\rho_{1,n}$

6) $P(STATIC)_{1,n} = P_{1,n} - \frac{V^2_{1,n}}{2g}\ \frac{P_{1,n}}{144}$

CALCULATION OF $\widetilde{W}_{R,n}$ =

$$D^*_{R,n} = \frac{\cos\beta_{2,n}\ VZ_{1,n}}{\cos\beta_{1,n}\ VZ_{2,n}}\left[1.12 + .61\ \frac{\cos^2\beta_{1,n}}{\sigma_{R,n}\ V_{1,n}\ VZ_{1,n}}\ (V_{1,n}\ WT_{1,n} - V_{2,n}\ WT_{2,n})\right]$$

$$D^{**}_{R,n} = 1 - \frac{W_{2,n}}{W_{1,n}} + \frac{V_{1,n}\ WT_{1,n} - V_{2,n}\ WT_{2,n}}{(V_{1,n}+V_{2,n})\sigma_{R,n}\ W_{1,n}}$$

$$Rotor_n = f\ (D^{**}_{R,n})$$

$$\widetilde{W}_{R,n} = \frac{2\sigma_{R,n}\ ROTOR_n}{\cos\beta_{2,n}}$$

COMPUTATION OF $\widetilde{W}_{s,n}$ =

$$D^*_{s,n} = \frac{\cos\gamma_{3,n}\ VZ_{2,n}}{\cos\gamma_{2,n}\ VZ_{3,n}}\left[1.12 + .61\ \frac{\cos^2\gamma_{2,n}}{\sigma_{s,n}\ V_{2,n}\ VZ_{2,n}}\ (V_{2,n}\ VT_{2,n} - V_{3,n}\ VT_{3,n})\right]$$

$$D^{**}_{s,n} = 1 - \frac{V_{3,n}}{V_{2,n}} + \frac{V_{2,n}\ VT_{2,n} - V_{3,n}\ VT_{3,n}}{(V_{2,n} + V_{3,n})\ \sigma_{3,n}\ V_{2,n}}$$

$$STATOR_n = f\left(D^{**}_{s,n}\right)$$

$$\tilde{W}_{s,n} = \frac{2\,\sigma_{s,n}\,STATOR_n}{\cos V_{3,n}}$$

CALCULATION OF $\Delta\beta_{ns}$:

$$A = \frac{\cos \beta_{2,n}\, VZ_{2,n}}{\cos \sigma_{1,n}\, VZ_{1,n}}$$

$$B = 1.12 + .61\,\frac{\cos^2 \beta_{1,n}}{V_{1,n}\,\sigma_{R,n}\,VZ_{1,n}}\left(V_{1,n}\,WT_{1,n} - V_{2,n}\,WT_{2,n}\right)$$

$$\Delta\beta_{ns} = \left[\frac{1}{a}\left(\frac{DFS}{A} - B\right)\right]^{.699}$$

where a = .007 if C-4 blade type

a = 1 if DCA blade type

a = .0117 if NACA-65 blade type

CALCULATION OF $\Delta\gamma_{ns}$:

$$A = \frac{\cos \gamma_{c,n}\, VZ_{3,n}}{\cos \gamma_{2,n}\, VZ_{2,n}}$$

$$B = 1.12 + .61\,\frac{\cos^2 \gamma_{2,n}}{V_{2,n}\;\; S,n\, VZ_{2,n}}\left(V_{2,n}\,VT_{2,n} - V_{3,n}\,VT_{3,n}\right)$$

$$\Delta\gamma_{ns} = \left[\frac{1}{a}\left(\frac{DFS}{A} - B\right)\right]^{.699}$$

REPORT NASA CR 54822 DISTRIBUTION LIST

W. W. Wilcox (5 Copies)
National Aeronautics and Space Administration
Lewis Research Center
21000 Brookpark Road
Cleveland, Ohio 44135
Mail Stop 500-305

W. F. Dankhoff (1 Copy)
Mail Stop 3-13

H. H. Hinckley, (1 Copy)
Mail Stop 500-210

Lewis Library (2 Copies)
Mail Stop 60-3

M. J. Hartmann (1 Copy)
Mail Stop 5-9

J. C. Montgomery (1 Copy)
Mail Stop 501-1

Office of Reliability and Quality Assurance (1 Copy)
Mail Stop 500-203

F. J. Dutee (1 Copy)
Mail Stop 23-1

D. F. Lange (1 Copy)
Mail Stop 501-1

Patent Counsel (1 Copy)
Mail Stop 77-1

Lewis Technical Information Division (1 Copy)
Mail Stop 5-5

Robert Connelly (1 Copy)
Mail Stop 5-9

AFSC Liaison Office
Major E. H. Karalis (1 Copy)
Mail Stop 4-1

NASA (6 Copies)
Scientific and Technical Information Facility
Box 5700
Bethesda, Maryland

Library (1 Copy)
NASA
Ames Research Center
Moffett Field, California 94035

Library (1 Copy)
NASA
Flight Research Center
P. O. Box 273
Edwards AFB, California 93523

Library (1 Copy)
NASA
Goddard Space Flight Center
Greenbelt, Maryland 20771

Library (1 Copy)
NASA
Langley Research Center
Langley Station
Hampton, Virginia 23365

Library (1 Copy)
NASA
Manned Spacecraft Center
Houston, Texas 77058

J. W. Thomas, Jr. (5 Copies)
I-E-E
NASA
George C. Marshall Space Flight Center
Huntsville, Alabama 35812

Library (1 Copy)
NASA
Western Operations
150 Pico Boulevard
Santa Monica, California 90406

Library (1 Copy)
Jet Propulsion Laboratory
4800 Oak Grove Drive
Pasadena, California 91103

A. O. Tischler (1 Copy)
Code RP
NASA
Washington, D. C. 20546

E. W. Gomersall (1 Copy)
NASA
Mission Analysis Division
Office of Advanced Research and Technology
Moffett Field, California 94035

F. C. Schwenk (1 Copy)
Code NPO
NASA
Washington, D. C. 20546

Dr. E. B. Konecci (1 Copy)
National Aeronautics and Space Council
Executive Office of the President
Executive Office Building
Washington, D. C.

H. V. Main (1 Copy)
Air Force Rocket Propulsion Laboratory
Edwards Air Force Base
Edwards, California

T. Iura (1 Copy)
Aerospace Corporation
2400 East El Segundo Blvd.
P. O. Box 95085
Los Angeles, California 90045

Pratt and Whitney Aircraft Corporation (1 Copy)
Florida Research and Development Center
P. O. Box 2691
West Palm Beach, Florida 33402

Dr. Kurt Rothe (1 Copy)
Rocketdyne
(Library Dept. 586-306)
Division of North American Aviation
6633 Canoga Avenue
Canoga Park, California 91304

Arnold Engineering Development Center (1 Copy)
Arnold Air Force Station
Tullahoma, Tennessee

Dr. K. Boyer (1 Copy)
Los Alamos Scientific Laboratory
CMF-9
P. O. Box 1663
Los Alamos, New Mexico

Dr. A. Acosta (1 Copy)
California Institute of Technology
1201 East California Street
Pasadena, California

Aeronautical Systems Division (1 Copy)
Air Force Systems Command
Wright Patterson Air Force Base
Dayton, Ohio 45433

Chemical Propulsion Information Agency (1 Copy)
John Hopkins University
Applied Physics Laboratory
8621 Georgia Ave.
Silver Spring, Maryland

Dr. G. Wislicenus (1 Copy)
Penn State University
Naval Ordnance Laboratory
University Park, Pennsylvania

Dr. M. Vavra (1 Copy)
Naval Post Graduate School
Monterey, California 93900

Dr. George Serovy (1 Copy)
Iowa State University
Ames, Iowa 50010